Simulation and Analysis of Photoinduced Charge Migration Processes

Inaugural-Dissertation

to obtain the academic degree
Doctor rerum naturalium (Dr. rer. nat.)

submitted to
the Department of Biology, Chemistry and Pharmacy
of Freie Universität Berlin

by

Gunter Hermann

from Eisenhüttenstadt

2018

This work was prepared under supervision of

Jean Christophe Tremblay, Ph.D. (Freie Universität Berlin)

from

June 2014 until April 2018

1st Reviewer	Jean Christophe Tremblay, Ph.D.
2nd Reviewer	Prof. Dr. Beate Paulus
Date of Defense	June 15th, 2018

Diese Doktorarbeit ist meinem Vater gewidmet

Uwe Hermann
(1955 – 2017)

"Nothing really matters, nothing really matters

when the one you love is gone"

Nick Cave

Abstract

The ultrafast migration of electrons and holes triggered by light-matter interactions is the elementary step for a vast number of photoinduced processes in molecules and solid-state materials. The simulation and mechanistic understanding of such charge migration scenarios are the central objectives of ultrafast science. In order to enable the time- and space-resolved analysis and visualization of this correlated many-electron dynamics in molecular systems, this dissertation first presents the capabilities and applications of the open-source post-processing toolbox DETCI@ORBKIT. This program provides a library of transition moments and expectation values of one-electron operators including, e.g., the electron density and the electronic flux density. These analysis tools provide mechanistic insights into electron migration processes by revealing both the time-dependent probability distribution of the electrons and their spatially-resolved instantaneous flow. In order to offer an additional analysis tool for solid-state materials, a novel wave function analysis technique is developed enabling the characterization of their excitonic properties.

In the second part of this dissertation, the established methodological framework is applied to various light-induced charge migration scenarios in three different types of molecular systems. First, the ultrafast electron migration in localized electronic superposition states is investigated for the hydrogen molecular ion and for the benzene molecule. While the former study yields analytical expressions and fundamental spatio-temporal symmetry properties for the electron density and the electronic flux density, the latter investigation provides a quantum mechanical verification of the arrows used to express the mechanism of electronic motion in Lewis structures.

The second application focuses on the simulation of photoinduced charge injection processes in different dye-sensitized solar cells. For their dynamical simulation, a single active electron approach proves its suitability as an appropriate and low-cost method. Apart from the mechanistic insights into the electron dynamics in such systems, the findings add knowledge to the role of many-body effects during charge migration.

In the last application, the charge carrier confinement in the presence of dissipation is examined for a model quantum dot during laser-controlled correlated electron dynamics. For this purpose, the study introduces new microscopic perturbative expressions for energy relaxation and pure dephasing rates and defines a robust and effective pathway to trap a charge carrier in the quantum dot.

In conclusion, the contributions of this dissertation are twofold. First, it provides novel, insightful analysis and imaging tools for the examination of ultrafast correlated electron dynamics. Second, it thereby contributes to the mechanistic understanding of various charge migration processes.

Kurzzusammenfassung

Ultraschnelle Ladungsmigrationsprozesse spielen eine elementare Rolle für eine Vielzahl photoinduzierter Prozesse in Molekülen und Festkörpersystemen. Die Simulation dieser Ladungswanderungen sowie deren mechanistische Aufklärung gehören zu den Hauptzielen der Forschung zu ultraschnellen Phänomenen. Um eine zeit- und ortsaufgelöste Analyse und Visualisierung dieser korrelierten Elektronendynamiken zu ermöglichen, wird in der vorliegenden Dissertation das Open-Source Programm DETCI@ORBKIT präsentiert. Dieses Programm ist in der Lage eine Reihe von Übergangsmomenten und Erwartungswerten von Ein-Elektronen-Operatoren zu berechnen, beispielsweise die Elektronendichte und die elektronische Flussdichte. Diese Größen sind ideal geeignet den Mechanismus von Ladungswanderungen aufzuklären, da sie sowohl die Aufenthaltswahrscheinlichkeit der Elektronen als auch deren ortsaufgelösten Elektronenfluss abbilden können. Um zusätzlich ein Analysewerkzeug für Festkörpermaterialien anzubieten, wird eine neue Methode zur Charakterisierung ihrer exzitonischen Eigenschaften eingeführt.

Diese Analysewerkzeuge werden zur Untersuchung unterschiedlicher Ladungsmigrationsprozesse in drei verschiedenen Arten von molekularen Systemen angewendet. Die erste Anwendung fokussiert sich auf den ultraschnellen Elektronentransfer in lokalisierten Superpositionszuständen im molekularen Wasserstoffion und im Benzolmolekül. Während in der ersten Studie analytische Ausdrücke und fundamentale Symmetrieeigenschaften der Elektronendichte und der elektronischen Flussdichte formuliert werden, liefert die zweite Studie eine quantenmechanische Überprüfung der Pfeil-Mechanismen, die zur Darstellung von Elektronenbewegung verwendet werden.

Der Schwerpunkt der zweiten Anwendung liegt auf photoinduzierten Ladungsinjektionen in verschiedenen Farbstoff-sensibilisierten Solarzellen. Deren dynamische Simulation wird durch einen Einteilchenansatz beschrieben, welcher sich als rechnerisch günstige und qualitativ valide Methode herausstellt. Neben Details zum Mechanismus der Elektronendynamik in solchen Systemen liefert diese Studie tiefe Einblicke zur Rolle von Mehrelektroneneffekten.

Die letzte Untersuchung befasst sich mit der räumlichen Einschränkung von Ladungsträgern in einem Quantenpunkt. Zur Simulation der dissipativen Elektronendynamik werden störungstheoretische Ausdrücke für die Raten der Energierelaxation und der reinen Dephasierung hergeleitet. Darüber hinaus wird ein robuster Anregungspfad zur effektiven räumlichen Einschränkung von Ladungsträgern im Quantenpunkt definiert.

Zusammenfassend stellt diese Dissertation neuartige und aufschlussreiche Analyse- und Visualisierungswerkzeuge zur Untersuchung ultraschneller Elektronendynamiken bereit und trägt damit zum mechanistischen Verständnis verschiedener Ladungsmigrationsprozesse bei.

Contents

List of Publications

Toolkit for Analyzing and Imaging Charge Migration

Paper TK1 V. Pohl, G. Hermann, and J. C. Tremblay

"An Open-Source Framework for Analyzing N-Electron Dynamics. I. Multideterminantal Wave Functions"

J. Comput. Chem. **38**, 1515–1527 (2017)

DOI: 10.1002/jcc.24792

Paper TK2 G. Hermann, V. Pohl, and J. C. Tremblay

"An Open-Source Framework for Analyzing N-Electron Dynamics. II. Hybrid Density Functional Theory/Configuration Interaction Methodology"

J. Comput. Chem. **38**, 2378–2387 (2017)

DOI: 10.1002/jcc.24896

Paper TK3 G. Hermann, L. E. Marsoner Steinkasserer, B. Paulus, and J. C. Tremblay

"Dipole-Induced Transition Orbitals - A Novel Tool for Investigating Optical Transitions in Extended Systems and its Application to Dye-Sensitized MoS_2"

Manuscript in preparation

Charge Migration in Small Molecules

Paper SM1 D. J. Diestler, G. Hermann, and J. Manz

"Charge Migration in Eyring, Walter and Kimball's 1944 Model of the Electronically Excited Hydrogen-Molecule Ion"

J. Phys. Chem. A **121**, 5332–5340 (2017)

DOI: 10.1021/acs.jpca.7b04714

Paper SM2 G. Hermann, C. Liu, J. Manz, B. Paulus, J. F. Pérez-Torres, V. Pohl, and J. C. Tremblay
"Multidirectional Angular Electronic Flux during Adiabatic Attosecond Charge Migration in Excited Benzene"
J. Phys. Chem. A **120**, 5360–5369 (2016)
DOI: 10.1021/acs.jpca.6b01948

Paper SM3 G. Hermann, C. Liu, J. Manz, B. Paulus, V. Pohl, and J. C. Tremblay
"Attosecond Angular Flux of Partial Charges on the Carbon Atoms of Benzene in Non-Aromatic Excited State"
Chem. Phys. Lett. **683**, 553–558 (2017)
DOI: 10.1016/j.cplett.2017.01.030

Charge Migration in Solar Cells

Paper SC1 T. Gomez, G. Hermann, X. Zarate, J. F. Pérez-Torres, and J. C. Tremblay
"Imaging the Ultrafast Photoelectron Transfer Process in Alizarin-TiO_2"
Molecules **20**, 13830–13853 (2015)
DOI: 10.3390/molecules200813830

Paper SC2 G. Hermann and J. C. Tremblay
"Ultrafast Photoelectron Migration in Dye-Sensitized Solar Cells: Influence of the Binding Mode and Many-Body Interactions"
J. Chem. Phys. **145**, 174704 (2016)
DOI: 10.1063/1.4966260

Paper SC3 G. Hermann, F. Witte, and J. C. Tremblay
"Comparison of Donor-Acceptor π-Conjugated Dyes in Model Solar Cells: A Study of Interfacial Ultrafast Electron Migration"
arXiv preprint arXiv:1707.01419 (2017)

Charge Migration in Quantum Dots

Paper QD1 G. Hermann and J. C. Tremblay

"Laser-Driven Hole Trapping in a Ge/Si Core-Shell Nanocrystal: An Atomistic Configuration Interaction Perspective"

J. Phys. Chem. C **119**, 25606–25614 (2015)

DOI: 10.1021/acs.jpcc.5b08606

Additional Publications

Paper AP1 G. Hermann, B. Paulus, J. F. Pérez-Torres, and V. Pohl

"Electronic and Nuclear Flux Densities in the H_2 Molecule"

Phys. Rev. A **89**, 052504 (2014)

DOI: 10.1103/physreva.89.052504

Paper AP2 G. Hermann, V. Pohl, J. C. Tremblay, B. Paulus, H.-C. Hege, and A. Schild

"ORBKIT: A Modular Python Toolbox for Cross-Platform Postprocessing of Quantum Chemical Wavefunction Data"

J. Comput. Chem. **37**, 1511–1520 (2016)

DOI: 10.1002/jcc.24358

Chapter 1

Introduction

Charge transfer at the molecular level plays a fundamental role in many physical and chemical processes in nature.[1–5] Over the last decades, significant theoretical and experimental efforts have been devoted to this field of research due to its importance to both basic research and applications in molecular electronics.[6,7] While charge transfer phenomena are traditionally assumed to be driven by nuclear motion, another purely electronic and extremely fast process is typically involved at the same time. This phenomenon, known as charge migration, was theoretically predicted by Cederbaum and coworkers.[8] It describes the periodic spatial redistribution of electronic charges in molecular or solid-state systems taking place on a timescale ranging from few femtoseconds down to hundreds attoseconds. In particular, it is expected that this ultrafast electronic motion is mediated by many-electron effects, i.e., electronic coherences and relaxations in an electronic superposition state induced by light-matter interactions.[8–14]

Charge migration is seen to be the elementary dynamical step in many photoinduced charge transfer processes such as photochemical reactions in biological relevant systems[11,15–19], charge injection in solar cells[20,21], or charge transfer exciton formation and separation in molecular systems and nanoclusters[22,23]. Its experimental observation requires an extremely high temporal resolution in order to follow and eventually control the ultrafast charge flow on their natural time scale. Following the advent of femtochemistry by the seminal experiments of Zewail and colleagues,[24,25] the recent advances in laser technologies offer the prospect for its direct monitoring on an attosecond temporal scale. Starting from the first experimental evidence of charge migration[26–28] to its indirect monitoring using attosecond laser pulses[29–39], it meanwhile became feasible to induce, directly probe, and control the attosecond charge migration in molecular cationic systems.[40,41] While in these experiments, the ultrafast charge oscillation is triggered by photoionization, electronic superposition states can also be prepared in neutral molecules.[42,43]

As charge migration processes bear an immense potential to gain a profound understanding of a variety of chemical reactions and processes, many theoretical studies of ultrafast electron dynamics in molecular systems have been conducted over the last decades.[8,9,40,44–61] A remaining theoretical challenge is the time- and space-resolved analysis and visualization of charge migration processes to unravel their mechanistic characteristics. A necessary step towards this aim is the development of a computational framework for the post-processing of many-electron wave functions. That forms the basis for the calculation of the crucial quantum chemical quantities for the visual representation of the ultrafast electronic motion. While the time-dependent electron density is the most widespread quantity for this purpose, a potential insightful quantity is the electronic flux density or electronic current density.[62,63] It supplements the information about the probability distribution of the electrons with their instantaneous flow. Thus, it yields at a first glance a very intuitive and microscopic picture of the electronic mechanism during charge migration.[AP1] In addition to a suitable set of analysis tools, such a computational framework needs to meet two requirements. First, general applicability of the program is necessary to enable the post-processing of a broad diversity of many-electron wave functions from various quantum chemistry programs. Second, the framework requires an easily expandable and comprehensible modular architecture. While several post-processing tools in modern computational chemistry exist, none of these programs meet all requirements.[64–68]

To fill this gap, this dissertation introduces the open-source framework detCI@ORBKIT (cf. **Paper TK1** and **Paper TK2**), which extends the functionalities of the recently published modular Python toolbox ORBKIT[AP2]. The new detCI@ORBKIT program is in general capable to determine the expectation values of any one-electron operator from multi-determinantal configuration interaction wave functions. The corresponding computational study (cf. **Paper TK1**) presents the applicability of the implemented one-electron quantities for the mechanistic enlightenment of a variety of charge migration processes. As nanostructured systems are often the focus of such charge migration studies, theoretical approaches are needed that are capable of dealing with ultrafast electron dynamics induced by strong laser fields in large systems. Approaches that require a satisfactory level of approximation and an affordable computational effort remain scarce. For this purpose, a hybrid density functional theory/configuration interaction methodology is developed in **Paper TK2**.

Another challenge regarding the increasing size of a quantum system is the examination of the charge transfer character for extended and condensed systems. While the optical spectra of such systems can be calculated with routinely applied methods like the linear response time-dependent density functional theory within the random-phase approximation, the excitonic nature of a specific transition cannot be determined on their basis. For molecular systems, the formalism associated with

the natural transition orbitals[69] offers a direct, graphical procedure for the interpretation of electronic excitations. As the transfer of the underlying concept to solids is desirable, **Paper TK3** proposes an equivalent perturbative ansatz yielding the excitonic properties for a specific optical transition in extended systems.

Apart from the technical and methodological prerequisites for the study of charge migration processes, the next logical step is the examination of this process in small molecules. In light of its simplicity and the extensive research on its properties[52,53,70–78], the hydrogen molecular ion H_2^+ is considered as a benchmark system being highly amenable for a theoretical treatment. While previous studies report on the simulation of attosecond charge migration in a superposition state of H_2^+[52,53,73], a first hypothetical conjecture of this process was already anticipated by Eyring, Walter, and Kimball (EWK) in their quantum chemistry textbook published in 1944.[79] Their simple analytical description for the electronic wave function of H_2^+ allows for the analytical derivation of the crucial dynamical quantities, i.e., the electron density and the electronic flux density. While the former is already given in their textbook, the latter in combination with a few other quantities is presented within **Paper SM1**. Besides, their model predicted the charge oscillation between the two protons starting with the electron localized on one of the hydrogen atoms. In order to supplement their description with mechanistic details on the charge migration, **Paper SM1** investigates the pathway of the migrating electron and focuses on the pivotal symmetry properties of the dynamical quantities.

A more complex molecule serving as a benchmark system for the fundamental research of both charge migration and charge transfer phenomena is the benzene molecule. In particular, it has been extensively used as the prototype for aromatic compounds in order to develop and describe the concepts of chemical bonding and aromaticity.[80,81] Previous research has specifically focused on the simulation of the oscillating electron dynamics between the two symmetrically equivalent Kekulé structures of benzene.[82,83] In these well-known structures, the six delocalized π-electrons in an oriented[84–90] benzene molecule are localized on alternating carbon-carbon bonds. A widespread model for their simplified representation are Lewis structures. Within this picture, the chemical reaction, i.e., double bond breaking and formation, leading to the oscillation between the two Kekulé localization patterns is usually indicated by curved arrows.[91] They generally symbolize the electronic motion of one or two valence electrons. An open question regarding this simple model concerns the validity of its mechanistic and quantitative statements in comparison to realistic dynamical simulations.

The two scenarios studied in the literature to initiate the electron dynamics between the Kekulé structures are the stimulation of the vibrational motion along the Kekulé mode[81,82] and the electronic excitation to a non-aromatic superposition state[83]. While the former is an example for a charge trans-

fer process mediated by nuclear motion, the latter is a charge migration phenomenon. The first attempt to verify the simple Lewis structure model was conducted by Schild and colleagues[82] using the charge transfer scenario. In contradiction to the six valence electrons indicated by the mechanistic arrows, they found a significantly smaller fraction of electrons being transferred during the vibrational dynamics. In addition, the examination of the mechanism revealed that the electrons rearrange according to the nuclear motion. These findings have been likewise corroborated in several studies on similar rearrangement reactions.[92–95] In order to obtain a corresponding quantitative and qualitative description for the charge migration scenario, Ulusoy and Nest prepared a non-aromatic electronic superposition state of the electronic ground and first excited state in the benzene molecule using a sequence of laser pulses.[83] While they proposed a pincer-type motion for the Rabi-type charge oscillation between the Kekulé structures on the attosecond time scale, their study lacks a quantitative analysis. The analyses of **Paper SM2** aim to fill this void. The necessary methodology for this task is transferred from previous studies on concerted electronic and nuclear fluxes during coherent tunneling.[95] On its basis, it is not only supposed to quantify the number of electrons migrating during the electron dynamics, but also to validate the charge migration mechanism proposed in Ref. [83]. Furthermore, the mechanistic characterization for the charge migration in another electronic superposition state is targeted (cf. **Paper SM3**). This superposition of the ground and second excited state generates negative and positive partial charges on alternating carbon atoms, and the associated dynamical mechanism has not been explored yet.

Besides the basic research on small molecules, the study of electron migration processes in nanostructured systems is relevant for their potential application in molecular electronics. For instance, the research on electron injection processes as a key step of the solar energy conversion can contribute to the efficiency improvement of solar cells.[96] An environmentally friendly and cost-effective representative for photovoltaic devices are Dye-Sensitized Solar Cells (DSSC). These so-called Grätzel cells[97–103] are potential alternatives to conventional silicon-based solar cells in order to satisfy the steadily increasing global energy needs. In DSSC devices, a nanostructured mesoporous film of a semiconductor, usually titanium dioxide TiO_2, is functionalized with a transition-metal or organic dye molecule enabling the absorption of visible light. This photoexcitation induces an interfacial electron injection from the dye into the conduction band of the semiconductor substrate. Subsequently, the electron migrates to the anode of the solar cell, while the oxidized dye is regenerated by the redox pair in the surrounding electrolyte. The redox pair is in turn restored at the cathode of the photovoltaic system. The key step for this conversion of solar energy into electrical energy is the electron-hole separation at the dye/semiconductor interface, which follows immediately after the photoinduced electron injection. This

process was experimentally observed to proceed on the femtosecond time scale.[104,105] Its efficiency and thus the performance of the solar cell are strongly affected by the structural, optical, and electronic properties of the DSSC. In this context, many theoretical aspects ranging from the energetic alignment of the dye and the semiconductor to the dynamical simulation of the electron injection process have been examined to understand the physics involved and to evaluate the efficiency of such a DSSC.[103,106–113]

A void in this field constitutes the time- and space-resolved imaging and analysis of the photoinduced charge injection processes to gain mechanistic insights and the determination of many-electron effects on the electron dynamics. A well-suited system for this purpose is the alizarin dye attached to a TiO_2 nanocrystallite, which has been investigated in great detail by experimentalists and theoreticians.[104,105,114–124] **Paper SC1** and **Paper SC2** examine the photoinduced charge injection process from the alizarin to a TiO_2 nanocluster with a particular focus on the many-body interactions. The mechanism of the electron flow is aimed to be specified using the time-dependent electronic flux density for the first time in such DSSC systems. A remaining challenge is the comprehensive examination of the relation between the structural characteristics of the dye and the mechanistic features of the charge injection process. For this research objective, the dyes under investigation require a similar architecture. In **Paper SC3**, the effects of minor structural differences on the light absorption and electron injection process are examined for the family of donor-acceptor π-conjugated dyes based on a pyridinium core.

A further system being potentially relevant for the usage in future electronic devices are semiconductor nanocrystals, known as quantum dots. These zero-dimensional structures exhibit unique optical and electronic properties, which considerably differ from those of their bulk counterparts.[125–127] One of these special characteristics is their natural tendency to confine charge carriers in all three spatial dimensions. In this context, the most appealing attribute of these semiconductor heterostructures is the tunability of their material properties by modifying their size and/or composition. This opens up the possibility for their usage in a variety of light emitting/absorbing applications such as solar cells[128,129] or quantum computers[130,131]. Consequently, a myriad of experimental and theoretical studies has been conducted over the last decades focusing on their design, fabrication, and characterization.[132–137]

An open challenge of theoretical research is the microscopic examination of the size-dependent excitonic properties of these quantum dots and the control of charge carrier confinement during light-induced charge transfer dynamics. While quantum dots have been extensively studied by means of large-scale methods, e.g., the pseudopotential method[133] or the effective-mass approximation[138], the approximate nature of these approaches prohibits a microscopic description. A more precise picture of the electronic structure and the transient electron dynamics on an atomistic level can be yielded using

systematically improvable wave function-based methods. Although they are restricted to size-reduced quantum dot models, they can serve as a benchmark for the more approximate methods and can take into account electronic correlations properly.

A typical and experimentally well-studied example for a quantum dot is a self-assembled core-shell Ge/Si nanocrystal.[132,134,136,137,139–143] In these type-II semiconductors, the large valence-band offset (~ 0.7 eV) generates a hole confinement in the Ge regions and an electron localization in the Si matrix. Recently, it was shown that their crucial structural features and excitonic properties can be reproduced by a configuration interaction formalism[144,145] for a size-reduced core-shell model system.[146] Based on this, **Paper QD1** attempts to simulate a laser-driven hole confinement in such a quantum dot model in the presence of energy and phase relaxations.

This doctoral dissertation is organized as follows: Chapter 2 gives an overview of the theoretical foundations and quantum chemical and dynamical methods applied in this thesis. The fundamental equation of motion for molecular systems, the time-dependent Schrödinger equation, and the separation of nuclear and electronic motion within the Born-Oppenheimer approximation are recapitulated in Sections 2.1 and 2.2. Various wave function-based and density functional theory methods to determine the molecular electronic structure for the ground state and excited states as well as the wave function analysis are discussed in Section 2.3. Section 2.4 reviews the theoretical treatment of electron dynamics for closed and open quantum systems and recalls an analytical expression for electric laser fields applied to drive the molecular system out of equilibrium. The theory chapter is completed with a description on the time- and space-resolved analysis of correlated many-electron dynamics (cf. Section 2.4). Chapter 3 summarizes and interrelates the results of the scientific publications. The contributions of each author are outlined as an introductory remark to each publication, which are presented in Chapter 4. Finally, Chapter 5 concludes with the main research contributions of the present thesis.

Chapter 2

Theoretical Framework

The following chapter describes the conceptual framework and theoretical methodologies being necessary to conduct the present research project. The main focus is on the presentation of electronic structure methods on various levels of accuracy and efficiency, the theoretical treatment of electron dynamics, and the analysis of the static and time-dependent electronic wave function.

2.1 The Time-Dependent Schrödinger Equation

In a non-relativistic treatment, the time evolution of a molecular quantum system is governed by the time-dependent Schrödinger equation[147]

$$\imath\hbar\frac{\partial}{\partial t}\Phi_{\mathrm{tot}}\left(\boldsymbol{q},\boldsymbol{Q},t\right)=\hat{H}_{\mathrm{tot}}\left(\boldsymbol{r},\boldsymbol{R},t\right)\Phi_{\mathrm{tot}}\left(\boldsymbol{q},\boldsymbol{Q},t\right) \tag{2.1}$$

with the reduced Planck constant $\hbar$ and the imaginary unit $\imath$. The molecular quantum system is completely described by the total molecular wave function $\Phi_{\mathrm{tot}}\left(\boldsymbol{q},\boldsymbol{Q},t\right)$ which depends on time t and the electronic and nuclear coordinates, $\boldsymbol{q}$ and $\boldsymbol{Q}$. These comprise the set of spatial and spin coordinates of the N_{el} electrons, $\boldsymbol{q}=\left\{\boldsymbol{r},\boldsymbol{\theta}\right\}\equiv\left\{\vec{r}_i,\theta_i\right\}_{i=1}^{N_{\mathrm{el}}}$, and N_{nuc} nuclei, $\boldsymbol{Q}=\left\{\boldsymbol{R},\boldsymbol{\Theta}\right\}\equiv\left\{\vec{R}_A,\Theta_A\right\}_{A=1}^{N_{\mathrm{nuc}}}$. It should be noted that the nuclear spin dependence is neglected in the current treatment and that the total non-relativistic Hamiltonian $\hat{H}_{\mathrm{tot}}\left(\boldsymbol{r},\boldsymbol{R},t\right)$ in Eq. (2.1) makes no reference to the nuclear and electronic spin coordinates. $\hat{H}_{\mathrm{tot}}\left(\boldsymbol{r},\boldsymbol{R},t\right)$ is composed of the time-independent molecular Hamiltonian $\hat{H}_{\mathrm{mol}}\left(\boldsymbol{r},\boldsymbol{R}\right)$ and the time-dependent interaction Hamiltonian $\hat{H}_{\mathrm{int}}\left(\boldsymbol{r},\boldsymbol{R},t\right)$

$$\hat{H}_{\mathrm{tot}}\left(\boldsymbol{r},\boldsymbol{R},t\right)=\hat{H}_{\mathrm{mol}}\left(\boldsymbol{r},\boldsymbol{R}\right)+\hat{H}_{\mathrm{int}}\left(\boldsymbol{r},\boldsymbol{R},t\right). \tag{2.2}$$

The latter describes, for example, the interaction of the molecular system with an external electric field, which can be defined by means of the semiclassical dipole approximation[148]

$$\hat{H}_{\mathrm{int}}\left(\boldsymbol{r},\boldsymbol{R},t\right)=-\hat{\mu}\left(\boldsymbol{r},\boldsymbol{R}\right)\cdot\vec{F}\left(t\right). \tag{2.3}$$

Here, $\hat{\mu}\left(\boldsymbol{r},\boldsymbol{R}\right)$ is the molecular dipole operator, and $\vec{F}\left(t\right)$ stands for the electric field operator, whose explicit form is defined in Sec. (2.4.3). The expression for the field-free molecular Hamiltonian $\hat{H}_{\mathrm{mol}}\left(\boldsymbol{r},\boldsymbol{R}\right)$, which describes the interaction of N_{el} electrons and N_{nuc} nuclei within the molecular framework, is given by

$$\begin{aligned}\hat{H}_{\mathrm{mol}}\left(\boldsymbol{r},\boldsymbol{R}\right) \;=\; & \underbrace{-\sum_{i=1}^{N_{\mathrm{el}}}\frac{\hbar^2}{2m_e}\nabla_{\vec{r}_i}^2}_{\hat{T}_{\mathrm{el}}(\boldsymbol{r})}\underbrace{-\sum_{A=1}^{N_{\mathrm{nuc}}}\frac{\hbar^2}{2M_A}\nabla_{\vec{R}_A}^2}_{\hat{T}_{\mathrm{nuc}}(\boldsymbol{R})}\underbrace{-\sum_{i=1}^{N_{\mathrm{el}}}\sum_{A=1}^{N_{\mathrm{nuc}}}\frac{Z_A e^2}{4\pi\epsilon_0\left|\vec{r}_i-\vec{R}_A\right|}}_{\hat{V}_{\mathrm{el-nuc}}(\boldsymbol{r},\boldsymbol{R})} \\ & \underbrace{+\sum_{i=1}^{N_{\mathrm{el}}}\sum_{j>i}^{N_{\mathrm{el}}}\frac{e^2}{4\pi\epsilon_0\left|\vec{r}_i-\vec{r}_j\right|}}_{\hat{V}_{\mathrm{el-el}}(\boldsymbol{r})}\underbrace{+\sum_{A=1}^{N_{\mathrm{nuc}}}\sum_{B>A}^{N_{\mathrm{nuc}}}\frac{Z_A Z_B e^2}{4\pi\epsilon_0\left|\vec{R}_A-\vec{R}_B\right|}}_{\hat{V}_{\mathrm{nuc-nuc}}(\boldsymbol{R})},\end{aligned} \tag{2.4}$$

where the mass M_A and the atomic number Z_A belong to the Ath nucleus, and $\nabla_{\vec{r}_i}^2$ and $\nabla_{\vec{R}_A}^2$ are the Laplace operators with respect to the Cartesian coordinates of electron i and nucleus A. Furthermore, m_e and e are the rest mass and charge of the electron, and ϵ_0 stands for the permittivity of vacuum. In Eq. (2.4), the first and second term correspond to the kinetic energy operator of the electrons $\hat{T}_{\mathrm{el}}\left(\boldsymbol{r}\right)$ and nuclei $\hat{T}_{\mathrm{nuc}}\left(\boldsymbol{R}\right)$, respectively. The last three operators can be assigned to intra-molecular Coulomb interactions consisting of the Coulomb attraction between electrons and nuclei $\hat{V}_{\mathrm{el-nuc}}\left(\boldsymbol{r},\boldsymbol{R}\right)$, the Coulomb repulsion between the electrons $\hat{V}_{\mathrm{el-el}}\left(\boldsymbol{r}\right)$, and the Coulomb repulsion between the nuclei $\hat{V}_{\mathrm{nuc-nuc}}\left(\boldsymbol{R}\right)$.[149,150]

The solution of the time-dependent Schrödinger equation, Eq. (2.1), is a highly demanding many-body problem which is numerically exactly accessible only for small molecular systems, such as the hydrogen molecular ion (H_2^+). Hence, basic simplifications and approximations have to be invoked for the numerical characterization of more sophisticated molecular systems.

2.2 The Born-Oppenheimer Approximation

The central simplification in quantum chemistry is the separation between electronic and nuclear motion, which is based on the significant difference in mass between the nuclei and the electrons and thus, on their different velocities. Following this assumption, the nuclei are considered as frozen in space

from the perspective of the electrons, while, from the perspective of the nuclei, the electrons react instantaneously to the nuclear motion.[149–151] Within this clamped nuclei approximation, an electronic Hamiltonian $\hat{H}_{\mathrm{el}}(\boldsymbol{r};\boldsymbol{R})$ can be defined from the molecular Hamiltonian $\hat{H}_{\mathrm{mol}}(\boldsymbol{r},\boldsymbol{R})$ (cf. Eq. (2.4))

$$\hat{H}_{\mathrm{el}}(\boldsymbol{r};\boldsymbol{R}) = \quad \hat{T}_{\mathrm{el}}(\boldsymbol{r}) + \hat{V}_{\mathrm{el-nuc}}(\boldsymbol{r};\boldsymbol{R}) + \hat{V}_{\mathrm{el-el}}(\boldsymbol{r}) + \hat{V}_{\mathrm{nuc-nuc}}(\boldsymbol{R}), \tag{2.5}$$

where the nuclear kinetic energy operator $\hat{T}_{\mathrm{nuc}}(\boldsymbol{R})$ is set to zero, and the internuclear repulsion term $\hat{V}_{\mathrm{nuc-nuc}}(\boldsymbol{R})$ becomes constant. It should be noted that any additive constant only affects the eigenvalue of an operator. In Eq. (2.5), $\hat{H}_{\mathrm{el}}(\boldsymbol{r};\boldsymbol{R})$ is an operator in the electronic space which depends only parametrically on the nuclear coordinates $\boldsymbol{R}$. This dependency is indicated by a semicolon.[149,150] For each fixed nuclear configuration $\boldsymbol{R}$, the electronic eigenvalue problem is governed by the time-independent electronic Schrödinger equation

$$\hat{H}_{\mathrm{el}}(\boldsymbol{r};\boldsymbol{R})\,\Psi_{\lambda}(\boldsymbol{q};\boldsymbol{R}) = E_{\lambda}(\boldsymbol{R})\,\Psi_{\lambda}(\boldsymbol{q};\boldsymbol{R}), \tag{2.6}$$

whose solution provides the stationary electronic eigenfunctions $\Psi_{\lambda}(\boldsymbol{q};\boldsymbol{R})$ of the electronic state λ and the associated electronic eigenvalues $E_{\lambda}(\boldsymbol{R})$. These expectation values are commonly denoted as the potential energy surface.[149,150] According to the Hermitian properties of the electronic Hamiltonian $\hat{H}_{\mathrm{el}}(\boldsymbol{r};\boldsymbol{R})$, the orthonormality condition

$$\int \mathrm{d}\boldsymbol{q}\,\Psi_{\lambda}^{\dagger}(\boldsymbol{q};\boldsymbol{R})\,\Psi_{\nu}(\boldsymbol{q};\boldsymbol{R}) \equiv \langle\Psi_{\lambda}|\Psi_{\nu}\rangle = \delta_{\lambda\nu} \tag{2.7}$$

applies for the set of electronic eigenfunctions $\{\Psi_{\lambda}(\boldsymbol{q};\boldsymbol{R})\}$ forming a complete basis in the electronic space $\boldsymbol{r}$ at every value of $\boldsymbol{R}$

$$\sum_{\lambda}\Psi_{\lambda}^{\dagger}(\boldsymbol{q}';\boldsymbol{R})\,\Psi_{\lambda}(\boldsymbol{q};\boldsymbol{R}) = \delta(\boldsymbol{q}-\boldsymbol{q}'). \tag{2.8}$$

Here, Eq. (2.7) introduces the Kronecker delta $\delta_{\lambda\nu}$ and the Dirac notation of the inner product of two wave functions $\langle\Psi_{\lambda}|\Psi_{\nu}\rangle$, which symbolizes the integration over the whole set of electronic coordinates $\boldsymbol{q}$.[149,150]

Returning to the description of the coupled electron-nuclear dynamics by the time-dependent Schrödinger equation, Eq. (2.1), an exact solution for the total molecular wave function $\Phi_{\mathrm{tot}}(\boldsymbol{q},\boldsymbol{R},t)$ can now be defined as

$$\Phi_{\mathrm{tot}}(\boldsymbol{q},\boldsymbol{R},t) = \sum_{\lambda}\Psi_{\lambda}(\boldsymbol{q};\boldsymbol{R})\,\chi_{\lambda}(\boldsymbol{R},t) \tag{2.9}$$

which is realized by an expansion in the complete set of electronic eigenfunctions $\{\Psi_\lambda(\boldsymbol{q};\boldsymbol{R})\}$. This expansion is known as the Born-Huang expansion and constitutes no approximation given that the summation is not truncated.[152] In Eq. (2.9), $\chi_\lambda(\boldsymbol{R},t)$ act as time-dependent expansion coefficients being a function of the nuclear coordinates. These are usually referred to as the nuclear wave functions. A coupled equation of motion for these expansion coefficients can be easily obtained by inserting the Born-Huang ansatz into the time-dependent Schrödinger equation (cf. Eq. (2.1)), multiplying from the left by $\Psi_\lambda^\dagger(\boldsymbol{q};\boldsymbol{R})$, and integrating over the electronic coordinates

$$\imath\hbar\frac{\partial}{\partial t}\chi_\lambda(\boldsymbol{R},t) = \left[\hat{T}_{\text{nuc}}(\boldsymbol{R}) + E_\lambda(\boldsymbol{R}) + \sum_\nu \Lambda_{\lambda\nu}(\boldsymbol{R}) + \hat{H}_{\text{int}}(\boldsymbol{R},t)\right]\chi_\lambda(\boldsymbol{R},t)\,. \tag{2.10}$$

In this formula, the dynamical interactions between the electronic and nuclear motion are characterized by the non-adiabatic coupling terms $\Lambda_{\lambda\nu}(\boldsymbol{R})$, which are expressed by

$$\Lambda_{\lambda\nu}(\boldsymbol{R}) = -\sum_A^{N_{\text{nuc}}} \frac{\hbar^2}{2M_A}\Big[\underbrace{2\langle\Psi_\lambda|\vec{\nabla}_{\vec{R}_A}|\Psi_\nu\rangle}_{\vec{\Lambda}^{(1)}_{\lambda\nu}(\boldsymbol{R})}\cdot\vec{\nabla}_{\vec{R}_A} + \underbrace{\langle\Psi_\lambda|\nabla^2_{\vec{R}_A}|\Psi_\nu\rangle}_{\Lambda^{(2)}_{\lambda\nu}(\boldsymbol{R})}\Big]. \tag{2.11}$$

Two elements for the non-adiabatic couplings are to be found in Eq. (2.11), i.e., a vectorial term $\vec{\Lambda}^{(1)}_{\lambda\nu}(\boldsymbol{R})$ of the first order and a scalar term $\Lambda^{(2)}_{\lambda\nu}(\boldsymbol{R})$ of the second order.[153,154] The neglect of these coupling elements leads to the Born-Oppenheimer approximation[151] which can be safely applied for a great number of molecular systems. However, it loses its validity in the case of energetically close lying electronic states.

Despite the simplifications arising from a non-relativistic Hamiltonian and the Born-Oppenheimer approximation, the solution of the time-independent electronic problem, Eq. (2.6), can only be achieved by approximate electronic structure methods.

2.3 Molecular Electronic Structure Theory

The two main classes of electronic structure models to find approximate solutions for the non-relativistic time-independent electronic Schrödinger equation, Eq. (2.6), are the wave function-based methods and the density functional theory. Both comprise methodologies to determine the electronic eigenfunctions and eigenvalues for the electronic ground state ($\lambda = 0$) as well as for excited electronic states. The associated standard methods as well as the underlying basic concepts, which are shared within each class and partly between both classes, are introduced in the following section. Their description in the ensuing section mainly follows Refs. [149], [150], [155], and [156].

2.3.1 The Hartree-Fock Method

The Hartree-Fock model constitutes the simplest wave function-based method in the electronic structure theory and belongs to the mean-field approaches.[157–159] In addition, it often serves as a favorable starting point for more sophisticated methods (cf. Sec. 2.3.2).

Within the mean-field approximation, each electron moves independently in the averaged potential of the remaining electrons and the potential created by the nuclei. Accordingly, the many-electron wave function can be expressed as a simple product of all one-electron wave functions (Hartree Product)

$$\Psi_{\mathrm{HP}}\left(\boldsymbol{q};\boldsymbol{R}\right) = \psi_1(\vec{q}_1;\boldsymbol{R})\psi_2(\vec{q}_2;\boldsymbol{R})\ldots\psi_{N_{\mathrm{el}}}(\vec{q}_{N_{\mathrm{el}}};\boldsymbol{R}). \tag{2.12}$$

Each one-electron wave function $\psi_a(\vec{q}_i;\boldsymbol{R})$ corresponds to an orthonormal spin orbital a occupied by an electron i

$$\psi_a(\vec{q}_i;\boldsymbol{R}) = \varphi_a(\vec{r}_i;\boldsymbol{R})\sigma(\theta_i) \tag{2.13}$$

and is defined as the product of a spatial molecular orbital $\varphi_a(\vec{r}_i;\boldsymbol{R})$ and a spin function $\sigma(\theta_i)$. The latter is either a spin up (α) or a spin down (β) function for fermions. In order to properly treat this ansatz, the many-electron wave function must be antisymmetric with respect to the interchange of the coordinates $\boldsymbol{q}$ of any two electrons[160,161]

$$\Psi\left(\vec{q}_1,\ldots,\vec{q}_i,\ldots,\vec{q}_j\ldots,\vec{q}_{N_{\mathrm{el}}};\boldsymbol{R}\right) = -\Psi\left(\vec{q}_1,\ldots,\vec{q}_j,\ldots,\vec{q}_i\ldots,\vec{q}_{N_{\mathrm{el}}};\boldsymbol{R}\right). \tag{2.14}$$

This antisymmetry requirement can be fulfilled by Slater determinants[162]

$$\begin{aligned}\Psi_{\mathrm{SD}}(\boldsymbol{q};\boldsymbol{R}) &= \frac{1}{\sqrt{N_{\mathrm{el}}!}}\begin{vmatrix} \psi_a(\vec{q}_1;\boldsymbol{R}) & \psi_a(\vec{q}_2;\boldsymbol{R}) & \ldots & \psi_a(\vec{q}_{N_{\mathrm{el}}};\boldsymbol{R}) \\ \psi_b(\vec{q}_1;\boldsymbol{R}) & \psi_b(\vec{q}_2;\boldsymbol{R}) & \ldots & \psi_b(\vec{q}_{N_{\mathrm{el}}};\boldsymbol{R}) \\ \vdots & \vdots & \ddots & \vdots \\ \psi_{N_{\mathrm{el}}}(\vec{q}_1;\boldsymbol{R}) & \psi_{N_{\mathrm{el}}}(\vec{q}_2;\boldsymbol{R}) & \ldots & \psi_{N_{\mathrm{el}}}(\vec{q}_{N_{\mathrm{el}}};\boldsymbol{R}) \end{vmatrix} \\ &\equiv \left|\psi_a\psi_b\ldots\psi_{N_{\mathrm{el}}}\right\rangle,\end{aligned} \tag{2.15}$$

which express the many-electron wave function as antisymmetrized products of spin orbitals. Here, the pre-determinant factor $\frac{1}{\sqrt{N_{\mathrm{el}}!}}$ ensures the normalization of the wave function. In the Hartree-Fock approximation, a single Slater determinant is used to model the total electronic wave function $\Psi_0^{\mathrm{HF}}\left(\boldsymbol{q};\boldsymbol{R}\right)$ of the ground state in the time-independent electronic Schrödinger equation, Eq. (2.6). In order to obtain the optimal Slater determinant, the variational principle is applied to determine the associated spin orbitals. This theorem states that the ground state energy $E_0(\boldsymbol{R})$ for any trial function

$\left|\tilde{\Psi}\right\rangle$ constitutes an upper bound to the exact expectation value of the electronic Hamiltonian[149]

$$\frac{\left\langle\tilde{\Psi}\middle|\hat{H}_{\mathrm{el}}(\boldsymbol{r};\boldsymbol{R})\middle|\tilde{\Psi}\right\rangle}{\left\langle\tilde{\Psi}\middle|\tilde{\Psi}\right\rangle} \geq \quad E_0(\boldsymbol{R}). \tag{2.16}$$

This means that an optimal set of orthonormal spin orbitals is sought yielding the minimum ground state energy.

Following the single Slater determinant wave function ansatz, a set of effective one-electron eigenvalue equations, the Hartree-Fock equations, can be derived

$$\hat{f}(\vec{r}_i;\boldsymbol{R})\,\psi_a^{\mathrm{HF}}(\vec{q}_i;\boldsymbol{R}) = \varepsilon_a^{\mathrm{HF}}(\boldsymbol{R})\,\psi_a^{\mathrm{HF}}(\vec{q}_i;\boldsymbol{R}). \tag{2.17}$$

In this formula, $\varepsilon_a^{\mathrm{HF}}(\boldsymbol{R})$ represents the orbital energy of the ath spin orbital, and $\hat{f}(\vec{r}_i;\boldsymbol{R})$ denotes the effective Hamiltonian of this one-electron eigenvalue equation

$$\hat{f}(\vec{r}_i;\boldsymbol{R}) = -\frac{\hbar^2}{2m_e}\nabla_{\vec{r}_i}^2 - \sum_A^{N_{\mathrm{nuc}}} \frac{Z_A e^2}{4\pi\epsilon_0\left|\vec{r}_i - \vec{R}_A\right|} + \hat{v}_{\mathrm{eff}}^{\mathrm{HF}}(\vec{r}_i;\boldsymbol{R}) \tag{2.18}$$

which is designated as the Fock operator. The first term of Eq. (2.18) signifies the electronic kinetic energy operator, and the second term stands for the electron-nuclear potential energy operator. Recalling the mean-field approximation, the last term $\hat{v}_{\mathrm{eff}}^{\mathrm{HF}}(\vec{r}_i;\boldsymbol{R})$ describes the potential experienced by one electron due to the presence of all other electrons.[149] It is composed of the classical Coulomb potential energy operator $\hat{J}_b(\vec{r}_i;\boldsymbol{R})$ and the non-classical exchange potential energy operator $\hat{K}_b(\vec{r}_i;\boldsymbol{R})$

$$\hat{v}_{\mathrm{eff}}^{\mathrm{HF}}(\vec{r}_i;\boldsymbol{R}) = \sum_b^{N_{\mathrm{el}}} \Big(\hat{J}_b(\vec{r}_i;\boldsymbol{R}) - \hat{K}_b(\vec{r}_i;\boldsymbol{R})\Big). \tag{2.19}$$

These two components acting on a spin orbital $\psi_a^{\mathrm{HF}}(\vec{q}_i;\boldsymbol{R})$ are defined as

$$\hat{J}_b(\vec{r}_i;\boldsymbol{R})\,\psi_a^{\mathrm{HF}}(\vec{q}_i;\boldsymbol{R}) = \left[\int \mathrm{d}\vec{q}_j\, \left(\psi_b^{\mathrm{HF}}(\vec{q}_j;\boldsymbol{R})\right)^\dagger \frac{e^2}{4\pi\epsilon_0\left|\vec{r}_i - \vec{r}_j\right|}\psi_b^{\mathrm{HF}}(\vec{q}_j;\boldsymbol{R})\right] \psi_a^{\mathrm{HF}}(\vec{q}_i;\boldsymbol{R}) \tag{2.20}$$

and

$$\hat{K}_b(\vec{r}_i;\boldsymbol{R})\,\psi_a^{\mathrm{HF}}(\vec{q}_i;\boldsymbol{R}) = \left[\int \mathrm{d}\vec{q}_j\, \left(\psi_b^{\mathrm{HF}}(\vec{q}_j;\boldsymbol{R})\right)^\dagger \frac{e^2}{4\pi\epsilon_0\left|\vec{r}_i - \vec{r}_j\right|}\psi_a^{\mathrm{HF}}(\vec{q}_j;\boldsymbol{R})\right] \psi_b^{\mathrm{HF}}(\vec{q}_i;\boldsymbol{R}). \tag{2.21}$$

In order to make the Hartree-Fock equations (cf. Eq. (2.17)) numerically solvable, Roothaan and Hall independently introduced an expansion of the spatial molecular orbitals into a set of known basis functions.[163,164] This MO-LCAO ansatz (Molecular Orbitals as Linear Combination of Atomic

Orbitals) expresses the spatial molecular orbitals as a linear combination of a finite set of atomic orbitals

$$\varphi_a(\vec{r}_i;\boldsymbol{R}) = \sum_{A}^{N_{\mathrm{nuc}}} \sum_{k_A}^{n_{\mathrm{AO}}(A)} C_{a,k_A}(\boldsymbol{R})\,\phi_{k_A}(\vec{r}_i - \vec{R}_A), \tag{2.22}$$

where $C_{a,k_A}(\boldsymbol{R})$ is the k_Ath molecular orbital coefficient of MO a, and $\left\{\phi_{k_A}(\vec{r}_i - \vec{R}_A)\right\}$ denote the $n_{\mathrm{AO}}(A)$ atomic orbitals centered at atom A. The application of this MO-LCAO ansatz leads to the Hartree-Fock-Roothaan-Hall matrix eigenvalue equation[163,164]

$$\boldsymbol{FC} = \boldsymbol{SC}\boldsymbol{\varepsilon} \tag{2.23}$$

with the Fock matrix $\boldsymbol{F}_{kk'} = \langle\phi_k|\hat{f}(\vec{r}_i;\boldsymbol{R})|\phi_{k'}\rangle$ expressed in the AO basis and the AO overlap matrix $\boldsymbol{S}_{kk'} = \langle\phi_k|\phi_{k'}\rangle$. Furthermore, the diagonal MO energy matrix $\boldsymbol{\varepsilon}$ contains the orbital energies $\boldsymbol{\varepsilon}_{aa} = \varepsilon_a$, and the matrix $\boldsymbol{C}$ comprises the molecular orbital expansion coefficients. In the sense of the variational method, the solution of this non-linear generalized eigenvalue equation yields the MO coefficients $\boldsymbol{C}$ that produce the lowest possible ground state energy within the single Slater determinant ansatz for a specific basis set. The N_{el} lowest spin orbitals, i.e., the occupied spin orbitals, contribute to this total molecular energy. The remaining orbitals are referred to as unoccupied or virtual spin orbitals.[149]

The major deficit of the Hartree-Fock method stems from the description of the molecular wave function with a single Slater determinant. Hence, electron interactions are solely treated in an average fashion. In consequence, the energy from Hartree-Fock calculations is always greater than the lowest possible ground state energy in a given basis. The difference between the Hartree-Fock energy and the exact energy is defined as the correlation energy. In order to properly include electron correlation effects, many post-Hartree-Fock methods have been developed to approach the exact ground state and to access excited electronic states.

2.3.2 The Configuration Interaction Method

The most straightforward extension to the Hartree-Fock ansatz is the Configuration Interaction (CI) method.[149,150,156] In this framework, the exact electronic wave function of an N_{el}-electron system for an electronic state λ is expressed as a linear combination of all possible Slater determinants for a given set of spin orbitals

$$|\Psi_\lambda^{\mathrm{CI}}\rangle = \sum_p D_{p,\lambda}|\Psi_p\rangle. \tag{2.24}$$

Here, $|\Psi_p\rangle$ denote the orthonormal Slater determinants formed from the complete basis of spin orbitals, and $D_{p,\lambda}$ are the linear expansion coefficients. The latter are determined by variational optimization

solving the secular equation

$$\boldsymbol{HD} = \boldsymbol{DE}, \tag{2.25}$$

where $\boldsymbol{D}$ is the coefficient matrix, the diagonal energy matrix $\boldsymbol{E}$ comprises the electronic energies E_λ^{CI}, and the elements of the Hamiltonian matrix $\boldsymbol{H}$ are defined as

$$\boldsymbol{H}_{pq} = \left\langle \Psi_p \middle| \hat{H}_{\mathrm{el}}(\boldsymbol{r};\boldsymbol{R}) \middle| \Psi_q \right\rangle . \tag{2.26}$$

Since these matrix elements $\boldsymbol{H}_{pq}$ can be expressed in terms of one- and two-electron integrals, the Slater-Condon rules can be employed to reduce the number of non-zero elements.[165–167] The only non-vanishing matrix elements exist between two Slater determinants, which are identical or differ by one or two spin orbitals.

In general, the different Slater determinants are constructed by excitations of spin orbitals from a single reference $\left|\Psi_0\right\rangle$, usually the Hartree-Fock determinant. That means that n electrons have been promoted from occupied $\{a, b, \dots\}$ to virtual $\{r, s, \dots\}$ spin orbitals in the reference determinant to form singly, doubly, etc., excited determinants $\left|\Psi_{ab\dots}^{rs\cdots}\right\rangle$. Accordingly, the CI electronic wave function can be reformulated as

$$\left|\Psi_\lambda^{\mathrm{CI}}\right\rangle = D_{0,\lambda}\left|\Psi_0\right\rangle + \left(\frac{1}{1!}\right)^2 \sum_{ar} D_{a,\lambda}^{r}\left|\Psi_a^r\right\rangle + \left(\frac{1}{2!}\right)^2 \sum_{abrs} D_{ab,\lambda}^{rs}\left|\Psi_{ab}^{rs}\right\rangle + \dots . \tag{2.27}$$

Alternatively to the description in the basis of Slater determinants, Configuration State Functions (CSF) can be used to expand the CI wave function (cf. Eq. (2.24)). These CSFs are symmetry-adapted linear combinations of Slater determinants and eigenfunctions of the spin angular momentum operator. Taking advantage of the spin symmetry or molecular symmetry, this ansatz reduces the number of non-zero CI matrix elements (cf. Eq. (2.25)).[149]

The CI wave function expansion (cf. Eq. (2.27)) including all possible Slater determinants is known as the Full CI ansatz and corresponds to the exact solution of the time-independent Schrödinger equation (cf. Eq. (2.6)) within the limit of the given one-electron basis set and the Born-Oppenheimer approximation. However, as the number of determinants grows factorially with the number of electrons and basis functions, the computational expense for this exact ansatz is only tractable for very small systems. In order to reduce the number of excited determinants, two main strategies have been developed. The first is based on the truncation of the CI expansion (cf. Eq. (2.27)) to a certain level of excitation, for example, singly (S) or doubly (D) excited determinants with respect to the reference. This leads to the two commonly used variants, the CIS and CISD scheme.[168] While the doubly excited determinants mainly contribute to the correction of the ground state energy, the singly excited deter-

minants do not affect the ground state according to the Brillouin theorem.[149] The second strategy restricts the number of active electrons in a specified number of active orbitals, i.e., the active space. Both strategies are combined in the Restricted Active Space CI (RASCI) scheme.[169] An unfavorable consequence of these truncation strategies is the loss of size consistency and size extensivity.

Up to this point, the CI wave function is expanded on the basis of a single Hartree-Fock determinant which is assumed to provide a physically meaningful description of the electronic structure. This ansatz is no longer an adequate description for conical intersections or bond forming or breaking situations. In such cases, the Multi-Configuration Self-Consistent Field (MCSCF) method[170] is used to generate a qualitatively correct description. Within this method, the orbital coefficients and the CI coefficients are simultaneously optimized for a certain set of active orbitals, while the orbitals outside the active space remain unchanged. The MCSCF approach can be performed for a single state or in a state-averaged fashion to receive a set of orbitals that optimally characterize the selected states. Including all determinants generated by allocating the active electrons to the selected active space leads to the popular Complete Active Space Self-Consistent Field (CASSCF) approach.[171–173] In order to truncate this ansatz and thus to avoid a large number of unnecessary highly excited configurations, the CASSCF method can be additionally restricted to a certain excitation rank (RASSCF).[150,169] In these MCSCF approaches, the different treatment of the active and inactive orbitals results in an imbalanced description of the configuration space. This drawback can be compensated with the Multi-Reference CI (MRCI) ansatz[174,175], which is generally based on the usual CI wave function expansion (cf. Eq. (2.27)) but with an MCSCF wave function as reference.

All these CI variants can provide very accurate descriptions of the electronic structure for the ground state and the excited states. However, the number of relevant configurations for a proper characterization can readily become unmanageable large. This makes them only tractable for moderately sized molecular systems.

2.3.3 The Density Functional Theory

Density Functional Theory (DFT) represents an alternative approach to the wave function-based electronic structure methods for solving the time-independent Schrödinger equation (cf. Eq. (2.6)) of an N_{el}-electron system.[150,155,176–179] While the post-Hartree-Fock methods presented above are based on $4N_{\mathrm{el}}$ dimensional (three spatial and one spin coordinate for each electron) wave functions, DFT determines the electronic structure of an N_{el}-electron system by means of the ground state one-electron density. The latter is defined as the absolute square of the electronic wave function integrated over all

electronic coordinates except one and additionally integrated over the remaining spin coordinate

$$\rho_0(\vec{r};\boldsymbol{R}) = N_{\mathrm{el}} \int \mathrm{d}\theta \int \mathrm{d}\vec{q}_2 \ldots \int \mathrm{d}\vec{q}_{N_{\mathrm{el}}} \left|\Psi_0(\vec{r},\theta,\vec{r}_2,\theta_2,\ldots,\vec{r}_{N_{\mathrm{el}}},\theta_{N_{\mathrm{el}}};\boldsymbol{R})\right|^2. \tag{2.28}$$

Here, the indices of the remaining spatial coordinate $\vec{r}$, which is also denoted as the observation point, and the spin coordinate are omitted in consequence of the indistinguishability of the electrons. In Eq. (2.28), the electron density is normalized to the electron number

$$\int \mathrm{d}\vec{r}\rho_0(\vec{r};\boldsymbol{R}) = N_{\mathrm{el}} \tag{2.29}$$

and has the interpretation that $\rho_0(\vec{r};\boldsymbol{R})\mathrm{d}\vec{r}$ specifies the probability of finding any of the N_{el} electrons in the volume element $\mathrm{d}\vec{r}$ irrespective of its spin. Thus, it depends solely on three spatial coordinates, independently of the system size. This drastic reduction of the dimensionality in comparison to the wave function-based methods results in a favorable computational scaling.

The theoretical basis for the DFT method relies on the two Hohenberg-Kohn theorems.[180] The first theorem, known as the existence theorem, proves that the exact electronic energy of a non-degenerate ground state is completely characterized by the one-electron ground state density. Hence, there exists a functional $E_0\big[\rho_0\big]$, which uniquely connects the exact ground state energy with the corresponding exact electron density. The second theorem states that this functional depending on any trial electron density $\tilde{\rho}_0(\vec{r};\boldsymbol{R})$ satisfies the variational principle

$$E_0 \leq E_0\big[\tilde{\rho}_0\big], \tag{2.30}$$

i.e., the ground state energy is minimized by the exact ground state electron density. Unfortunately, the exact mathematical form of this universal functional and thus the exact ground state energy are not known.

The first seminal concept to practically realize DFT was introduced by Kohn and Sham.[181] They suggested a mapping of the true system consisting of N_{el} interacting electrons onto an equivalent reference system of non-interacting electrons moving in an effective potential. This fictitious system is exactly described by a single Slater determinant (cf. Eq. (2.15)), which is formed by a set of one-electron basis functions, the Kohn-Sham (KS) orbitals $\big\{\psi_a^{\mathrm{KS}}(\vec{r},\theta;\boldsymbol{R})\big\}$. These can be constructed in analogy to the MO-LCAO ansatz (cf. Eq. (2.22)). The associated non-interacting one-electron density reads

$$\rho_0^{\mathrm{KS}}(\vec{r};\boldsymbol{R}) = \sum_a^{N_{\mathrm{el}}} \int \mathrm{d}\theta \left|\psi_a^{\mathrm{KS}}(\vec{r},\theta;\boldsymbol{R})\right|^2 \stackrel{!}{=} \rho_0(\vec{r};\boldsymbol{R}) \tag{2.31}$$

and is identical to the electron density of the real interacting system $\rho_0(\vec{r};\boldsymbol{R})$. In the framework of this Kohn-Sham DFT ansatz, an expression for the ground state energy as a functional of the one-electron density can be formulated

$$E_0\left[\rho_0^{\mathrm{KS}}\right] = T_{\mathrm{S}}^{\mathrm{KS}}\left[\rho_0^{\mathrm{KS}}\right] + V_{\text{el-nuc}}\left[\rho_0^{\mathrm{KS}}\right] + J\left[\rho_0^{\mathrm{KS}}\right] + E_{\mathrm{XC}}\left[\rho_0^{\mathrm{KS}}\right] + V_{\text{nuc-nuc}}, \tag{2.32}$$

where the functional for the nuclear-nuclear repulsion $V_{\text{nuc-nuc}}$ remains constant according to the Born-Oppenheimer approximation. In Eq. (2.32), the first term is the functional for the exact kinetic energy of the non-interacting system, which can be expressed in terms of the Kohn-Sham orbitals

$$T_{\mathrm{S}}^{\mathrm{KS}}\left[\rho_0^{\mathrm{KS}}\right] = -\frac{\hbar^2}{2m_e}\sum_a^{N_{\mathrm{el}}}\left\langle\psi_a^{\mathrm{KS}}\middle|\nabla_{\vec{r}}^2\middle|\psi_a^{\mathrm{KS}}\right\rangle. \tag{2.33}$$

The second and third term signify the functionals for the electron-nuclei interaction $V_{\text{el-nuc}}\left[\rho_0^{\mathrm{KS}}\right]$

$$V_{\text{el-nuc}}\left[\rho_0^{\mathrm{KS}}\right] = -\sum_A^{N_{\mathrm{nuc}}}\int \mathrm{d}\vec{r}\,\frac{Z_A e^2}{4\pi\epsilon_0\left|\vec{r}-\vec{R}_A\right|}\rho_0^{\mathrm{KS}}(\vec{r};\boldsymbol{R}) \tag{2.34}$$

and for the Coulomb repulsion $J\left[\rho_0^{\mathrm{KS}}\right]$

$$J\left[\rho_0^{\mathrm{KS}}\right] = \frac{1}{2}\iint \mathrm{d}\vec{r}\,\mathrm{d}\vec{r}\,'\,\frac{e^2}{4\pi\epsilon_0\left|\vec{r}-\vec{r}\,'\right|}\rho_0^{\mathrm{KS}}(\vec{r};\boldsymbol{R})\rho_0^{\mathrm{KS}}(\vec{r}\,';\boldsymbol{R}). \tag{2.35}$$

The latter is also referred to as the Hartree term and describes the self-interaction of the electron cloud. The remaining functional in Eq. (2.32) stands for the exchange-correlation energy functional $E_{\mathrm{XC}}\left[\rho_0^{\mathrm{KS}}\right]$, which is the only unknown quantity within the Kohn-Sham DFT approach.[177,179] It includes the lacking contributions for the kinetic correlation energy and for the electronic exchange and correlation energy

$$E_{\mathrm{XC}}\left[\rho_0^{\mathrm{KS}}\right] = \left(T\left[\rho_0^{\mathrm{KS}}\right] - T_{\mathrm{S}}^{\mathrm{KS}}\left[\rho_0^{\mathrm{KS}}\right]\right) + \left(V_{\text{el-el}}\left[\rho_0^{\mathrm{KS}}\right] - J\left[\rho_0^{\mathrm{KS}}\right]\right). \tag{2.36}$$

The practical calculation of the electron density is accomplished by applying the variational principle, whose validity is assured by the second Hohenberg-Kohn theorem. Here, the electronic energy is minimized by varying the orthonormal Kohn-Sham orbitals $\left|\psi_a^{\mathrm{KS}}\right\rangle$ which build the electron density (cf. Eq (2.31)). These one-electron functions and the respective orbital energies $\varepsilon_a^{\mathrm{KS}}(\boldsymbol{R})$ are variationally obtained by solving the single-particle Kohn-Sham equations

$$\left(-\frac{\hbar^2}{2m_e}\nabla_{\vec{r}}^2 + \hat{v}_{\mathrm{eff}}^{\mathrm{KS}}(\vec{r};\boldsymbol{R})\right)\left|\psi_a^{\mathrm{KS}}\right\rangle = \varepsilon_a^{\mathrm{KS}}(\boldsymbol{R})\left|\psi_a^{\mathrm{KS}}\right\rangle. \tag{2.37}$$

As stated above, the electrons are subject to the effective potential, which is defined as[155,176]

$$\hat{v}_{\text{eff}}^{\text{KS}}(\vec{r};\boldsymbol{R}) = -\sum_{A}^{N_{\text{nuc}}} \frac{Z_A e^2}{4\pi\epsilon_0 \left|\vec{r}-\vec{R}_A\right|} + \int \mathrm{d}\vec{r}\,' \, \frac{e^2 \rho_0^{\text{KS}}(\vec{r}\,';\boldsymbol{R})}{4\pi\epsilon_0 \left|\vec{r}-\vec{r}\,'\right|} + \hat{v}_{\text{XC}}(\vec{r};\boldsymbol{R}). \tag{2.38}$$

The last term, the exchange-correlation potential $\hat{v}_{\text{XC}}(\vec{r};\boldsymbol{R})$, is given by the derivative of the exchange-correlation functional E_{XC} with respect to the electron density $\rho_0^{\text{KS}}(\vec{r};\boldsymbol{R})$

$$\hat{v}_{\text{XC}}(\vec{r};\boldsymbol{R}) = \frac{\delta E_{\text{XC}}\left[\rho_0^{\text{KS}}\right]}{\delta \rho_0^{\text{KS}}(\vec{r};\boldsymbol{R})}. \tag{2.39}$$

Apart from this exchange-correlation potential, the Kohn-Sham equations closely resemble the Hartree-Fock equations (cf. Eq. (2.17)), i.e., reducing the N_{el}-electron problem to N_{el} one-electron problems. However, it is important to emphasize that the Hartree-Fock method is an approximation by definition. The underlying ansatz expressing the electronic wave function by a single Slater determinant causes a deficient description of electronic correlations. In contrast, the Kohn-Sham equations are formally exact under the condition that the exact expression of E_{XC} is known.[150,177,179] Unfortunately, an analytical form is not accessible from the Hohenberg-Kohn theorems. Thus, approximate expressions for E_{XC} are indispensable for the practical implementation of DFT, and their development turns out to be the main challenge in modern DFT. A plethora of non-empirical and semi-empirical density functionals with different levels of accuracy has emerged in the last three decades.[179] The major difficulty concerning this functional development is that the density functionals are not systematically improvable. However, a hierarchy of approximations for E_{XC}, called the Jacob's ladder[182], exists to rank the quality of the functionals.

The simplest approximation occupying the first rung of the ladder is the Local Density Approximation (LDA) which forms the basis for most approximate functionals. The central idea of LDA is the assumption that the inhomogeneous electron density can be locally treated as a homogeneous electron gas. This is a reasonable approximation for a slowly varying electron density. The associated exchange-correlation functional can be written as

$$E_{\text{XC}}^{\text{LDA}}\left[\rho_0^{\text{KS}}\right] = \int \mathrm{d}\vec{r}\; \rho_0^{\text{KS}}(\vec{r};\boldsymbol{R}) \varepsilon_{\text{XC}}^{\text{LDA}}\left[\rho_0^{\text{KS}}\right] \tag{2.40}$$

with $\varepsilon_{\text{XC}}^{\text{LDA}}$ as the exchange-correlation energy of the homogeneous electron gas. This quantity can be divided into an exchange and a correlation contribution

$$\varepsilon_{\text{XC}}^{\text{LDA}}\left[\rho_0^{\text{KS}}\right] = \varepsilon_{\text{X}}^{\text{LDA}}\left[\rho_0^{\text{KS}}\right] + \varepsilon_{\text{C}}^{\text{LDA}}\left[\rho_0^{\text{KS}}\right], \tag{2.41}$$

where the exchange term is analytically solvable,[183–185] and the correlation term is derived from highly accurate quantum Monte-Carlo simulations.[186–189] These functionals tend to perform surprisingly well, especially, in describing extended homogeneous systems, such as metal solids. However, they yield highly inaccurate results for most molecular systems, since they usually have highly inhomogeneous density distributions.[177,179] In order to take care of this inhomogeneity, the functional form depending solely on the information of the density $\rho_0^{\mathrm{KS}}(\vec{r};\boldsymbol{R})$ at a particular point can be supplemented by the information about the gradient $\vec{\nabla}\rho_0^{\mathrm{KS}}(\vec{r};\boldsymbol{R})$ of the density. This is taken into account in the Generalized Gradient Approximation (GGA) functionals, whose general form is given by

$$E_{\mathrm{XC}}^{\mathrm{GGA}}\left[\rho_0^{\mathrm{KS}}\right] = \int \mathrm{d}\vec{r}\; \rho_0^{\mathrm{KS}}(\vec{r};\boldsymbol{R})\varepsilon_{\mathrm{XC}}^{\mathrm{GGA}}\left[\rho_0^{\mathrm{KS}}, \vec{\nabla}\rho_0^{\mathrm{KS}}\right]. \tag{2.42}$$

Different flavors of these gradient-corrected correlation-energy functionals have been introduced in prior research. The most popular examples are PW91[190] and PBE[191] functionals. In order to further improve the flexibility of the GGA functionals, the Laplacian of the density $\nabla^2\rho_0^{\mathrm{KS}}(\vec{r};\boldsymbol{R})$ or the kinetic energy density can be incorporated as an additional ingredient. This leads to the meta-GGA functionals.[177,179]

Apart from improving the systematic error of the LDA by adding physically meaningful components, both, GGA and meta-GGA functionals, struggle in properly characterizing long-range dynamic correlations, strong correlations, and the self-interaction of the electrons.[179] A possible solution for the latter is to include a fraction of the exact exchange functional $K^{\mathrm{HF}}\left[\{\psi_a^{\mathrm{KS}}\}\right]$, which is determined within the Hartree-Fock formalism using Kohn-Sham orbitals. These functionals are referred to as hybrid functionals[192] and have the general form

$$E_{\mathrm{XC}}^{\mathrm{hybrid}}\left[\rho_0^{\mathrm{KS}}\right] = \varpi\left(K^{\mathrm{HF}}\left[\{\psi_a^{\mathrm{KS}}\}\right] - E_{\mathrm{X}}^{\mathrm{LDA/GGA}}\left[\rho_0^{\mathrm{KS}}, \vec{\nabla}\rho_0^{\mathrm{KS}}\right]\right) + E_{\mathrm{XC}}^{\mathrm{LDA/GGA}}\left[\rho_0^{\mathrm{KS}}\right]. \tag{2.43}$$

The B3LYP[193,194] and PBE0[195] functional are the two most popular and widely used global hybrid functionals yielding remarkably reliable results for a broad range of chemical and physical ground state properties. Although the computational cost of density functionals increases climbing up the Jacob's ladder, DFT is much less expensive compared to the wave function-based methods. This renders DFT more suitable for the characterization of large quantum systems.

A weakness of all functional approximations presented above is the inadequate description of long-range electron correlations, known as dispersion. A way to account for those is the semi-empirical dispersion correction by Grimme (DFT-D)[196–198], which employs damped, pairwise potentials as an

additive term to the functionals. The corresponding attractive energy term is defined as

$$E_{\text{disp}}^{\text{DFT-D}} = \sum_{A=1}^{N_{\text{nuc}}} \sum_{B>A}^{N_{\text{nuc}}} \sum_{v=6,8,\ldots} h_v \frac{G_{AB,v}}{\left|\vec{R}_A - \vec{R}_B\right|^v} f_v^{\text{damp}}(R_{AB}), \tag{2.44}$$

where $f_v^{\text{damp}}(R_{AB})$ is the empirical damping function, $G_{AB,v}$ signifies an atom-dependent parameter, and h_v denotes a functional-depending scaling factor.

2.3.4 The Time-Dependent Density Functional Theory

The most widely used extension of the ground state density functional theory is the Linear Response Time-Dependent DFT (LR-TDDFT), which allows for the calculation of excited state properties, such as transition energies, oscillator strengths, or photoabsorption spectra. The following presentation of the TDDFT method is mainly based on the Refs. [199–204].

In analogy to ordinary DFT, the basic idea of TDDFT relies on solving the time-dependent Schrödinger equation (cf. Eq. (2.1)) for an N_{el}-electron system in terms of the time-dependent electron density, i.e., the derivation of a time-dependent variant of the KS equations (cf. Eq. (2.37)). The theory is based on two fundamental theorems, the Runge-Gross theorem[205] and the van Leeuwen theorem[206]. The former can be seen as the time-dependent analogue of the Hohenberg-Kohn theorem[180]. For the time evolution of a many-body system from a fixed initial state, it proves that there exists a one-to-one correspondence between the time-dependent one-electron density and the time-dependent potential. This implies that the potential and all quantum mechanical observables can be written as a functional depending on the time-dependent electron density and the initial state. Accordingly, the important question arises whether the exact time-dependent electron density of the fully interacting system can be reproduced by an auxiliary non-interacting system, which is subject to a time-dependent effective potential. This is justified by the van Leeuwen theorem (non-interacting v-representability). Hence, the corresponding time-dependent KS electron density can be constructed in terms of the time-dependent KS (TDKS) orbitals

$$\rho^{\text{TDKS}}(\vec{r}, t; \boldsymbol{R}) = \sum_{a}^{N_{\text{el}}} \int \mathrm{d}\theta \left|\psi_a^{\text{TDKS}}(\vec{r}, \theta, t; \boldsymbol{R})\right|^2. \tag{2.45}$$

As a result from the existence of a unique effective singe-particle potential $\hat{v}_{\text{eff}}^{\text{TDKS}}(\vec{r}, t; \boldsymbol{R})$ yielding this density, the time-dependent Kohn-Sham equations for the fictitious system of non-interacting electrons can be formulated

$$\imath\hbar \frac{\partial}{\partial t} \left|\psi_a^{\text{TDKS}}\right\rangle = \left(-\frac{\hbar^2}{2m_e} \nabla_{\vec{r}}^2 + \hat{v}_{\text{eff}}^{\text{TDKS}}(\vec{r}, t; \boldsymbol{R}) \right) \left|\psi_a^{\text{TDKS}}\right\rangle \tag{2.46}$$

with the time-dependent effective potential

$$\hat{v}_{\mathrm{eff}}^{\mathrm{TDKS}}(\vec{r},t;\boldsymbol{R}) = \hat{v}_{\mathrm{ext}}(\vec{r},t;\boldsymbol{R}) + \int \mathrm{d}\vec{r}\,' \; \frac{e^2\rho^{\mathrm{TDKS}}(\vec{r}\,',t;\boldsymbol{R})}{4\pi\epsilon_0\left|\vec{r}-\vec{r}\,'\right|} + \hat{v}_{\mathrm{XC}}(\vec{r},t;\boldsymbol{R}). \tag{2.47}$$

Here, $\hat{v}_{\mathrm{ext}}(\vec{r},t;\boldsymbol{R})$ is the time-dependent external potential, and $\hat{v}_{\mathrm{XC}}(\vec{r},t;\boldsymbol{R})$ denotes the exchange-correlation potential, which is history-dependent. In correspondence with ground state DFT, this time-dependent Kohn-Sham formalism is in principle an exact description. Nevertheless, some approximations have to be introduced to simplify the functional form of the unknown exchange-correlation potential $\hat{v}_{\mathrm{XC}}(\vec{r},t;\boldsymbol{R})$. In order to reduce its functional dependence, it is assumed that the quantum system starts initially from a non-degenerate ground state

$$\psi_a^{\mathrm{TDKS}}(\vec{r},\theta,t=t_0;\boldsymbol{R}) = \psi_a^{\mathrm{KS}}(\vec{r},\theta;\boldsymbol{R}). \tag{2.48}$$

This neglects the initial-state dependence of $\hat{v}_{\mathrm{XC}}(\vec{r},t;\boldsymbol{R})$. However, it still depends on the density at every point in space and at all previous times. The basic approximation to bypass this history dependence is the adiabatic approximation

$$\hat{v}_{\mathrm{XC}}\left[\rho^{\mathrm{TDKS}}\right](\vec{r},t;\boldsymbol{R}) = \hat{v}_{\mathrm{XC}}\left[\rho^{\mathrm{TDKS}}(t)\right](\vec{r};\boldsymbol{R}), \tag{2.49}$$

where $\hat{v}_{\mathrm{XC}}(\vec{r},t;\boldsymbol{R})$ is specified by means of the static exchange-correlation functional at the time-dependent instantaneous density. This local time-dependence of $\hat{v}_{\mathrm{XC}}(\vec{r},t;\boldsymbol{R})$ is justified for a slowly varying density, where the system remains in its instantaneous ground state.

The Linear Response Time-Dependent Density Functional Theory

The complete solution of the time-dependent KS equations tends to be a computationally highly demanding task and is often not required, for instance, to extract the excitation spectrum of a quantum system. For small perturbations causing solely a small deviation of the system from its initial state, the linear response theory can be used to access a first-order perturbative solution to the TDKS equations.[199–204] In general response theory, this weak perturbation is generated by an external stimulus $\hat{v}(\vec{r},t;\boldsymbol{R})$, e.g., a weak electric field,

$$\begin{aligned}\hat{v}_{\mathrm{ext}}(\vec{r},t;\boldsymbol{R}) &= \hat{v}_0(\vec{r};\boldsymbol{R}) + \vartheta(t-t_0)\hat{v}(\vec{r},t;\boldsymbol{R}) \\ &= -\sum_A^{N_{\mathrm{nuc}}} \frac{Z_A e^2}{4\pi\epsilon_0\left|\vec{r}-\vec{R}_A\right|} + \vartheta(t-t_0)\hat{v}(\vec{r},t;\boldsymbol{R})\end{aligned} \tag{2.50}$$

which is turned on at time t_0 by a Heaviside step function $\vartheta(t-t_0)$. Here, $\hat{v}_0(\vec{r};\boldsymbol{R})$ is the external

potential of the unperturbed system in its ground state. The response of the system due to the perturbation $\hat{v}(\vec{r},t;\boldsymbol{R})$ is represented by the time-dependent density response, which can be expressed as a functional Taylor series[207]

$$\rho(\vec{r},t;\boldsymbol{R})-\rho_0(\vec{r};\boldsymbol{R})=\rho^{(1)}(\vec{r},t;\boldsymbol{R})+\rho^{(2)}(\vec{r},t;\boldsymbol{R})+\rho^{(3)}(\vec{r},t;\boldsymbol{R})+\ldots, \tag{2.51}$$

where the superscripts in parenthesis denote the order of the expansion, and $\rho_0(\vec{r};\boldsymbol{R})$ is the unperturbed ground state density of the interacting system. In the linear response regime, the first term on the right side of Eq. (2.51), $\rho^{(1)}(\vec{r},t;\boldsymbol{R})$, is sufficient to describe the density response to small changes in the external potential $\hat{v}_{\text{ext}}(\vec{r},t;\boldsymbol{R})$

$$\rho^{(1)}(\vec{r},t;\boldsymbol{R})=\iint \mathrm{d}t'\,\mathrm{d}\vec{r}'\;\boldsymbol{\chi}(\vec{r},t,\vec{r}',t';\boldsymbol{R})\,\hat{v}(\vec{r}',t';\boldsymbol{R}) \tag{2.52}$$

with the density-density response function of the fully interacting system defined as

$$\boldsymbol{\chi}(\vec{r},t,\vec{r}',t';\boldsymbol{R})=\left.\frac{\delta\rho[\hat{v}_{\text{ext}}](\vec{r},t;\boldsymbol{R})}{\delta\,\hat{v}_{\text{ext}}(\vec{r}',t';\boldsymbol{R})}\right|_{\hat{v}_0(\vec{r};\boldsymbol{R})}. \tag{2.53}$$

Exploiting the KS formalism, the linear density response function can be expressed in terms of the non-interacting system subject to the linear variation of the effective KS potential

$$\rho^{(1)}(\vec{r},t;\boldsymbol{R})=\iint \mathrm{d}t'\,\mathrm{d}\vec{r}'\;\boldsymbol{\chi}_{\text{eff}}(\vec{r},t,\vec{r}',t';\boldsymbol{R})\,\hat{v}_{\text{eff}}^{(1)\text{TDKS}}(\vec{r}',t';\boldsymbol{R}). \tag{2.54}$$

The associated linearized effective potential $\hat{v}_{\text{eff}}^{(1)\text{TDKS}}(\vec{r}',t';\boldsymbol{R})$ includes contributions for the external perturbation, the Hartree potential, and the exchange-correlation potential

$$\hat{v}_{\text{eff}}^{(1)\text{TDKS}}(\vec{r}',t';\boldsymbol{R})=\hat{v}(\vec{r}',t';\boldsymbol{R})+\iint \mathrm{d}t''\mathrm{d}\vec{r}''\frac{e^2\delta(t'-t'')\rho^{(1)}(\vec{r}'',t'';\boldsymbol{R})}{4\pi\epsilon_0\left|\vec{r}'-\vec{r}''\right|}+\hat{v}_{\text{XC}}^{(1)}(\vec{r}',t';\boldsymbol{R}). \tag{2.55}$$

An expression for $\hat{v}_{\text{XC}}^{(1)}(\vec{r}',t';\boldsymbol{R})$ can be obtained by applying the chain-rule for functional derivatives

$$\hat{v}_{\text{XC}}^{(1)}(\vec{r}',t';\boldsymbol{R})=\iint \mathrm{d}t''\,\mathrm{d}\vec{r}''\;\hat{f}_{\text{XC}}(\vec{r}',t',\vec{r}'',t'';\boldsymbol{R})\,\rho^{(1)}(\vec{r}'',t'';\boldsymbol{R}). \tag{2.56}$$

Eq. (2.56) introduces the time-dependent exchange-correlation kernel

$$\hat{f}_{\text{XC}}(\vec{r}',t',\vec{r}'',t'';\boldsymbol{R})=\left.\frac{\delta\,\hat{v}_{\text{XC}}^{(1)}[\rho](\vec{r}',t';\boldsymbol{R})}{\delta\rho(\vec{r}'',t'';\boldsymbol{R})}\right|_{\rho_0(\vec{r}';\boldsymbol{R})}, \tag{2.57}$$

which is the functional derivative of the exchange-correlation potential with respect to the density. The

exchange-correlation kernel also becomes time-independent by virtue of the adiabatic approximation. As the time-dependent density response for the interacting and for the non-interacting system have to be identical, equating the corresponding equations, Eq. (2.52) and Eq. (2.54), and inserting the expression for the linearized effective potential $\hat{v}_{\mathrm{eff}}^{(1)\mathrm{TDKS}}(\vec{r}\,',t';\boldsymbol{R})$ (cf. Eq. (2.55)) yields

$$\begin{aligned}\iint \mathrm{d}t'\,\mathrm{d}\vec{r}\,'\;\boldsymbol{\chi}(\vec{r},t,\vec{r}\,',t';\boldsymbol{R})\,\hat{v}(\vec{r}\,',t';\boldsymbol{R}) &= \iint \mathrm{d}t'\,\mathrm{d}\vec{r}\,'\;\boldsymbol{\chi}_{\mathrm{eff}}(\vec{r},t,\vec{r}\,',t';\boldsymbol{R})\,\hat{v}_{\mathrm{eff}}^{(1)\mathrm{TDKS}}(\vec{r}\,',t';\boldsymbol{R}) \\ &+ \iint \mathrm{d}t'\,\mathrm{d}\vec{r}\,'\;\boldsymbol{\chi}_{\mathrm{eff}}(\vec{r},t,\vec{r}\,',t';\boldsymbol{R}) \cdot \iint \mathrm{d}t''\,\mathrm{d}\vec{r}\,''\left[\frac{e^2\delta(t'-t'')}{4\pi\epsilon_0\left|\vec{r}\,'-\vec{r}\,''\right|} + \hat{f}_{\mathrm{XC}}(\vec{r}\,',t',\vec{r}\,'',t'';\boldsymbol{R})\right] \\ &\cdot \iint \mathrm{d}t'''\,\mathrm{d}\vec{r}\,'''\;\boldsymbol{\chi}_{\mathrm{eff}}(\vec{r}\,'',t'',\vec{r}\,''',t''';\boldsymbol{R})\,\hat{v}_{\mathrm{eff}}^{(1)\mathrm{TDKS}}(\vec{r}\,''',t''';\boldsymbol{R}).\end{aligned} \tag{2.58}$$

This relation holds independently for any arbitrary perturbation in the linear regime, since the density response function is an intrinsic ground state property. Thus, the connection between the interacting and non-interacting response function can be expressed by

$$\begin{aligned}\boldsymbol{\chi}(\vec{r},\vec{r}\,',\omega;\boldsymbol{R}) = \boldsymbol{\chi}_{\mathrm{eff}}(\vec{r},\vec{r}\,',\omega;\boldsymbol{R}) + \iint \mathrm{d}\vec{r}\,''\,\mathrm{d}\vec{r}\,'''\;\boldsymbol{\chi}(\vec{r},\vec{r}\,'',\omega;\boldsymbol{R}) \\ \cdot \left[\frac{e^2}{4\pi\epsilon_0\left|\vec{r}\,''-\vec{r}\,'''\right|} + \hat{f}_{\mathrm{XC}}(\vec{r}\,'',\vec{r}\,''',\omega;\boldsymbol{R})\right]\boldsymbol{\chi}_{\mathrm{eff}}(\vec{r}\,''',\vec{r}\,',\omega;\boldsymbol{R})\end{aligned} \tag{2.59}$$

which is a Dyson-type equation in the frequency space ω obtained from a Fourier transformation. This equation represents the formally correct expression for the density response of the fully interacting system. Incidentally, the neglect of the exchange-correlation kernel $\hat{f}_{\mathrm{XC}}$ leads to the random-phase approximation (RPA).[208,209] In Eq. (2.59), the frequency-dependent Kohn-Sham density-density response function can be formulated in terms of the static unperturbed Kohn-Sham orbitals

$$\boldsymbol{\chi}_{\mathrm{eff}}(\vec{r},\vec{r}\,',\omega;\boldsymbol{R}) = \lim_{\eta\to 0^+}\sum_{ar}\left[\frac{\rho_{ra}^{\mathrm{KS}}(\vec{r};\boldsymbol{R})\rho_{ar}^{\mathrm{KS}}(\vec{r}\,';\boldsymbol{R})}{\omega-\omega_{ar}^{\mathrm{KS}}+\imath\eta} - \frac{\rho_{ar}^{\mathrm{KS}}(\vec{r};\boldsymbol{R})\rho_{ra}^{\mathrm{KS}}(\vec{r}\,';\boldsymbol{R})}{\omega+\omega_{ar}^{\mathrm{KS}}+\imath\eta}\right]. \tag{2.60}$$

Here, the summation runs over the occupied $\{a,b,\dots\}$ and unoccupied orbitals $\{r,s,\dots\}$, whose transition density is defined as

$$\rho_{ar}^{\mathrm{KS}}(\vec{r};\boldsymbol{R}) = \int \mathrm{d}\theta\big(\psi_r^{\mathrm{KS}}(\vec{r},\theta;\boldsymbol{R})\big)^{\dagger}\psi_a^{\mathrm{KS}}(\vec{r},\theta;\boldsymbol{R}), \tag{2.61}$$

and their respective transition frequency is given by

$$\omega_{ar}^{\mathrm{KS}}(\boldsymbol{R}) = [\varepsilon_r^{\mathrm{KS}}(\boldsymbol{R}) - \varepsilon_a^{\mathrm{KS}}(\boldsymbol{R})]/\hbar. \tag{2.62}$$

From Eq. (2.60), it is apparent that there exist poles Ω for frequencies ω that match the Kohn-Sham

transition frequencies $\omega_{ar}^{\mathrm{KS}}(\boldsymbol{R})$. These resonant transitions correspond to the excitation energies of the system's electronically excited states, which, in principle, can be exactly calculated in the linear regime by means of a non-Hermitian eigenvalue equation. This is known as the Casida equation[210]

$$\begin{bmatrix} \boldsymbol{A} & \boldsymbol{B} \\ \boldsymbol{B}^{\star} & \boldsymbol{A}^{\star} \end{bmatrix} \begin{bmatrix} \boldsymbol{X}_{\lambda} \\ \boldsymbol{Y}_{\lambda} \end{bmatrix} = \Omega_{\lambda} \begin{bmatrix} \mathbf{1} & \mathbf{0} \\ \mathbf{0} & -\mathbf{1} \end{bmatrix} \begin{bmatrix} \boldsymbol{X}_{\lambda} \\ \boldsymbol{Y}_{\lambda} \end{bmatrix}. \tag{2.63}$$

Here, the matrix elements $\boldsymbol{A}$ and $\boldsymbol{B}$ are defined as

$$\begin{aligned} \boldsymbol{A}_{ra,bs}(\omega;\boldsymbol{R}) &= \omega_{ar}^{\mathrm{KS}}(\boldsymbol{R})\,\delta_{ab}\delta_{rs} + \boldsymbol{B}_{ar,bs}(\omega;\boldsymbol{R}), \\ \boldsymbol{B}_{ar,bs}(\omega;\boldsymbol{R}) &= \iint \mathrm{d}\vec{r}\,\mathrm{d}\vec{r}\,'\ \rho_{ra}^{\mathrm{KS}}(\vec{r};\boldsymbol{R}) \left[\frac{e^2}{4\pi\epsilon_0\left|\vec{r}-\vec{r}\,'\right|} + \hat{f}_{\mathrm{XC}}(\vec{r},\vec{r}\,',\omega;\boldsymbol{R})\right] \rho_{bs}^{\mathrm{KS}}(\vec{r}\,';\boldsymbol{R}), \end{aligned} \tag{2.64}$$

and $\boldsymbol{X}_{\lambda}$ and $\boldsymbol{Y}_{\lambda}$ are the response vectors for the excitation from an occupied orbital a to a virtual orbital r and for the de-excitation from a virtual orbital r to an occupied orbital a. A practically solvable formulation for the Casida equation emerges under the condition of real-valued Kohn-Sham orbitals and a frequency-independent exchange-correlation kernel. Its solution does not only provide the excitation energies but also the associated oscillator strengths. The elimination of the de-excitation processes can be achieved by setting the off-diagonal elements $\boldsymbol{B}$ to zero. This is known as the Tamm-Dancoff approximation (TDA)[211]

$$\boldsymbol{A}\boldsymbol{X}_{\lambda} = \Omega_{\lambda}\boldsymbol{X}_{\lambda} \tag{2.65}$$

and coincides with the configuration interaction singles (CIS) formalism. Consequently, a CIS-type wave function can be uniquely defined for each excited state within the TDA approach.

2.3.5 Solvation Models

Within the electronic structure methods presented so far, the molecular properties are characterized for the isolated system in the gas phase. However, environmental effects, such as the influence of a solvent, can cause changes in energy, stability, or molecular structure. To evaluate solvent effects, two main approaches are applied: the supermolecule approach explicitly treating the individual solvent molecules, which interact with the system, and the dielectric continuum solvation model describing the solvent as a continuous entity. As computational cost of the former model can grow prohibitively high, the second model is most commonly used in current computational chemistry and presented in the following section.[150,212,213] Within its framework, the solvent is considered as a uniform polarizable medium characterized by its macroscopic properties, i.e., the dielectric constant, and the solute occupies an appropriately shaped cavity in this continuous medium. The free energy, which emerges from the

introduction of the solute in the solvent and their interaction, is known as the solvation energy. It can be divided into three essential components: the energy required to create the cavity, the dispersion interaction energy between the solute and the solvent, and the electrostatic energy resulting from the polarization of the solvent by the electric charge distribution of the solute. Obviously, the size and shape of the cavity, which should ideally match the molecular charge distribution, are fundamental parameters to evaluate the solvation energy. Both parameters define the Solvent Accessible Surface (SAS), which is usually constructed by interlocking spheres centered on different nuclei. These overlapping spheres have scaled van der Waals atomic radii, and their surface, the SAS, is often additionally smoothed for a more adequate description. This concept of molecular-shaped cavities is employed in the popular Polarizable Continuum Model (PCM)[214] and the COnductor-like Screening MOdel (COSMO)[215–219]. Both methods can be applied to quantum chemical calculations of various electronic structure methods.

2.3.6 Basis Set

Within the aforementioned molecular electronic structure methods, the molecular electronic wave function is expressed in terms of Slater determinants, which are formed by antisymmetric products of molecular orbitals. According to the MO-LCAO ansatz (cf. Eq. (2.22)), these spatial molecular orbitals are constructed by linear combinations of a finite set of real-valued basis functions, the atomic orbitals. This set of functions is referred to as the basis set.[149] For molecular systems, the most widely used functional form for the atomic basis functions is the atom-centered Gaussian-type orbital.[220] In Cartesian coordinates, a primitive Cartesian Gaussian function is given by

$$\phi^{\mathrm{GTO}}_{\upsilon,l_x l_y l_z}(\vec{r}) = N x^{l_x} y^{l_y} z^{l_z} \exp\left(-\upsilon r^2\right), \tag{2.66}$$

where N stands for the normalization constant, x, y, and z are the Cartesian coordinates, υ labels the orbital exponent, and $r = \sqrt{x^2 + y^2 + z^2}$ denotes the radius of the function. The sum of the exponents l_x, l_y, and l_z determines the type of the orbital. These primitive Gaussian functions are very convenient from a computational viewpoint, since analytical solutions for their integrals are available, and the product of any number of Gaussian functions can be simplified by employing the Gaussian product rule. Both vastly accelerate the evaluation of numerous expectation values. This is the reason for the r^2-dependence in the exponential, although a r-dependence provides a better description of the atomic orbitals. Two issues arise from this r^2-dependence: A zero slope at the nucleus instead of a cusp and a too rapid decay for larger values of r that cause a poor representation of the radial shape of the electronic wave function.[149] In order to compensate for this behavior, the atomic basis functions are modeled by linear combinations of numerous primitive Gaussian functions yielding the contracted

Gaussian type functions

$$\phi_{k_A}^{\mathrm{cGTO}}(\vec{r}-\vec{R}_A)=\sum_{f}^{N_{\mathrm{basis}}} c_f \phi_{\upsilon_f,l_x l_y l_z}^{\mathrm{GTO}}(\vec{r}-\vec{R}_A). \tag{2.67}$$

Here, c_f are the contraction coefficients, and N_{basis} defines the length of the contraction.[150]

2.3.7 Wave Function Analysis

The electronic structure of a molecular system is fully characterized by its electronic wave function, which is obtained from the solution of the time-independent electronic Schrödinger equation. In order to derive further molecular properties besides the electronic energy, the molecular wave function has to be analyzed by exploiting its functional form or decomposing the associated electron density. A variety of available analysis tools exists that range from projection operators based on the electron density or on the molecular orbitals to various wave function transformation techniques. (For a comprehensive overview of wave function analysis methods, see Refs. [149, 150].)

Population Analysis

The population analysis is the study of the electronic charge distribution within a molecular system by assigning a partial charge to each atom in the molecule. As the partial atomic charges are no observable molecular properties, no unique definition is available. The two most common methods for defining partial charges are based on the partitioning of the wave function in terms of the basis functions and on the decomposition of the electron density into atomic domains. (For an overview, see Ref. [150].)

The simplest scheme for assigning charges based on the atomic basis functions is the Mulliken population analysis.[221–224] Within its framework, the number of electrons associated to a specific atom is determined by its atomic orbital contribution to the molecular wave function. Since this type of scheme strongly depends on the basis set and does not necessarily converge with increasing basis set size, it is advantageous to employ atomic charge determination methods based on the numerical analysis of the one-electron density as a function of space. Its general form in terms of a multi-determinantal, many-electron wave function for the electronic state λ reads

$$\rho_\lambda(\vec{r};\boldsymbol{R})=N_{\mathrm{el}}\int \mathrm{d}\theta \int \mathrm{d}\vec{q}_2 \ldots \int \mathrm{d}\vec{q}_{N_{\mathrm{el}}} \left|\Psi_\lambda(\vec{r},\theta,\vec{r}_2,\theta_2,\ldots,\vec{r}_{N_{\mathrm{el}}},\theta_{N_{\mathrm{el}}};\boldsymbol{R})\right|^2. \tag{2.68}$$

An example for this type of population analysis is the Hirshfeld method.[225] It partitions the one-electron density according to a weighting function $\mathcal{W}_A^{\mathrm{Hirshfeld}}$, which is defined as the ratio of the ground state electron density $\rho_{A,0}(\vec{r};\boldsymbol{R})$ for the isolated atom A to a fictitious promolecular density

constructed as the sum over the spherically-averaged $\rho_{A,0}(\vec{r};\boldsymbol{R})$

$$\rho^{\mathrm{pro}}(\vec{r};\boldsymbol{R}) = \sum_{A}^{N_{\mathrm{nuc}}} \rho_{A,0}(\vec{r};\boldsymbol{R}). \tag{2.69}$$

The resulting atomic charge is then determined by subtraction of the integral of the density associated with atom A from the corresponding nuclear charge Z_A

$$\mathcal{Q}_{A,\lambda}^{\mathrm{Hirshfeld}} = Z_A - \int \mathrm{d}\vec{r}\, \mathcal{W}_A^{\mathrm{Hirshfeld}} \rho_\lambda(\vec{r};\boldsymbol{R}) = Z_A - \int \mathrm{d}\vec{r}\, \frac{\rho_{A,0}(\vec{r};\boldsymbol{R})}{\rho^{\mathrm{pro}}(\vec{r};\boldsymbol{R})} \rho_\lambda(\vec{r};\boldsymbol{R}). \tag{2.70}$$

An alternative approach for dividing the real-space electron density into atomic contributions is the Voronoi Deformation Density (VDD) method.[226] The underlying concept relies on a Voronoi partitioning that divides the space into atomic domains known as Voronoi Cells (VC). These cells are defined as the region in space closer to the selected atom A than to the remaining atoms. In order to properly account for the electron density change due chemical bonding, the VDD formalism uses the deformation density, which is the difference between the electron density $\rho_\lambda(\vec{r};\boldsymbol{R})$ and the promolecular density $\rho^{\mathrm{pro}}(\vec{r};\boldsymbol{R})$

$$\rho_\lambda^{\mathrm{def}}(\vec{r};\boldsymbol{R}) = \rho_\lambda(\vec{r};\boldsymbol{R}) - \rho^{\mathrm{pro}}(\vec{r};\boldsymbol{R}). \tag{2.71}$$

Accordingly, the VDD atomic charge is obtained by the spatial integration of $\rho_\lambda^{\mathrm{def}}(\vec{r};\boldsymbol{R})$ over the Voronoi cells

$$\mathcal{Q}_{A,\lambda}^{\mathrm{VDD}} = \int\limits_{\mathrm{VC\,of}\,A} \mathrm{d}\vec{r} \rho_\lambda^{\mathrm{def}}(\vec{r})\,. \tag{2.72}$$

An ambiguity for both methods can arise from the atomic densities especially when choosing between the neutral or cationic/anionic species of an atom in a molecular system.

Natural Transition Orbitals

The characterization of electronically excited states, which are exclusively or predominantly described by single excitations from a single-determinant reference, can be facilitated by constructing Natural Transition Orbitals (NTO).[69] The benefit of the NTO analysis relies on transforming the multi-determinantal wave function of such an excited state into a compact representation in which the excited state is expressed as correlated pairs of particle and hole functions. The central quantity containing the amplitudes for the single excitation from an occupied to a virtual orbital with respect to the reference is the one-electron transition density matrix between this reference Ψ_{ref} and the excited state Ψ_λ. An

element of this matrix is defined as

$$\boldsymbol{T}_{ra,\lambda} = \left\langle \Psi_\lambda \middle| \hat{a}_r^\dagger \hat{a}_a \middle| \Psi_{\text{ref}} \right\rangle . \tag{2.73}$$

Here, $\hat{a}_r^\dagger$ is the creation operator of molecular orbital φ_r, and $\hat{a}_a$ denotes the annihilation operator of molecular orbital φ_a. Such an excitation matrix can be obtained from single-reference electronic structure methods, such as CIS, TDA or LR-TDDFT, with the single-determinant ground state Ψ_0 as reference Ψ_{ref}. Within the CIS scheme, $\boldsymbol{T}_\lambda$ contains the CI expansion coefficients $D^r_{a,\lambda}$ (cf. Eq. (2.27)), while it is directly related to the response vector $\boldsymbol{X}_\lambda$ (cf. Eq. (2.63) and Eq. (2.65)) for the TDA and the LR-TDDFT method. In order to define the NTOs, a single value decomposition of $\boldsymbol{T}_\lambda$ is applied

$$\boldsymbol{T}_\lambda = \boldsymbol{V}_\lambda \text{diag}\left(\zeta_{1,\lambda}, \zeta_{2,\lambda}, \dots\right) \boldsymbol{W}_\lambda^{\text{T}} \tag{2.74}$$

yielding two unitary matrices $\boldsymbol{V}_\lambda$ and $\boldsymbol{W}_\lambda$, which contain the eigenvectors of the hole and particle functions. Consequently, the hole NTOs can be constructed from $\boldsymbol{V}_\lambda$,

$$\varphi^{\text{h}}_{\ell,\lambda}(\vec{r};\boldsymbol{R}) = \sum_a^{N_{\text{occ}}} \boldsymbol{V}_{a,\ell,\lambda} \varphi_a(\vec{r};\boldsymbol{R}), \tag{2.75}$$

and the particle NTOs can be built up using $\boldsymbol{W}_\lambda$

$$\varphi^{\text{el}}_{\ell,\lambda}(\vec{r};\boldsymbol{R}) = \sum_r^{N_{\text{virt}}} \boldsymbol{W}_{r,\ell,\lambda} \varphi_r(\vec{r};\boldsymbol{R}), \tag{2.76}$$

where $\varphi_a(\vec{r};\boldsymbol{R})$ and $\varphi_r(\vec{r};\boldsymbol{R})$ are the occupied and virtual orbitals from the reference. In Eq. (2.74), the squared eigenvalues $\zeta_{\ell,\lambda}$ correspond to the weighting factors for the particle-hole transitions. Accordingly, the normalized hole and particle densities can be formulated as weighted sums over the squared NTOs

$$\begin{aligned} \rho^{\text{h}}_\lambda(\vec{r};\boldsymbol{R}) &= \sum_\ell \left| \zeta_{\ell,\lambda} \varphi^{\text{h}}_{\ell,\lambda}(\vec{r};\boldsymbol{R}) \right|^2 \\ \rho^{\text{el}}_\lambda(\vec{r};\boldsymbol{R}) &= \sum_\ell \left| \zeta_{\ell,\lambda} \varphi^{\text{el}}_{\ell,\lambda}(\vec{r};\boldsymbol{R}) \right|^2 . \end{aligned} \tag{2.77}$$

Typically only a small fraction of the particle and hole functions is required to express the multi-determinantal wave function of an excited state. Thus, its representation as NTOs is a practical and straightforward analysis technique to characterize the excitonic properties of a molecular systems.[227]

2.4 Electron Dynamics

In general, the theoretical treatment of electron dynamics can be classified according to the two different types of molecular systems: the closed and the open quantum system. The term closed quantum system refers to systems, which are not subject to the influence of environmental forces. This includes isolated molecular systems, which are described by a time-independent Hamiltonian and whose time evolution is coherent. This situation can be completely modeled by the time-dependent Schrödinger equation (cf. Eq. (2.1)), where the system remains in a pure state described by a single molecular wave function.

As this isolated system is an oversimplification, physically realistic quantum systems are treated as open quantum systems, which are in contact with a surrounding environment. Its general concept relies on the separation of the total system into an open molecular subsystem S and a subsystem representing the environment or bath B. The combined total system (S + B) is again assumed to be a closed system. The interaction between the relevant subsystem S and its environment B, which strongly depends on the type of bath and on its coupling strength to S, can lead to dissipation and dephasing phenomena. As a consequence, it is not possible to describe the molecular subsystem S by a single quantum state. Instead, an incoherent statistical ensemble of pure states, called a mixed state, is used for its representation. In the ensuing section, the equation of motion for open quantum systems is derived, mainly following Refs. [1], [228], [229], and [230].

2.4.1 Time Evolution in Open Quantum Systems

The most general description of the time evolution for open quantum systems is given in the framework of the reduced density matrix formalism.[229] Here, the density operator $\hat{\varrho}(t)$ is employed to characterize the dynamics of a quantum system. In general, it is defined as the time-dependent mixture of pure states $\big|\Phi_n(t)\big\rangle$ weighted by the probability coefficients $P_n(t)$

$$\hat{\varrho}(t) = \sum_n P_n(t) \big|\Phi_n(t)\big\rangle\big\langle\Phi_n(t)\big| \tag{2.78}$$

with $\sum_n P_n(t) = 1$ for a closed system. For a pure state, this expression reduces to

$$\hat{\varrho}(t) = \big|\Phi(t)\big\rangle\big\langle\Phi(t)\big|. \tag{2.79}$$

Throughout this section, the coordinate dependence for all quantities is omitted for sake of simplicity. In accordance to the general definition of the density operator (cf. Eq. (2.78)), the expectation value of any arbitrary operator $\hat{\mathcal{O}}$ for a mixed state can be obtained by summing over the respective eigenvalues

for the pure states in the statistical mixture

$$\langle\hat{\mathcal{O}}\rangle = \sum_n P_n(t) \left\langle \Phi_n(t) \middle| \hat{\mathcal{O}} \middle| \Phi_n(t) \right\rangle . \tag{2.80}$$

This can be simplified by using the trace formula

$$\langle\hat{\mathcal{O}}\rangle = \mathrm{Tr}\left\{ \hat{\mathcal{O}}\, \hat{\varrho}(t) \right\} . \tag{2.81}$$

In practical applications, the density operator is usually expressed in its matrix form $\boldsymbol{\varrho}(t)$ by using a time-independent, orthonormal basis $\left\{ \left| \Psi_\kappa \right\rangle \right\}$. For a mixed state, the elements of this matrix are given by

$$\varrho_{\kappa\iota}(t) = \langle \Psi_\kappa | \hat{\varrho}(t) | \Psi_\iota \rangle = \sum_n P_n(t) d^\star_{\kappa,n}(t) d_{\iota,n}(t) \tag{2.82}$$

and for a pure state by

$$\varrho_{\kappa\iota}(t) = \langle \Psi_\kappa | \hat{\varrho}(t) | \Psi_\iota \rangle = d^\star_\kappa(t) d_\iota(t). \tag{2.83}$$

Here, the expansion coefficients $d_{\kappa,n}(t)$ are obtained from

$$d_{\kappa,n}(t) = \langle \Psi_\kappa | \Phi_n(t) \rangle . \tag{2.84}$$

The density matrix $\boldsymbol{\varrho}(t)$ is hermitian, i.e., it satisfies the condition $\varrho_{\kappa\iota}(t) = \varrho^\star_{\iota\kappa}(t)$. Its diagonal elements can be interpreted as the probability of finding the system in basis state $\left| \Psi_\kappa \right\rangle$ at time t, and are thus referred to as populations. As these populations are positive numbers, i.e.,

$$\varrho_{\kappa\kappa}(t) \geq 0, \tag{2.85}$$

it follows that the density operator $\hat{\varrho}(t)$ is a semi-definite operator. The off-diagonal terms of $\boldsymbol{\varrho}(t)$ represent the interferences between different basis state functions and are termed coherences. Both terms depend on the choice of the selected basis set $\left\{ \left| \Psi_\kappa \right\rangle \right\}$.

In order to derive an equation of motion for the density operator, the solution of the time-dependent Schrödinger equation is formulated by means of a unitary time evolution operator

$$\left| \Phi_n(t) \right\rangle = \hat{\mathcal{U}}(t, t_0) \left| \Phi_n(t_0) \right\rangle. \tag{2.86}$$

In analogy, the time evolution for the density operator can be written as

$$\hat{\varrho}(t) = \sum_n P_n(t)\,\hat{\mathcal{U}}(t,t_0)\big|\Phi_n(t_0)\big\rangle\big\langle\Phi_n(t_0)\big|\,\hat{\mathcal{U}}^\dagger(t,t_0) = \hat{\mathcal{U}}(t,t_0)\hat{\varrho}(t_0)\,\hat{\mathcal{U}}^\dagger(t,t_0). \tag{2.87}$$

The time derivative of the above equation directly results in the equation of motion for the density operator

$$\frac{\partial}{\partial t}\hat{\varrho}(t) = -\frac{\imath}{\hbar}\left[\hat{H}_{\mathrm{tot}}(t), \hat{\varrho}(t)\right] \tag{2.88}$$

which is known as the Liouville-von Neumann equation. This equation is often written in an alternative formulation

$$\frac{\partial}{\partial t}\hat{\varrho}(t) = -\imath\mathcal{L}\hat{\varrho}(t) \tag{2.89}$$

with $\mathcal{L}$ as the Liouville superoperator or Liouvillian. It should be noted that the solution of the Liouville-von-Neumann equation yields the same time evolution for a closed system as the solution of the time-dependent Schrödinger equation.

Considering a closed total system, which consists of a subsystem S coupled to a usually macroscopic bath B, the associated total Hamiltonian has the general form

$$\hat{H}_{\mathrm{tot}}(t) = \hat{H}_{\mathrm{S}} + \hat{H}_{\mathrm{B}} + \hat{H}_{\mathrm{SB}}(t). \tag{2.90}$$

Here, $\hat{H}_{\mathrm{S}}$ and $\hat{H}_{\mathrm{B}}$ are the time-independent Hamiltonians describing the subsystem S and the environment B, and $\hat{H}_{\mathrm{SB}}(t)$ expresses the interaction between the two. Under the assumption that $\hat{H}_{\mathrm{SB}}(t) = 0$ for $t \leq t_0$, the initial density operator at $t = t_0$ for the combined system $(\mathrm{S} + \mathrm{B})$ can be described by the following tensor product

$$\hat{\varrho}(t_0) = \hat{\varrho}_{\mathrm{S}}(t_0) \otimes \hat{\varrho}_{\mathrm{B}}(t_0). \tag{2.91}$$

In order to incorporate a time-dependent external stimulus to the situation in Eq. (2.90), the interaction Hamiltonian $\hat{H}_{\mathrm{int}}$ (cf. Eq. (2.2)) can be added to $\hat{H}_{\mathrm{S}}$ neglecting its influence on $\hat{H}_{\mathrm{B}}$ and $\hat{H}_{\mathrm{SB}}$.

2.4.2 The Liouville-von Neumann Equation in Lindblad Form

The unitary time evolution (cf. Eq. (2.87)) of the combined system is generally too intricate to solve in practice due to the huge number of environmental degrees of freedom. The common strategy to circumvent this issue is to trace over the degrees of freedom of the bath which leads to the reduced density operator. The associated equation of motion, the so-called quantum master equation, is non-unitary and can be derived by invoking several approximations. (For a complete derivation, see Ref. [228].) Its starting point is the Liouville-von Neumann equation for the total density operator in its interaction

picture form

$$\frac{\partial}{\partial t}\hat{\varrho}_{\mathrm{I}}(t) = -\frac{\imath}{\hbar}\left[\hat{H}_{\mathrm{SB,I}}(t), \hat{\varrho}_{\mathrm{I}}(t)\right] \tag{2.92}$$

with the subscript "I" indicating the interaction frame. The interaction picture for an arbitrary operator $\hat{\mathcal{O}}(t)$ is defined as

$$\hat{\mathcal{O}}_{\mathrm{I}}(t) = e^{\imath\left(\hat{H}_{\mathrm{S}}+\hat{H}_{\mathrm{B}}\right)t/\hbar}\,\hat{\mathcal{O}}(t)\,e^{-\imath\left(\hat{H}_{\mathrm{S}}+\hat{H}_{\mathrm{B}}\right)t/\hbar}. \tag{2.93}$$

Eq. 2.92 can be transformed in its integral form

$$\hat{\varrho}_{\mathrm{I}}(t) = \hat{\varrho}_{\mathrm{I}}(t_0) - \frac{\imath}{\hbar}\int_{t_0}^{t} \mathrm{d}t' \,\left[\hat{H}_{\mathrm{SB,I}}(t'), \hat{\varrho}_{\mathrm{I}}(t')\right]. \tag{2.94}$$

Inserting this integral into Eq. (2.92) and taking the partial trace over the bath leads to

$$\frac{\partial}{\partial t}\hat{\varrho}_{\mathrm{S,I}}(t) = -\frac{1}{\hbar^2}\int_{0}^{t} \mathrm{d}t' \,\mathrm{Tr}_{\mathrm{B}}\left\{\left[\hat{H}_{\mathrm{SB,I}}(t), \left[\hat{H}_{\mathrm{SB,I}}(t'), \hat{\varrho}_{\mathrm{I}}(t')\right]\right]\right\}. \tag{2.95}$$

Here, it is assumed that the initial correlation between the system and the bath at $t_0 = 0$ is zero

$$\mathrm{Tr}_{\mathrm{B}}\left\{\left[\hat{H}_{\mathrm{SB,I}}(t), \hat{\varrho}_{\mathrm{I}}(t_0)\right]\right\} = 0. \tag{2.96}$$

In order to simplify Eq. (2.95), the Born approximation is applied that assumes a weak coupling between the reduced system S and the bath B and neglects the effect of this coupling on the bath. This is justified for a macroscopic environment in its thermal equilibrium, whose excitations caused by the reduced system are not resolved within the time scale of S. Following these assumptions, the total density matrix can be expressed as the tensor product ignoring any time evolution of the environment density operator

$$\hat{\varrho}_{\mathrm{I}}(t) \approx \hat{\varrho}_{\mathrm{S,I}}(t) \otimes \hat{\varrho}_{\mathrm{B,I}}. \tag{2.97}$$

It can be used to rewrite Eq. (2.95) to

$$\frac{\partial}{\partial t}\hat{\varrho}_{\mathrm{S,I}}(t) = -\frac{1}{\hbar^2}\int_{0}^{t} \mathrm{d}t' \,\mathrm{Tr}_{\mathrm{B}}\left\{\left[\hat{H}_{\mathrm{SB,I}}(t), \left[\hat{H}_{\mathrm{SB,I}}(t'), \hat{\varrho}_{\mathrm{S,I}}(t') \otimes \hat{\varrho}_{\mathrm{B,I}}\right]\right]\right\}. \tag{2.98}$$

A further simplification on this equation can be achieved by the Markov approximation, which transforms the equation of motion for the density matrix into a time-local expression by replacing $\hat{\varrho}_{\mathrm{S,I}}(t')$ by $\hat{\varrho}_{\mathrm{S,I}}(t)$ inside the integral. That means that the time evolution of the density matrix solely depends

on its current state and that memory effects are neglected. This step yields the following equation

$$\frac{\partial}{\partial t}\hat{\varrho}_{\mathrm{S,I}}(t) = -\frac{1}{\hbar^2}\int_0^t \mathrm{d}t'\ \mathrm{Tr}_{\mathrm{B}}\left\{\left[\hat{H}_{\mathrm{SB,I}}(t),\left[\hat{H}_{\mathrm{SB,I}}(t'),\hat{\varrho}_{\mathrm{S,I}}(t)\otimes\hat{\varrho}_{\mathrm{B,I}}\right]\right]\right\}. \tag{2.99}$$

However, this equation still depends on the choice of the initial preparation at time $t = 0$. In order to eliminate this explicit dependence, the variable t is substituted by $t - t'$, and the upper limit of the integral is replaced by infinity. This gives a Markovian master equation

$$\frac{\partial}{\partial t}\hat{\varrho}_{\mathrm{S}}(t) = -\frac{1}{\hbar^2}\int_0^\infty \mathrm{d}t'\ \mathrm{Tr}_{\mathrm{B}}\left\{\left[\hat{H}_{\mathrm{SB}}(t),\left[\hat{H}_{\mathrm{SB}}(t-t'),\hat{\varrho}_{\mathrm{S}}(t)\otimes\hat{\varrho}_{\mathrm{B}}\right]\right]\right\}, \tag{2.100}$$

which is usually referred to as the Redfield master equation[229,231]. To ensure the validity of the complete Markov approximation, it is additionally assumed that the relaxation time τ_{R} of the reduced system S significantly exceeds the bath correlation time τ_{B}. As a consequence, these quickly decaying bath correlations are not resolved on a coarse-grained time axis, and thus the bath memory is neglected.

The two approximations just applied are usually summarized as the Born-Markov approximation. Despite yielding a master equation which is local in time and omits memory effects for the dynamics of S, it does not guarantee complete positivity and thus does not preserve the probabilistic interpretation of the density operator.[232,233] This attribute can be enforced by performing the secular approximation, which averages over the rapidly oscillating terms in the master equation. To start with its derivation, the interaction Hamiltonian $\hat{H}_{\mathrm{SB}}$ is expressed as a tensor product in the Schrödinger picture

$$\hat{H}_{\mathrm{SB}} = \sum_\alpha \hat{A}_\alpha \otimes \hat{B}_\alpha, \tag{2.101}$$

where $\hat{A}_\alpha$ and $\hat{B}_\alpha$ are Hermitian operators acting on the system and on the bath, respectively. The prerequisite for the secular approximation is the decomposition of the interaction Hamiltonian H_{SB} into eigenoperators of the system Hamiltonian H_{S}. For this purpose, the $\hat{A}_\alpha$ operator is projected on subspaces with a fixed frequency $\omega = (\varepsilon' - \varepsilon)/\hbar$

$$\hat{A}_\alpha(\omega) = \sum_{\omega=(\varepsilon'-\varepsilon)/\hbar} \hat{P}(\varepsilon)\hat{A}_\alpha\hat{P}(\varepsilon') \tag{2.102}$$

with ε as the eigenvalues of the system Hamiltonian H_{S} and $\hat{P}$ as the associated projectors. This

definition implies that $\hat{A}_\alpha(\omega)$ satisfies the commutation relation

$$\begin{aligned}\left[\hat{H}_\mathrm{S}, \hat{A}_\alpha(\omega)\right] &= -\omega \hat{A}_\alpha(\omega) \\ \left[\hat{H}_\mathrm{S}, \hat{A}^\dagger_\alpha(\omega)\right] &= +\omega \hat{A}^\dagger_\alpha(\omega).\end{aligned} \tag{2.103}$$

As the completeness relation holds for the eigenvectors of H_S, $\hat{A}_\alpha$ can be recovered by summing over all frequencies

$$\sum_\omega \hat{A}_\alpha(\omega) = \sum_\omega \hat{A}^\dagger_\alpha(\omega) = \hat{A}_\alpha. \tag{2.104}$$

This allows to rewrite the interaction Hamiltonian as

$$\hat{H}_\mathrm{SB}(t) = \sum_{\alpha,\omega} \hat{A}_\alpha(\omega) \otimes \hat{B}_\alpha = \sum_{\alpha,\omega} \hat{A}^\dagger_\alpha(\omega) \otimes \hat{B}^\dagger_\alpha. \tag{2.105}$$

By employing the expression of $\hat{A}_\alpha(\omega)$ in the interaction picture

$$e^{\imath \hat{H}_\mathrm{S} t/\hbar} \hat{A}_\alpha(\omega) e^{-\imath \hat{H}_\mathrm{S} t/\hbar} = e^{-\imath\omega t} \hat{A}_\alpha(\omega), \tag{2.106}$$

H_SB can likewise be written in its interaction frame

$$\hat{H}_\mathrm{SB,I}(t) = \sum_{\alpha,\omega} e^{-\imath\omega t} \hat{A}_\alpha(\omega) \otimes \hat{B}_\alpha(t) \quad = \sum_{\alpha,\omega} e^{+\imath\omega t} \hat{A}^\dagger_\alpha(\omega) \otimes \hat{B}^\dagger_\alpha(t). \tag{2.107}$$

Here, the operator for the bath in the interaction picture is defined as

$$\hat{B}_\alpha(t) = e^{\imath \hat{H}_\mathrm{B} t/\hbar} \hat{B}_\alpha e^{-\imath \hat{H}_\mathrm{B} t/\hbar}. \tag{2.108}$$

Inserting Eq. (2.107) into the Markovian master equation (cf. Eq. (2.100)) leads to

$$\frac{\partial}{\partial t} \hat{\varrho}_\mathrm{S,I}(t) = \sum_{\omega\omega'} \sum_{\alpha\beta} e^{\imath(\omega'-\omega)t} \, \Xi_{\alpha\beta}(\omega) \left(\hat{A}_\beta(\omega) \hat{\varrho}_\mathrm{S,I}(t) \hat{A}^\dagger_\alpha(\omega') - \hat{A}^\dagger_\alpha(\omega') \hat{A}_\beta(\omega) \hat{\varrho}_\mathrm{S,I}(t) \right) + \mathrm{h.c.}, \tag{2.109}$$

where "h.c." signifies the Hermitian conjugate expression. In Eq. (2.109), the one-sided Fourier transform for the bath correlation function is used

$$\begin{aligned}\Xi_{\alpha\beta}(\omega) &= \frac{1}{\hbar^2} \int_0^\infty \mathrm{d}t' \; e^{+\imath\omega t'} \left\langle \hat{B}^\dagger_\alpha(t) \hat{B}_\beta(t - t') \right\rangle \\ &= \frac{1}{\hbar^2} \int_0^\infty \mathrm{d}t' \; e^{+\imath\omega t'} \left\langle \hat{B}^\dagger_\alpha(t') \hat{B}_\beta(0) \right\rangle,\end{aligned} \tag{2.110}$$

where the bath correlation function $\left\langle \hat{B}_\alpha^\dagger(t)\hat{B}_\beta(t-t')\right\rangle = \mathrm{Tr_B}\left\{\left[\hat{B}_\alpha^\dagger(t)\hat{B}_\beta(t-t')\hat{\varrho}_{\mathrm{B,I}}\right]\right\}$ becomes stationary, since $\hat{\varrho}_{\mathrm{B,I}}$ is an eigenstate of the bath Hamiltonian $\hat{H}_\mathrm{B}$. This in turn means that $\Xi_{\alpha\beta}(\omega)$ does not depend on time. The general condition of the secular approximation builds upon the consideration that the characteristic timescale of a system τ_S, given by $|\omega' - \omega|^{-1}$, is small compared to the relaxation time of the system τ_R, i.e., $\tau_\mathrm{R} \gg \tau_\mathrm{S}$. Consequently, all terms for which $\omega' \neq \omega$ holds can safely be neglected, since these terms oscillate fast in comparison to τ_R. This is known as the strict secular approximation. Hence, the subsequent master equation emerges

$$\frac{\partial}{\partial t}\hat{\varrho}_{\mathrm{S,I}}(t) = \sum_\omega \sum_{\alpha\beta} \Xi_{\alpha\beta}(\omega)\left(\hat{A}_\beta(\omega)\hat{\varrho}_{\mathrm{S,I}}(t)\hat{A}_\alpha^\dagger(\omega) - \hat{A}_\alpha^\dagger(\omega)\hat{A}_\beta(\omega)\hat{\varrho}_{\mathrm{S,I}}(t)\right) + \mathrm{h.c.}, \tag{2.111}$$

which can be cast into a simple general form

$$\frac{\partial}{\partial t}\hat{\varrho}_{\mathrm{S,I}}(t) = -\frac{\imath}{\hbar}\left[\hat{H}_\mathrm{LS}, \hat{\varrho}_{\mathrm{S,I}}(t)\right] + \mathcal{L}_\mathrm{D}\hat{\varrho}_{\mathrm{S,I}}(t). \tag{2.112}$$

Here, $\hat{H}_\mathrm{LS}$ is the Lamb shift Hamiltonian

$$\hat{H}_\mathrm{LS} = \sum_\omega \sum_{\alpha\beta} S_{\alpha\beta}(\omega)\hat{A}_\alpha^\dagger(\omega)\hat{A}_\beta(\omega), \tag{2.113}$$

which commutes with the system Hamiltonian, and thus renormalizes the energy levels of the unperturbed system. The coefficients $S_{\alpha\beta}(\omega)$ in Eq. (2.113) arise from the decomposition of the Fourier transforms of the reservoir correlation functions $\Xi_{\alpha\beta}(\omega)$ into its real and imaginary part

$$\Xi_{\alpha\beta}(\omega) = \frac{1}{2}\xi_{\alpha\beta}(\omega) + \imath S_{\alpha\beta}(\omega) \tag{2.114}$$

with

$$S_{\alpha\beta}(\omega) = \frac{1}{2\imath}\left(\Xi_{\alpha\beta}(\omega) - \Xi_{\beta\alpha}^\dagger(\omega)\right) \tag{2.115}$$

and

$$\xi_{\alpha\beta}(\omega) = \Xi_{\alpha\beta}(\omega) + \Xi_{\beta\alpha}^\dagger(\omega). \tag{2.116}$$

On this basis, an expression for the dissipative Liouvillian or dissipator in Eq. (2.112) can be written

$$\mathcal{L}_\mathrm{D}\hat{\varrho}_{\mathrm{S,I}}(t) = \frac{1}{2}\sum_\omega \sum_{\alpha\beta} \xi_{\alpha\beta}(\omega)\left\{\left[\hat{A}_\beta(\omega), \hat{\varrho}_{\mathrm{S,I}}(t)\hat{A}_\alpha^\dagger(\omega)\right] + \left[\hat{A}_\beta(\omega)\hat{\varrho}_{\mathrm{S,I}}(t), \hat{A}_\alpha^\dagger(\omega)\right]\right\}. \tag{2.117}$$

The master equation of Eq. (2.112) can be easily transformed to the Liouville-von Neumann equation in Lindblad form[234]

$$\frac{\partial}{\partial t}\hat{\varrho}_{\mathrm{S}}(t) = -\frac{\imath}{\hbar}\left[\hat{H}_{\mathrm{S}}(t), \hat{\varrho}_{\mathrm{S}}(t)\right] + \mathcal{L}_{\mathrm{D}}\hat{\varrho}_{\mathrm{S}}(t) \tag{2.118}$$

by transforming it to its Schrödinger picture, i.e., adding the system Hamiltonian $\hat{H}_{\mathrm{S}}$, neglecting the Lamb shift Hamiltonian $\hat{H}_{\mathrm{LS}}$, and diagonalizing the matrices $\xi_{\alpha\beta}(\omega)$. The first term on the right-hand side of Eq. (2.118) accounts for the unitary time evolution of the density operator of the system which is often expressed in terms of the time-independent electronic eigenstates derived from electronic structure calculations

$$\hat{\varrho}_{\mathrm{S}}(t) = \sum_{\lambda\nu} \mathcal{P}_{\lambda\nu}(t)\big|\Psi_\lambda\big\rangle\big\langle\Psi_\nu\big| \tag{2.119}$$

with $\mathcal{P}_{\lambda\nu}(t)$ as expansion coefficients. The second term in Eq. (2.118), i.e., the dissipative Liouvillian, describes the interaction between the system and the bath. An expression for the latter in the Lindblad representation reads

$$\mathcal{L}_{\mathrm{D}}\hat{\varrho}_{\mathrm{S}}(t) = \frac{1}{2}\sum_{d}\left\{\left[\hat{C}_d\hat{\varrho}_{\mathrm{S}}(t), \hat{C}_d^\dagger\right] + \left[\hat{C}_d, \hat{\varrho}_{\mathrm{S}}(t)\hat{C}_d^\dagger\right]\right\}, \tag{2.120}$$

which likewise ensures the semipositivity of the reduced density operator. In Eq. (2.120), $\hat{C}_d$ is a Lindblad operator representing the nature and strength of a dissipative channel d. These operators enable the investigation of energy relaxation and/or dephasing phenomena. A convenient definition for $\hat{C}_d$ to describe energy relaxations are raising/lowering operators given by

$$\hat{C}_d \rightarrow \sqrt{\hbar\Gamma_{\nu\rightarrow\lambda}}\big|\Psi_\lambda\big\rangle\big\langle\Psi_\nu\big|. \tag{2.121}$$

The associated dissipation rates $\Gamma_{\nu\rightarrow\lambda}$ can be calculated perturbatively using Fermi's Golden Rule formula[235,236]

$$\Gamma_{\nu\rightarrow\lambda} = \frac{2\pi}{\hbar}\sum_{mm'}\left|\left\langle\Psi_\lambda, \Upsilon_m\middle|\hat{H}_{\mathrm{SB}}\middle|\Psi_\nu, \Upsilon_{m'}\right\rangle\right|^2 \varsigma_m\left(1-\varsigma_{m'}\right)\delta\left(\epsilon_{m'} - \epsilon_m - \hbar\omega_{\nu\lambda}\right), \tag{2.122}$$

where Ψ_λ and Ψ_ν denote the electronic states of the system, and Υ_m and $\Upsilon_{m'}$ are the initial and final bath states with energies ϵ_m and $\epsilon_{m'}$ and the thermal distribution function ς_m and $\varsigma_{m'}$.

2.4.3 The Electric Field

An intuitive strategy to drive the molecular subsystem S out of equilibrium rests on the application of external laser pulses inducing transitions between electronic states. There exist different formula-

tions for modeling these electric fields.[236] The most straightforward expression for a laser field is the analytical form of a π-pulse promoting a selective transition between two states Ψ_λ and Ψ_ν[237]

$$\vec{F}(t) = \vec{F}_0 s(t) \cos(\omega_{\lambda\nu} t), \tag{2.123}$$

where $\vec{F}(t)$ is the time-dependent electric field with the components $F_x(t)$, $F_y(t)$, and $F_z(t)$ that interact with the molecular dipole operator $\hat{\mu}$ within the semiclassical dipole approximation (cf. Eq. (2.3)).[148] Furthermore, $\omega_{\lambda\nu}$ refers to the carrier frequency of the laser field resonant with the respective transition energy, and $\vec{F}_0$ signifies the amplitude of the laser field. $s(t)$ specifies the temporal envelope function with a $\sin^2$ type shape

$$s(t) = \begin{cases} \sin^2\left(\frac{\pi t}{t_h}\right) & \text{if } 0 \leq t \leq t_h \\ 0 & \text{else} \end{cases} \tag{2.124}$$

with t_h as the pulse length. A complete population inversion for the state-to-state transition can be accomplished in an idealized isolated two-level system, if the π-pulse condition is fulfilled

$$\left|\vec{\mu}_{\lambda\nu}\vec{F}_0\right| \int_0^{t_h} \mathrm{d}t s(t) = \pi\hbar. \tag{2.125}$$

Here, $\vec{\mu}_{\lambda\nu}$ is the transition dipole moment comprising the components $\mu_{\lambda\nu,x}$, $\mu_{\lambda\nu,y}$, and $\mu_{\lambda\nu,z}$, and $\vec{F}_0$ is the pulse amplitude, which reads

$$F_{0,x} = \frac{2\pi\hbar}{t_h \left|\mu_{\lambda\nu,x}\right|} \tag{2.126}$$

for a x-linearized laser field. Eq. (2.125) results from the (two-state) rotating wave approximation and can be approximately applied for multi-level systems.[238,239] A series of interlevel transitions in a multi-level system can be achieved by a superposition of linearly polarized laser fields

$$\vec{F}_g(t) = \begin{cases} \vec{F}_{0,g} \sin^2\left(\frac{\pi(t-t_g)}{t_{h,g}}\right) \cos(\omega_g t) & \text{if } t_g \leq t \leq t_g + t_{h,g} \\ 0 & \text{else} \end{cases}, \tag{2.127}$$

where t_g and $t_{h,g}$ are the starting time and the pulse length of the gth laser pulse, respectively.

2.4.4 Analysis of Electron Dynamics

The time- and space-resolved analysis of ultrafast electron migration processes in molecular systems is the cornerstone to obtain a complete picture of its intrinsic mechanism. The commonly used quantity for the characterization of such a correlated electron dynamics is the time-dependent one-electron

density[62,63,240]

$$\rho(\vec{r},t) = \sum_{\lambda\nu} \int \mathrm{d}\boldsymbol{R}\big(\chi_\nu^\dagger(\boldsymbol{R},t)\chi_\lambda(\boldsymbol{R},t)\big)\rho_{\lambda\nu}(\vec{r};\boldsymbol{R}) \tag{2.128}$$

with $\chi_\lambda(\boldsymbol{R},t)$ as the nuclear wave function and $\rho_{\lambda\nu}(\vec{r};\boldsymbol{R})$ as the time-independent electronic transition density

$$\rho_{\lambda\nu}(\vec{r};\boldsymbol{R}) = \int \mathrm{d}\theta \int \mathrm{d}\vec{q}_2 \ldots \int \mathrm{d}\vec{q}_{N_\mathrm{el}}\, \Psi_\lambda(\boldsymbol{q};\boldsymbol{R})\, \Psi_\nu(\boldsymbol{q};\boldsymbol{R}). \tag{2.129}$$

Throughout this section, the general ansatz for a multi-determinantal, many-electron wave function (cf. Eq. (2.24)) is used to define an electronic state. The time-dependent one-electron density can be intuitively interpreted as a conserved probability fluid of electrons. The complementary quantity revealing the mechanistic details of the spatially resolved instantaneous flow of electrons is the time-dependent electronic flux density (cf. **Paper AP1**)

$$\vec{j}(\vec{r},t) = \sum_{\lambda\nu} \int \mathrm{d}\boldsymbol{R}\big(\chi_\nu^\dagger(\boldsymbol{R},t)\chi_\lambda(\boldsymbol{R},t)\big)\vec{j}_{\lambda\nu}(\vec{r};\boldsymbol{R}) \tag{2.130}$$

with the time-independent electronic transition flux density between state λ and state ν

$$\vec{j}_{\lambda\nu}(\vec{r};\boldsymbol{R}) = -\frac{\imath\hbar}{2m_e} \int \mathrm{d}\theta \int \mathrm{d}\vec{q}_2 \ldots \int \mathrm{d}\vec{q}_{N_\mathrm{el}} \left(\Psi_\nu(\boldsymbol{q};\boldsymbol{R})\vec{\nabla}_{\vec{r}}\,\Psi_\lambda(\boldsymbol{q};\boldsymbol{R}) - \Psi_\lambda(\boldsymbol{q};\boldsymbol{R})\vec{\nabla}_{\vec{r}}\,\Psi_\nu(\boldsymbol{q};\boldsymbol{R})\right). \tag{2.131}$$

Within the clamped nuclei approximation, the electronic flux density $\vec{j}_{\lambda\lambda}(\vec{r};\boldsymbol{R})$ for two identical states, known as the adiabatic electronic flux density, vanishes as the electronic states are real-valued. A few theoretical approaches exist trying to bypass this unphysical phenomenon.[241–248]

The central conservation relation between the time-dependent electron density $\rho(\vec{r},t)$ and the electronic flux density $\vec{j}(\vec{r},t)$ is the electronic continuity equation[147]

$$\frac{\partial}{\partial t}\rho(\vec{r},t) = -\vec{\nabla}_{\vec{r}} \cdot \vec{j}(\vec{r},t). \tag{2.132}$$

The left-hand side of this equation, the time-derivative of the electron density, is designated as the electron flow, while on the right-hand side it is described as the divergence of the electronic flux density.

A derived quantity from the electron density often used to supplement the analysis of a charge migration process is the difference density. It specifies the variation of the electron density within a certain time interval $[0,t]$ from a given initial condition and is defined by integrating the electron flow over time[249,250]

$$\Delta\rho(\vec{r},t) = \int_{t_0}^{t} \mathrm{d}t' \frac{\partial\rho(\vec{r},t')}{\partial t'} = \rho(\vec{r},t) - \rho(\vec{r},t_0). \tag{2.133}$$

In analogy to the time-independent population analysis (cf. Sec. (2.3.7)), a projector formalism acting on the different real-space scalar fields can be applied to yield quantitative information about the instantaneous and total contributions of a molecular fragment during the charge migration. Accordingly, the number of electrons assigned to a certain atom/fragment or volume V at any given time can be defined as

$$N_V(t) = \int \mathrm{d}\vec{r}\, \hat{\mathcal{P}}_V \rho(\vec{r}, t). \tag{2.134}$$

Here, the projector operator $\hat{\mathcal{P}}_V$ can be based either on the spatial decomposition of the electron density in specific volume elements as in the Voronoi formalism or on the partitioning by means of the atomic orbital contributions to the electron density as in the Mulliken scheme. Two additional quantities arising from this projector formalism are the time-dependent net electronic yield

$$Y_V(t) = \int \mathrm{d}\vec{r}\, \hat{\mathcal{P}}_V \Delta\rho(\vec{r}, t) = N_V(t) - N_V(t_0) \tag{2.135}$$

and the time-dependent net electronic flow

$$\mathcal{F}_V(t) = \int \mathrm{d}\vec{r}\, \hat{\mathcal{P}}_V \frac{\partial}{\partial t} \rho(\vec{r}, t). \tag{2.136}$$

Both reveal the quantitative change of the number of electrons and the flow of electrons within a certain time interval assigned to a specific molecular fragment, respectively.[249,250]

An interesting property of the transition electronic current density is its direct relation to the transition electric dipole moment $\mu^{\mathrm{v}}_{\lambda\nu}(\boldsymbol{R})$ in velocity gauge and thus to the absorption intensity of an electronic transition. Accordingly, the general form for the electronic contribution to $\mu^{\mathrm{v}}_{\lambda\nu}(\boldsymbol{R})$ can be written as

$$\mu^{\mathrm{v}}_{\lambda\nu}(\boldsymbol{R}) = -e \int \mathrm{d}\vec{r}\, \vec{j}_{\lambda\nu}(\vec{r}; \boldsymbol{R}) \tag{2.137}$$

with e as the elementary charge. Alternatively, an expression for the transition electric dipole moment in length gauge can be formulated in terms of the time-independent electronic transition density

$$\mu^{\mathrm{r}}_{\lambda\nu}(\boldsymbol{R}) = -e \int \mathrm{d}\vec{r}\, \vec{r} \cdot \vec{\rho}_{\lambda\nu}(\vec{r}; \boldsymbol{R}). \tag{2.138}$$

Both forms of $\mu_{\lambda\nu}(\boldsymbol{R})$ are directly related via[251]

$$\left(\mu^{\mathrm{v}}_{\lambda\nu}(\boldsymbol{R})\right)^{\mathrm{r}} = \frac{\imath\hbar}{(E_\nu(\boldsymbol{R}) - E_\lambda(\boldsymbol{R}))} \mu^{\mathrm{v}}_{\lambda\nu}(\boldsymbol{R}) \tag{2.139}$$

which has to be identical to the expression in Eq. (2.138) in the limit of an exact wave function. This

relation can be useful to estimate the quality of an electronic structure calculation concerning the level of theory and the underlying basis set.

Chapter 3

Results

This chapter provides a brief summary of the central findings from the scientific publications produced in the framework of this thesis. A detailed description of the entire results as well as the methodologies, which have been both applied and specifically developed for the study purposes, can be found in the respective papers presented in Chapter 4. These studies are thematically divided into four groups: The first group (**TK**) presents novel and routinely used tools for the analysis and imaging of electronic excitations and many-electron dynamics which are implemented in an open-source framework. The latter three groups investigate different scenarios for charge migration processes in three diverse molecular systems including various small molecules (**SM**), dye-sensitized solar cells (**SC**), and a semiconductor quantum dot (**QD**).

The **Paper TK1** and **Paper TK2** demonstrate the capabilities and applications of the open-source framework DETCI@ORBKIT, which is a Python post-processing toolbox for multi-determinantal wave functions and builds upon the functionalities of ORBKIT[AP2]. The latter was developed by the author and a colleague and is listed as an additional publication (cf. **Paper AP2**). The main objective for the development of the DETCI@ORBKIT program was to provide a suitable toolset for the time- and space-resolved study and visualization of correlated many-electron dynamics. For this purpose, it evaluates transition moments and expectations values of various one-electron operators for explicitly time-dependent electronic wavepackets that are expressed as linear combinations of multi-determinantal wave functions. The necessary data to reconstruct these multi-determinantal wave functions are directly extracted from the output of Configuration Interaction (CI) calculations at various levels of theory. The electron density, the electronic flux density, and several derived quantities and observables are among these one-electron properties. In general, the modular design of DETCI@ORBKIT enables to straightforwardly implement any type of one-electron quantity. In **Paper TK1**, the capabilities of the

proposed set of analysis tools to unravel the mechanistic features of ultrafast charge migration processes are substantiated for a few benchmark systems. In particular, the combination of derived quantities from the electron density, such as the electronic flow, complemented by the electronic flux density reveal extensive dynamical details about the motion and flow of the electrons during the investigated charge migration scenarios. The convergence of these tools with respect to different levels of CI calculations and the basis set size exhibit a high robustness concerning the qualitative statements gained on their basis. In addition, the derived quantities from the electron density show a rapid quantitative convergence.

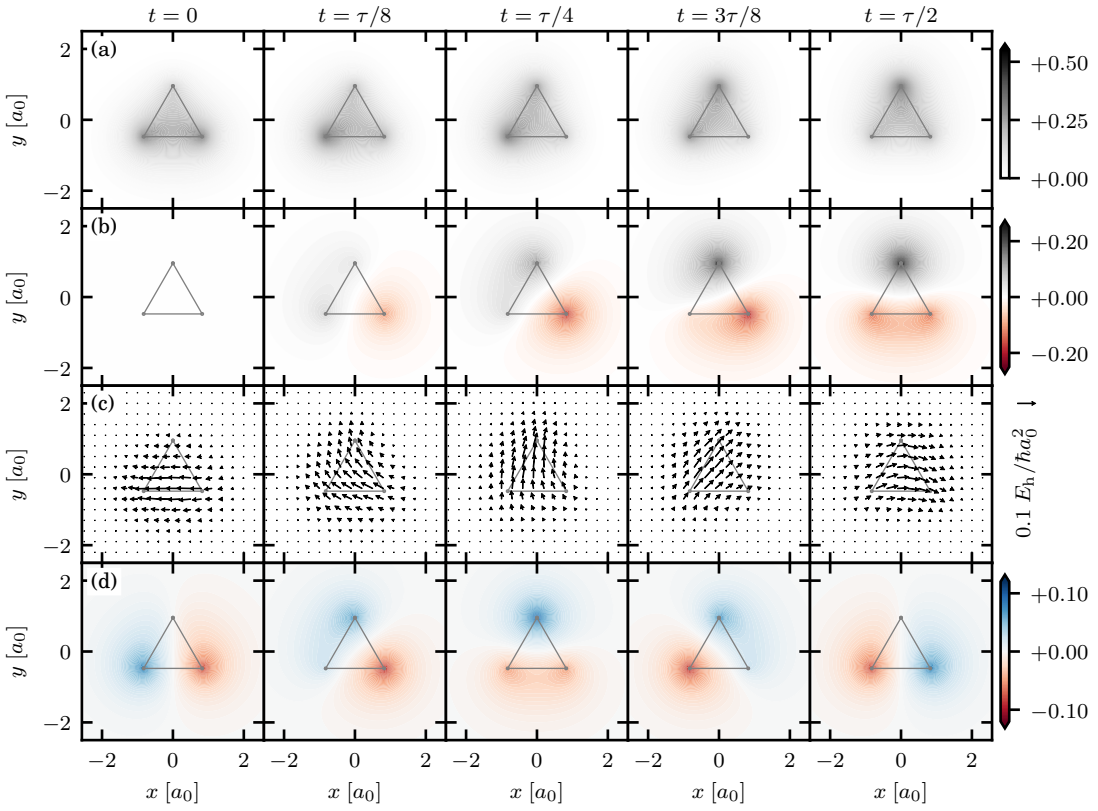

Figure 3.1: Selection of the analysis tools implemented in the DETCI@ORBKIT framework including (a) the electron density $\rho(\vec{r},t)$ (in units of $1/a_0^3$), (b) the difference density $\Delta\rho(\vec{r},t)$ (in units of $1/\mathrm{a_0}^3$), (c) the electronic flux density $\vec{j}(\vec{r},t)$ (in units of $E_\mathrm{h}/\hbar a_0^2$), and (d) the electronic flow $\frac{\partial}{\partial t}\rho(\vec{r},t)$ (in units of $E_\mathrm{h}/\hbar a_0^3$). These are displayed for representative time steps during the first half period of the charge migration process in a superposition state of the trihydrogen cation H_3^+. The superposition state is prepared by the ground state $1\,^1A_1^{'}$ and degenerate excited state $1\,^1E^{'}$, the molecule is sketched as a gray stick model, and the analysis quantities are determined with the Full CI method using a cc-pVTZ basis set. A reference arrow for $\vec{j}(\vec{r},t)$ is shown at the right side of panel (c). This figure is created on the basis of the data calculated for **Paper TK1** and **Paper TK2**.

As the computational expense of high-level wave function-based correlation methods scales poorly with increasing system size, their application is solely feasible for small molecular systems. To circum-

vent this issue, **Paper TK2** introduce a non-variational hybrid density functional theory/CI scheme. In the scope of this novel procedure, the multi-determinantal wave functions are constructed from Linear Response Time-Dependent Density Functional Theory (LR-TDDFT) calculations as pseudo CI singles eigenvectors. While the method benefits from the improved energetic description at virtually the same costs as a CI singles calculation, it maintains the simple electron-hole picture to characterize the transient many-electron dynamics. In order to confirm the applicability of this hybrid TDDFT/CIS scheme, it is benchmarked against different CI variants for the ultrafast charge migration process in the lithium hydride molecule. The mechanistic characteristics of the electron dynamics obtained from the hybrid scheme coincide semi-quantitatively with the results from the higher-level electronic structure methods. That means that the electronic flux density maps for the different methods agree qualitatively, while quantitative differences between the methods exist in the low electron density regions. Supplementary to this, the scalability of the hybrid approach is demonstrated by the charge migration in a moderately sized organic dye induced by a broadband laser excitation. In this context, a strategy to further speed-up the hybrid method is tested. That truncates the pseudo-CI basis to a few dominant configurations according to their contribution to the respective electronic state. Even for tight truncation criteria, the analysis tools, especially, the electronic flux density, reveal a robust predictive behavior for the major mechanistic features of the electron dynamics.

An overview of the most insightful analysis tools available within the DETCI@ORBKIT framework is depicted in Fig. 3.1. They are exemplary shown for the charge migration in a superposition state of the trihydrogen cation which is also used as a benchmark system in both DETCI@ORBKIT papers, **Paper TK1** and **Paper TK2**. As a final remark, it should be noted that the functionalities of the DETCI@ORBKIT framework as well as the underlying post-processing program ORBKIT are extensively exploited throughout the remaining publications.

In many photoinduced processes, the excitonic character of an optical transition plays a fundamental role, particularly, the spatial extent and intrinsic structure of an exciton as well as the electron-hole separation are of interest to understand such processes. While experimental optical spectra for extended and finite-sized systems can be satisfactorily reproduced by LR-TDDFT calculations within the Random-Phase Approximation (LR-TDDFT-RPA), the information about the excitonic nature of an optical transition cannot be obtained. To fill this void, **Paper TK3** extends the concept of Natural Transition Orbitals (NTO)[69] to semi-infinite periodic systems. This unitary orbital transformation technique uses the one-particle transition density matrix to provide a compact representation of many-body electronic wave functions as pairs of particle and hole functions (cf. Sec. 2.3.7). The novel approach approximates this transition density matrix with the transition dipole matrix, whose choice is

justified by first-order time-dependent perturbation theory. The obtained set of correlated particle-hole orbitals is termed Dipole-Induced Transition Orbitals (DITO). On the basis of the LR-TDDFT-RPA kernel, the DITOs are compared to the NTOs for a specific metal-to-ligand transfer in a typical metal complex. Both reveal the qualitatively identical picture for the physics of the studied optical excitation. A comparison between the NTOs and DITOs for a specific metal-to-ligand charge transfer band in this benchmark system is illustrated in Fig. 3.2 with the associated difference density as a reference. The suitability of the DITOs to characterize extended systems is presented for a model dye-sensitized solar cell composed of a MoS_2 surface with different coverages of phenol molecules. The analysis of the spatial distributions of the particle-hole functions for a low- and a high-energy optical band exhibits a clear distinction regarding their charge transfer nature. In particular, the findings indicate a charge transfer character for the low-energy band and a charge separated character for the high-energy band.

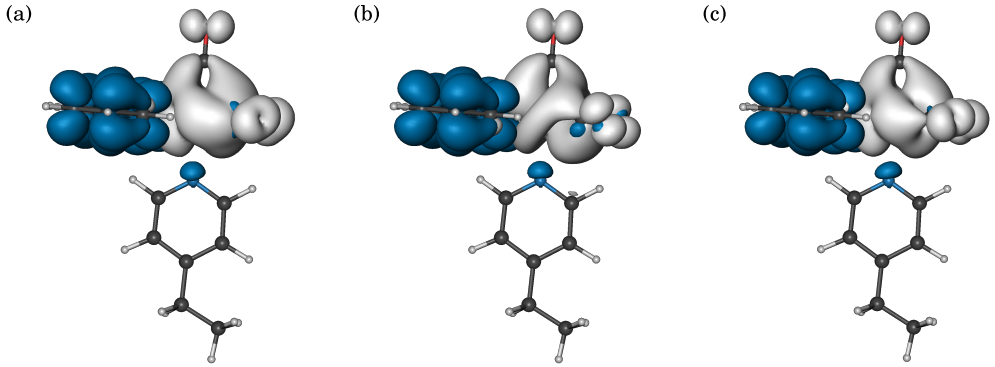

Figure 3.2: Comparison of particle (blue) and hole (gray) densities obtained from (a) NTOs and (b) (rotationally averaged) DITOs for the lowest-lying Metal-to-Ligand Charge Transfer transition (MLCT) in $[Re(bpy)(CO)_3(4\text{-}Etpy)]^+$. The ball-and-stick model of the molecule represents the rhenium, carbon, hydrogen, oxygen, and nitrogen atoms as cyan, dark gray, light gray, red, and blue beads. As a reference, the difference density (c) between the ground state and the excited states belonging to the MLCT excitation is depicted revealing regions of density depletion (gray) and concentration (blue). All quantities are in units of $1/a_0^3$ with an isosurface value of $10^{-3}a_0^{-3}$. These depictions are adapted from the **Paper TK3**.

In general, the set of analysis tools collected in the **Papers TK1–TK3** allows for the quantitative and qualitative mechanistic description of intricate many-electron dynamics. Starting with small molecular systems, **Papers SM1–SM3** focus on the investigation of ultrafast charge migration processes in different electronic superposition states of the hydrogen molecular ion and the benzene molecule. The **Paper SM1** applies a time-dependent analysis of the electron density, electronic flux density, and axial electronic flux to the hydrogen molecular ion in a coherent superposition state between the ground state (σ_g) and an excited state (σ_u) (cf. Figs. 3.4(a) and (c)). Both are represented in a minimal basis set at a frozen nuclear geometry. This state combination results in a spatial localization of the electron on one of the protons (cf. Fig. 3.4(c)). Its ultrafast time evolution shows a periodic oscillation

of the electron density between the two protons with a period, $\tau = 551\,\text{as}$, inversely proportional to the energy difference between the states. Based on the model of the electronically excited hydrogen molecular ion from Eyring, Walter, and Kimball[79], analytical expressions are derived for many dynamical properties including the electron density, the electronic yield, and the electronic flux density. Building upon these, fundamental symmetry relations for the electron density and electronic flux density are established revealing an abundance of spatial-temporal features. Among these, two fundamental findings are deduced from these relations. First, the electronic flux density unveils a unidirectional charge migration mechanism. Second, the electronic flux density on the internuclear axis reaches its maximum in time and space, where the electron density has a local minimum. As the hydrogen molecular ion is a one-electron system, another novel observation arises stating that the electron migration can occur without the influence of electron correlation.

In analogy, **Paper SM2** and **Paper SM3** elucidate the mechanism of two different charge migration processes in the benzene molecule by means of a qualitative and quantitative analysis of the time-dependent electron density. These studies were motivated by previous theoretical work from Ulusoy and Nest on the control of the aromaticity in benzene.[83] They demonstrated that two different non-aromatic electronic superposition states can be selectively prepared using a train of linearly polarized laser pulses which were designed by optimal control theory. These superposition states were generated by equally populating, on the one hand, the ground state $S_0(1^1A_{1g})$ and the first excited state $S_1(1^1B_{2u})$ and, on the other hand, the ground state $S_0(1^1A_{1g})$ and the second excited state $S_2(1^1B_{1u})$. As a criterion to measure their aromaticity, the bond order and Mulliken charges were determined for the respective target states. The results revealed that the aromaticity of the molecule can be switched off by a partial electron density localization on alternating carbon-carbon bonds for the target state, $S_0 + S_1$ (cf. Fig 3.3(a)), and on alternating carbon atoms for the target state, $S_0 + S_2$ (cf. Fig 3.3(b)). While the former resembles the Kekulé structure of benzene with an alternating bond pattern of single and double bonds, the second initiates a localization of negative and positive partial charges on alternating carbon atoms. Both scenarios lead to an oscillating charge migration between the two symmetrically equivalent localization patterns on an attosecond time scale (cf. Fig. 3.3). Their underlying mechanism was hypothesized as a pincer-type motion.

In order to corroborate these findings and to supplement them with the mechanistic and quantitative details of the electron motion, an expression for the angular electronic flux during the charge migration processes is developed for excited ring-shaped molecules. The underlying theory is transferred from previous work on concerted electronic and nuclear fluxes during coherent tunneling.[252] It employs the continuity equation and invokes suitable boundary conditions in order to convert the time-dependent

electron density to the angular electronic flux. This quantity allows to determine the angular direction of the electron flow and the number of migrating electrons during the charge migration in a ring-shaped system. In order to reconstruct the two superposition states investigated by Ulusoy and Nest, the electronic eigenstates were determined by a state-averaged CASSCF(6,6) calculation. The associated excitation energies were additionally improved by a MRCI singles and doubles calculation. The latter reveal the periods of $\tau = 830\,\text{as}$ and $\tau = 590\,\text{as}$ for the charge migration in the $S_0 + S_1$ and in the $S_0 + S_2$ superposition state, respectively. The time-resolved analysis of the angular electronic fluxes for both states unravels the mechanistic features of the electron motion which are depicted in Figs. 3.3(a) and (b). Both scenarios show a multidirectional pincer-type motion of the electrons migrating periodically from the regions of electron density concentration to regions of electron density deficiency on an attosecond timescale. These sources and sinks of the electron fluxes are located on the carbon-carbon bonds ($S_0 + S_1$) or on the carbon atoms ($S_0 + S_2$), respectively. Thus, the original conjecture of Ulusoy and Nest concerning the charge migration mechanism is proven unequivocally. Supplementary to this, the maximum number of electrons flowing concertedly during these processes is quantified to $N_{\text{el}} = 6 \times 0.12 = 0.72$ for state $S_0 + S_1$ and $N_{\text{el}} = 6 \times 0.2 = 1.2$ for state $S_0 + S_2$. This corresponds to the quantification of the arrows representing the electronic motion in Lewis structures as depicted in Fig. 3.3.

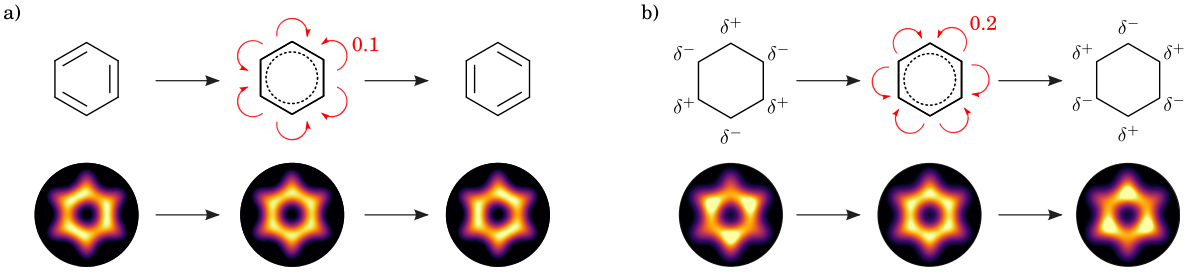

Figure 3.3: Schematic depiction of the charge migration mechanism during the first half period in the benzene molecule starting from two different superposition states: (a) $S_0(1^1A_{1g}) + S_1(1^1B_{2u})$ and (b) $S_0(1^1A_{1g}) + S_2(1^1B_{1u})$. Top row: Sequence of Lewis-type structures depicted at representative time steps of the charge migration, starting from a non-aromatic superposition state ($t = 0$) via a transition state with equally distributed electron density ($t = \tau/4$) to the symmetry equivalent non-aromatic superposition state ($t = \tau/2$). The red arrows indicate the angular direction of the electron flow revealing a multidirectional, pincer-type mechanism. Each arrow represents the migration of (a) 0.1 and (b) 0.2 electrons. Bottom row: Corresponding snapshots of the time-dependent electron density $\rho(\vec{r}, t)$ disclosing the electron localization patterns. These depictions are adapted from the **Paper SM2** and **Paper SM3**.

In order to give access to a more transparent formalism to the angular electronic fluxes, the calculations in **Paper SM2** were restricted to the dominant Slater determinants. This allows to reduce the complete wave function expansion to a few molecular orbital contributions facilitating the interpretation of the electronic fluxes. The outcomes obtained from this simplification demonstrate a robustness

with respect to the qualitative features of the electron motion as well as the quantification of the electron flow. Admittedly, the small variance in the magnitude of the flux can be ascribed to the omitted renormalization of the approximate wave functions.

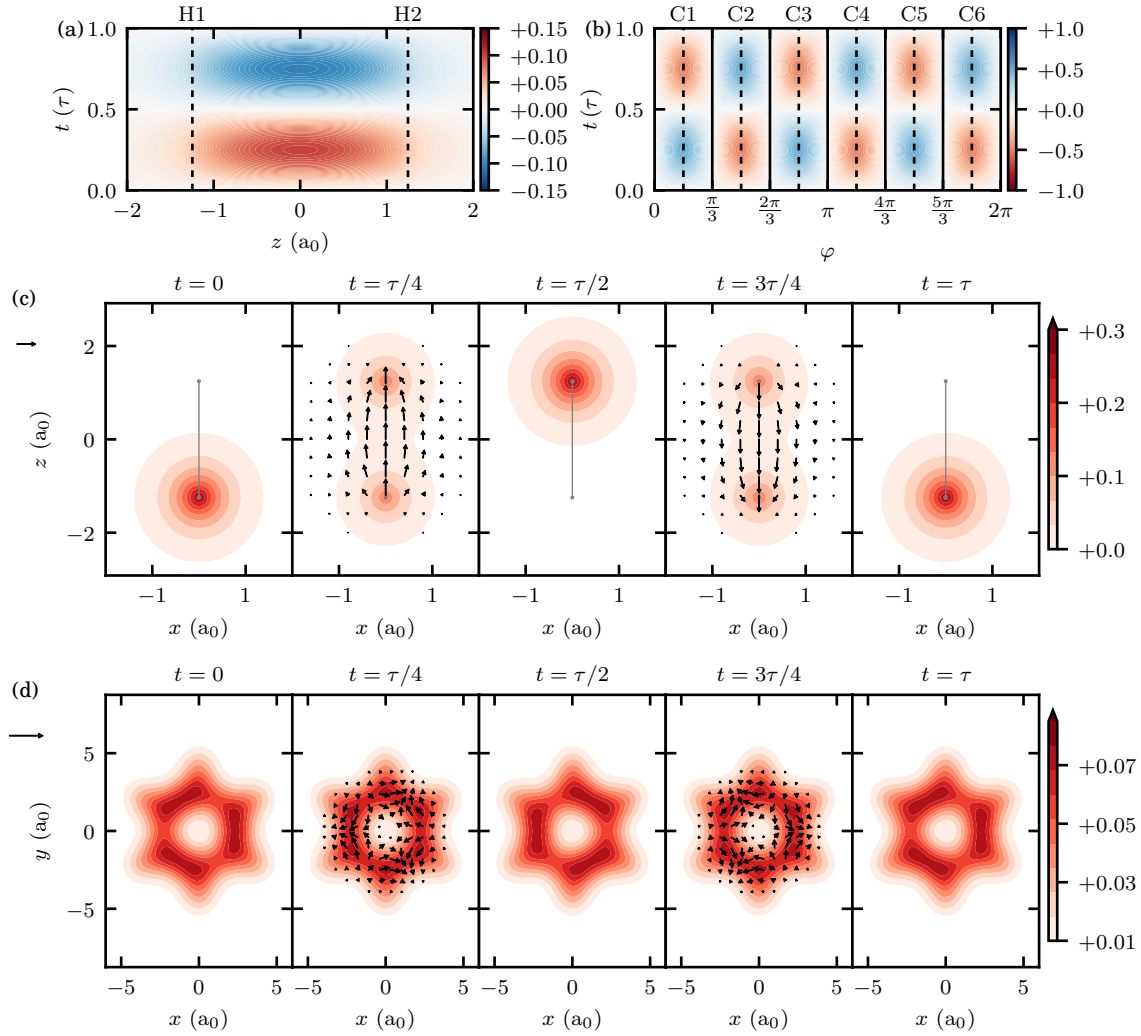

Figure 3.4: Comparison of the analysis tools applied in the **Papers SM1–SM3** to examine the mechanism of ultrafast charge migration processes in molecular systems. (a) Axial electronic flux as a function of time and (c) time evolution of the electron density and electronic flux density at representative time steps during one period of the charge migration process for the hydrogen molecular ion in the superposition state $\sigma_g + \sigma_u$. (b) Angular electronic flux as a function of time and (d) time evolution of the electron density and electronic flux density at representative time steps during one period of the charge migration process for the benzene molecule prepared in its superposition state $S_0(1^1A_{1g}) + S_1(1^1B_{2u})$. One reference vector for the flux density of each molecular system is located at the ordinate with the length of $3.0 \cdot 10^{-2}\, E_h/\hbar a_0^2$ for the hydrogen molecular ion (c) and with the length of $2.5 \cdot 10^{-3}\, E_h/\hbar a_0^2$ for the benzene molecule (d). These figures are adapted and created on the basis of **Paper SM1** and **Paper SM3**.

To summarize the analysis tools applied in the **Papers SM1–SM3**, Fig. 3.4 compares the axial/angular electronic flux and the combination of the time-dependent electron density with the associated electronic flux density for the hydrogen molecular ion and the benzene molecule. While the

latter offers an intuitive picture of the instantaneous flow of electrons, the former is a powerful tool for the quantitative investigation of ultrafast electron dynamics. However, convenient boundary conditions based on the system's symmetry have to be invoked for the determination of the axial/angular electronic fluxes.

In order to demonstrate the applicability of these analysis tools for more extended systems, the **Papers SC1–SC3** investigate photoinduced electron injection processes in different Dye-Sensitized Solar Cell (DSSC) models at the interface of an organic dye anchored to a TiO_2 nanoparticle. The general objectives of these studies comprised the modeling of a realistic DSSC and the simulation and time- and space-resolved examination of the electron migration from the dye into the TiO_2-cluster.

To accomplish the first goal, the following protocol was pursued in the three publications: First, the dye was attached via an anchoring group to a finite TiO_2 nanocrystallite mimicking either a colloidal nanoparticle or a thin film of titania. The geometry of this model system was optimized by means of a DFT calculation at a convenient level of theory. Second, the absorption spectra of the DSSC models were determined within the LR-TDDFT framework. Third, the electronic and optical properties of the model systems were verified by the comparison to experimental data, i.e., the energetic alignment and hybridization between the dye and the substrate and the optical absorption spectra. This ensured that the finite cluster models mimic the fundamental characteristics of a realistic solar cell.

As the prototypical DSSCs are constructed as finite cluster models to enable the analysis of the electron injection on an atomistic level, a fundamental component of the electron dynamical simulation is a complex absorbing potential. This suppresses artificial recurrences in the electron dynamics and reflections at the edges of the TiO_2 cluster. In the series of studies (**Papers SC1–SC3**), a projector formalism is developed affecting the boundary atoms of the TiO_2 cluster to simulate the contact with an infinite substrate. While the formulation of the absorbing potential in the **Paper SC1** and **Paper SC2** relies on a user-defined scaling factor to reproduce the experimental injection rates, a parameter-free expression is established in **Paper SC3**. The typical experimental injection time amounts to 6 fs for a colloidal TiO_2 substrate[104] and 60 fs for a thin film[105] and is considered as an intrinsic property of the TiO_2 cluster, independently of the dye.

The first application of the analysis and imaging tools, e.g., electronic flux density, electron density, electronic yield, and electronic flow, to unravel charge migration processes in complex molecular systems is presented in the **Paper SC1**. Here, it is exemplary shown for the alizarin dye attached to a colloidal $(TiO_2)_{15}$ cluster (cf. Fig. 3.5(a)). In order to facilitate the interpretation of the introduced analysis tools, an explicitly time-dependent single active electron approach is used to simulate the ultrafast photoinduced electron transfer from the dye into the cluster. Within this ansatz, an active electron

of an occupied Kohn-Sham orbital located on the dye is excited with a δ-pulse to the complete set of energetically accessible molecular orbitals. A qualitative analysis of these orbitals indicates that after an intrachromophore excitation, the electron injection is mediated by orbitals, which are localized on the substrate or delocalized over the entire DSSC. The usage of this ansatz is substantiated by the observation that the optical excitations of the DSSC are dominated by transitions from the selected active Kohn-Sham orbital.

As the formulation of the electronic flux from the **Paper SM2** and **Paper SM3** strictly requires to include a suitable symmetry condition of the molecular system, an alternative definition is derived on the basis of a projector formalism using a Voronoi partitioning. This enables to assign the quantitative contribution of the electron flow to a specific molecular fragment by following the time evolution of the integrated electronic flux and electronic yield. Thereby, the effect of coherences on the electron dynamics is investigated revealing that electron density located on the molecular fragments simply decays exponentially in the incoherent propagation. In contrast, the coherent dynamics exhibits a symmetric and synchronous Rabi oscillation between the two carbonyl groups (cf. Fig. 3.5(c)).

Due to the to some extent arbitrary definition of this projector formalism, electronic flux density maps are calculated to provide a more universal picture for the mechanistic features of the ultrafast charge migration. In detail, it is discovered that the charge injection is heavily affected by the carbonyl groups, while the aromatic rings solely act as mediators for the electron transfer between the carbonyl groups.

The main focus of the **Paper SC2** is to explore the effects of the dye-substrate binding mode and of many-electron correlations on the ultrafast electron migration promoted by a laser excitation. For the first study objective, two stoichiometric alizarin-TiO_2 complexes are constructed with two different dissociative anchoring motifs, i.e., the monodentate and the bidentate binding mode. The finite-sized TiO_2 cluster is modelled as a thin film carved out of the bulk anatase. To account for many-body effects in these DSSC models during electron migration, the single active electron approach from **Paper SC1** is compared to a time-dependent many-electron CI ansatz. The latter is based on the hybrid TDDFT/CIS scheme presented in **Paper TK2**. The validity of the one-electron ansatz is in turn corroborated by the prevailing contribution of the active orbital to the optically excitable states obtained from the TDDFT calculation.

Once again, the mechanistic pathway for the migrating electrons from the dye into the substrate is clarified using the previously introduced analysis tools in combination with the Voronoi projector technique. Independently of the binding mode in the DSSC complex and of the description of the electron dynamics, the space- and time-resolved evaluation of the electronic yields, electronic fluxes,

and electronic flux densities reveal similar charge transfer characteristics. They unveil an alternating electron flow from the dye to the TiO_2-cluster via the bonds of the anchoring groups. Comparing the two binding modes, it is observed that the electron injection process in the bidentate system proceeds one order of magnitude faster than in the monodentate complex. The methodological comparison of the one-electron and many-electron approach show a similar phenomenological behavior concerning the electronic structure and the overall electron dynamics. This indicates that many-body effects have only a marginal impact on the investigated DSSC models.

Thus, it is concluded that the single active electron approach is qualified for the description of electron migration processes in these type of systems. However, the many-body wave function ansatz shows more intricate mechanistic details of the charge migration. In addition, this ansatz opens up the possibility to shed light on the electron-electron and hole-hole contributions during the charge migration. For this purpose, a new decomposition technique for the electronic flux density is proposed revealing their spatial distribution and time evolution. While the electron-electron component is mainly localized on the TiO_2-substrate, the hole-hole component is mainly distributed on the dye. Both show a slower fluctuation compared to the complete electronic flux density.

In the last paper (SC3) of this series, a comparative examination is conducted for three different donor-acceptor π-conjugated dyes attached to a colloidal TiO_2-cluster. A special emphasis is put on the characterization of their potential performance and photon-to-current efficiency from a static point of view. The donor-π-acceptor-type dyes consist of an expanded π-conjugated molecular skeleton containing a pyridinium ring as electron acceptor, an amino group as electron donor, and a carboxylate group as anchoring group to the substrate (exemplary, cf. Fig. 3.5(b)). The three photosensitizers under investigation mainly differ by the extent of their condensed π-conjugated scaffold and by the type of their amino group.

In order to specify their achievable photovoltaic output from a static perspective, parameter-free expressions are established for the crucial properties determining their photon-to-current conversion efficiency, i.e., the state-resolved injection time and current. Their validity to yield quantitative correct statements is confirmed by the comparison to typical experimental values. On the basis of their analysis for the three DSSC complexes, it is deduced that the extent of the condensed π-conjugated system is the decisive structural feature for their photovoltaic efficiency. Additionally, this feature also influences the sunlight harvesting properties of the dyes. This observation is a consequence of the location of the absorption maxima in the simulated optical absorption spectra.

To supplement these findings with the dynamical aspects of a realistic ultrafast electron migration process, a broadband laser excitation of the optical band in each model system is simulated in real time

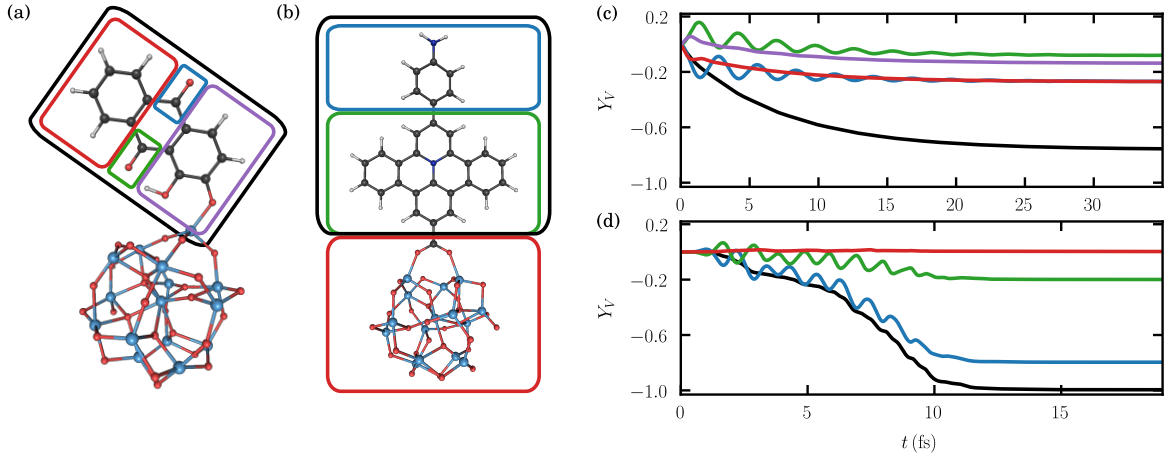

Figure 3.5: Time- and space-resolved analysis of different charge migration processes in two DSSC models by means of the projector formalism based on a Voronoi partitioning scheme. Ball-and-stick models for the optimized molecular structures of the selected dye-TiO_2 complexes investigated in (a) **Paper SC1** and (b) **Paper SC3**. The dark gray, light gray, blue, red, and cyan beads represent carbon, hydrogen, nitrogen, oxygen, and titanium, respectively. Time evolution of the electronic yields $Y_V(t)$ during the different charge migration dynamics from the dye into the TiO_2 semiconductor for the DSSC complexes in (c) **Paper SC1** and (d) **Paper SC3**. The electronic yields are determined for different characteristic molecular fragments. These are defined as boxes in the ball-and-stick models which are colored as the curves in the charts. The dynamical simulations were carried out using the single active electron approach initiated by a δ-pulse for the system in **Paper SC1** and a broadband laser excitation for the DSSC model in **Paper SC3**. The figures are adapted from **Paper SC1** and **Paper SC3**.

by means of the single active electron approach. The adequacy of this approach is again confirmed by the molecular orbital transition contributions to the excited states. In analogy to the previous studies, the time-dependent one-electron density and the electronic yields partitioned for selected molecular fragments are used to elucidate the mechanistic course of the migrating electron. A fluctuation of electron density between the electron donor and electron acceptor group with a contemporaneous injection into the TiO_2-substrate is observed for the three DSSC models (exemplary, cf. Fig. 3.5(d)). In accordance with the static investigation, the performance of the dyes is slightly enhanced by the size of the π-system.

In order to emphasize the usefulness of the projector formalism based on the Voronoi partitioning scheme, Fig. 3.5 shows the analysis of the charge migration in two selected DSSC model systems from **Paper SC1** and **Paper SC3**. It corroborates the suitability of the formalism to yield an time- and space-resolved evaluation of ultrafast electron dynamics with additional information about the contributions of specific molecular fragment during the dynamical process.

The last study in this thesis, **Paper QD1**, deals with the laser-controlled charge carrier confinement in a solid state quantum dot with a special focus on the enhancement of the charge trapping efficiency. To this end, a model quantum dot is constructed as a nanometer-size Ge/Si core-shell system maintaining the important structural and excitonic properties of experimentally observed self-

assembled pyramidal Ge/Si quantum dots. In detail, a small dome-shaped Ge impurity is embedded in a Si host matrix consisting of a few Si shells. The simulation of the electron dynamics in the Ge/Si model quantum dot is achieved by means of a fully atomistic, correlated many-electron ansatz. Specifically, the reduced density matrix variant of the time-dependent configuration interaction method (ρ-TDCI)[253–257] for open systems is applied for the first time to a nanostructured solid state system. It allows to incorporate the effects of energy relaxation and pure dephasing as couplings of the local core-shell structure with vibrations of the surrounding Si environment. For this purpose, a perturbative model for these nonadiabatic coupling rates is developed scaling with the inverse of the electronic energy difference squared. Interestingly, the same scaling is found in the Fermi liquid theory for three-dimensional metallic systems.[258]

Hole confinement in the Ge/Si nanocrystal is accomplished by state-selective laser excitations. In order to evaluate the degree of charge confinement for a certain interlevel transition path, the associated one-electron difference densities obtained from the correlated many-electron wave functions were analyzed from a static perspective. Two transition pathways, direct and indirect, are determined yielding the highest hole confinement in the vicinity of the Ge nanocrystal. The dynamical simulation following these two pathways reveal that the direct excitation mechanism is strongly affected by polarization and other nonlinear field-molecule effects, while the indirect mechanism offers a more efficient and robust way to confine a hole state in the Ge quantum dot and to create long-lived permanent dipoles in such systems. In addition, it is observed that energy relaxation and pure dephasing induced by the nonadiabatic couplings play a rather subordinate role in the electron dynamics.

Chapter 4

Publications

The subsequent chapter presents the scientific publications which form the core of this dissertation. These publications consist of published papers and papers to be submitted for publication. In order to give a thematic classification of these studies, they are assigned to four different groups:

- **TK** An open-source toolkit for analyzing electronic excitations and many-electron dynamics
- **SM** Mechanistic analyses of charge migration processes in small molecules
- **SC** Ultrafast photoelectron migration in dye-sensitized solar cells
- **QD** Laser-driven electron dynamics of a Ge/Si core-shell quantum dot

The contributions of the individual authors to the conceptualization, execution, and preparation of each publication are reported as introductory remarks in the following section.

Paper TK1

An Open-Source Framework for Analyzing N-Electron Dynamics. I. Multideterminantal Wave Functions

V. Pohl, G. Hermann, and J. C. Tremblay

J. Comput. Chem. **38**, 1515–1527 (2017)

DOI: 10.1002/jcc.24792

URL: https://doi.org/10.1002/jcc.24792

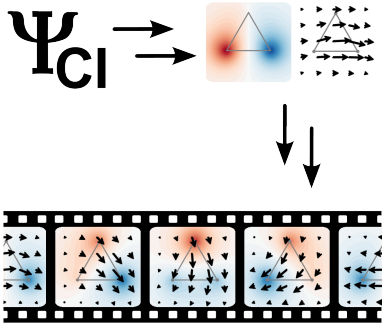

Figure 4.1: Graphical Abstract. Reprint with permission from Pohl et al.[TK1] (©2017 Wiley Periodicals, Inc.)

Author contributions

DETCI@ORBKIT is a modular post-processing toolkit for multi-determinantal wave functions based on the functionalities of ORBKIT (cf. **Paper AP2**). Vincent Pohl and I started to program the first modules for this toolkit during the work for **Paper AP1** which was supervised by Jhon Fredy Pérez Torres. Throughout the dissertations of Vincent Pohl and myself, we further developed the program in equal parts. A commonly usable version of the program was equally developed by Vincent Pohl and myself as a result of the work for **Paper SM3**. The implemented general methodology to post-process CI wave functions was derived in collaboration with Jean Christophe Tremblay. To benchmark the methodology, Vincent Pohl performed Full CI and different CASSCF calculations for a number of molecular test systems. For this purpose, he interfaced the respective quantum chemical programs, PSI4[259] and MOLPRO[260]. The quantities, i.e., electronic flux density and electron density, to analyze correlated many-electron dynamics in the test systems were calculated and illustrated by Vincent Pohl and myself for the different CI methods. The manuscript was prepared by myself with input from Jean Christophe Tremblay and Vincent Pohl.

Paper TK2

An Open-Source Framework for Analyzing N-Electron Dynamics. II. Hybrid Density Functional Theory/Configuration Interaction Methodology

G. Hermann, V. Pohl, and J. C. Tremblay

J. Comput. Chem. **38**, 2378–2387 (2017)

DOI: 10.1002/jcc.24896

URL: https://doi.org/10.1002/jcc.24896

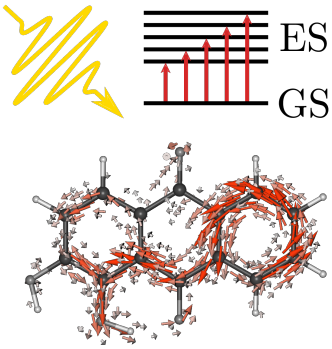

Figure 4.2: Graphical Abstract. Reprint with permission from Hermann et al.[TK2] (©2017 Wiley Periodicals, Inc.)

Author contributions

The hybrid DFT/CI methodology was initially developed and applied by Jean Christophe Tremblay and myself in **Paper SC2**. I implemented this approach into the post-processing toolkit DETCI@ORBKIT and additionally created interfaces to a number of quantum chemical programs, i.e., TURBOMOLE[261] and GAMESS (US)[262], providing an electronic structure characterization by means of LR-TDDFT. To benchmark the hybrid approach, Vincent Pohl and I performed LR-TDDFT calculations in comparison to different CI methods for selected model systems. The evaluation and visualization of the results were accomplished by Vincent Pohl and myself. Jean Christophe Tremblay and I wrote the manuscript with input from Vincent Pohl.

Paper TK3

Dipole-Induced Transition Orbitals - A Novel Tool for Investigating Optical Transitions in Extended Systems and its Application to Dye-Sensitized MoS_2

G. Hermann, L. E. Marsoner Steinkasserer, B. Paulus, and J. C. Tremblay

Manuscript in preparation

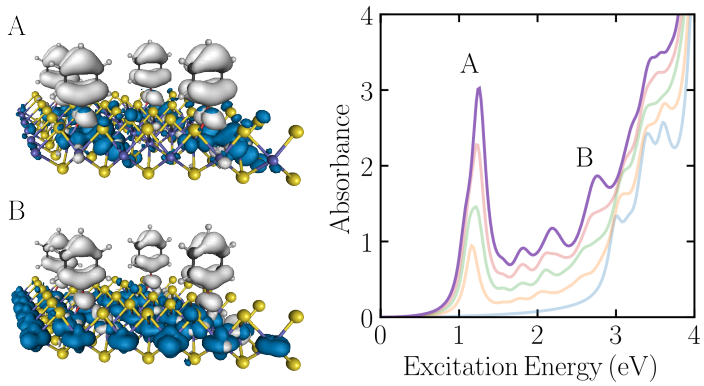

Figure 4.3: Graphical abstract, particularly created for this thesis on the basis of the figures from Paper TK3.

Author contributions

The initial proposal for the Dipole-Induced Transition Orbitals (DITO) was conceived by Lukas Eugen Marsoner Steinkasserer and myself. Together with Jean Christophe Tremblay, we developed the underlying theoretical framework. The implementation of the methodology in the open-source framework DETCI@ORBKIT[TK1] was conducted by myself. The suitability of the DITOs for the characterization of electronic excitations was verified by myself by comparing them to natural transition orbitals for a molecular metal complex. I likewise performed the necessary electronic structure calculation. For the application of the DITOs to semi-infinite systems, Lukas Eugen Marsoner Steinkasserer and myself characterized the electronic structure for different dye-sensitized MoS_2 systems. The DITOs for different optical transitions were calculated by myself. All coauthors discussed and interpreted the results. The first draft of the manuscript was prepared by Lukas Eugen Marsoner Steinkasserer and myself. The final version was revised by Jean Christophe Tremblay with contributions from all coauthors.

Dipole-Induced Transition Orbitals — A Novel Tool for Investigating Optical Transitions in Extended Systems and its Application to Dye-Sensitized MoS_2

Gunter Hermann,* Lukas Eugen Marsoner Steinkasserer,
Beate Paulus, and Jean Christophe Tremblay
Institut für Chemie und Biochemie, Freie Universität Berlin,
Takustraße 3, D-14195 Berlin, Germany

(Dated: July 19, 2018)

Abstract

Linear response time-dependent density functional theory within the random-phase approximation (LR-TDDFT-RPA) provides a quick and easy way to compute the optical spectra of extended and finite-sized systems from first principles. While the method is nowadays routinely applied, many important properties, such as the charge transfer character associated with a particular transition, cannot be obtained from it. Inspired by the concept of *natural transition orbitals* [J. Chem. Phys. **118**, 4775 (2003)], we formulate a perturbative orbital transformation theory based on the dipole induced transitions appearing in the LR-TDDFT-RPA kernel. This theory yields correlated pairs of particle and hole functions retaining the character of the natural transition orbitals. In order to demonstrate the potency of this new transformation formalism, we investigate the nature of excitations in dye-sensitized MoS_2 for potential solar cell applications. By applying our method, it is possible to extract mechanistic insights from the transitions observed in the optical spectrum, which are unattainable by conventional RPA calculations.

* gunter.hermann@zedat.fu-berlin.de

I. INTRODUCTION

First principle calculations of optical properties have become an invaluable tool for experimental physicists and chemists to corroborate as well as to interpret their results. On the other hand, the corresponding theoretical stream of research has seen a strong move towards the usage of high-throughput calculations to systematically screen for new materials with properties tailored towards specific applications[1–3]. Hence, both disciplines need tools capable to capture all important features associated with specific optical excitations in finite and periodic systems. While experimental spectra can often be reproduced with good accuracy by the linear response time-dependent density functional theory within the random-phase approximation (LR-TDDFT-RPA)[4–6], the excitonic nature of a particular transition and the spatial distribution of the corresponding particles and holes are not retrievable.

To address this issue, Richard L. Martin introduced the concept of *natural transition orbitals* (NTOs) as singular value vectors of the one-particle transition density matrix[7]. This formalism allows to characterize the nature of many-body electronic wave functions in terms of correlated particle-hole pairs. The NTOs provide a direct, graphical way of interpreting electronic excitations associated with specific spectral features and yield important parameters for the quantitative characterization of charge transfer states. Given the simplicity and the success of the method, an extension to semi-infinite periodic systems appears highly desirable. Unfortunately, the LR-TDDFT-RPA ansatz often used to study such systems precludes a direct application of the NTO theory. To fill this void, we define here a novel orbital transformation matrix motivated by the LR-TDDFT-RPA kernel and the time-dependent perturbation theory. We propose the usage of the transition dipole matrix as a measure to obtain what we term *dipole-induced transition orbitals* (DITOs). Although approximate, this new set of correlated particle-hole orbitals is shown to capture the same physics as the NTOs for optical excitations in isolated molecules. The underlying concept of the DITOs is general and not limited to the case of LR-TDDFT-RPA, as presented here. Generally, it can be further applied to any method, which allows for the calculation of the transition dipole matrix.

II. DIPOLE-INDUCED TRANSITION ORBITALS

Our derivation starts with the Bethe-Salpeter equation (BSE) for the electron-hole correlation function $L(\mathbf{12};\mathbf{1'2'})$, in the form given by Strinati[8–10] and by Rohlfing and Louie[11],

$$L(\mathbf{12};\mathbf{1'2'}) = L_0(\mathbf{12};\mathbf{1'2'}) + \int d(\mathbf{3456}) L_0(\mathbf{14};\mathbf{1'3}) K(\mathbf{35};\mathbf{46}) L_0(\mathbf{62};\mathbf{52'}). \tag{1}$$

Here, $K(\mathbf{35};\mathbf{46})$ corresponds to the electron-hole interaction kernel, and $L_0(\mathbf{12};\mathbf{1'2'})$ denotes the free electron-hole pairs. Each set of variables $(\mathbf{1})$ contains a spatial, a spin, and a time coordinate, $(\mathbf{1}) = \{\mathbf{x_1}, t_1\}$, with $\mathbf{x_1} = \{\mathbf{r_1}, s_1\}$. Although the electron-hole correlation function depends on four time variables, Eq. (1) can be simplified for optical transitions, which are characterized by simultaneous creations/annihilations of holes and particles. Taking the Fourier transform of the difference between the remaining two time variables finally yields the particle-hole response function, $L(\mathbf{x}_1, \mathbf{x}_2; \mathbf{x}'_1, \mathbf{x}'_2; \omega)$. In the quasi-particle approximation, the long-lived transitions describe electron-hole excitations, and the correlation function takes the following form

$$L(\mathbf{x}_1, \mathbf{x}'_1; \mathbf{x}_2, \mathbf{x}'_2; \omega) = i\hbar \sum_{\lambda} \left[\frac{\chi^{(\lambda)}(\mathbf{x}_1, \mathbf{x}'_1) \left(\chi^{(\lambda)}(\mathbf{x}'_2, \mathbf{x}_2)\right)^*}{(E^{(\lambda)} - E^{(0)}) - \hbar\omega} - \frac{\chi^{(\lambda)}(\mathbf{x}_2, \mathbf{x}'_2) \left(\chi^{(\lambda)}(\mathbf{x}'_1, \mathbf{x}_1)\right)^*}{(E^{(\lambda)} - E^{(0)}) + \hbar\omega} \right]. \tag{2}$$

The poles of the correlation function are associated with excitation energies $(E^{(\lambda)} - E^{(0)})$ from a reference state $\lambda = 0$. The residuals of these poles define the particle-hole amplitudes

$$\chi^{(\lambda)}(\mathbf{x}, \mathbf{x}') = \left\langle \Psi^{(0)} \left| \hat{\psi}^\dagger(\mathbf{x}) \hat{\psi}(\mathbf{x}') \right| \Psi^{(\lambda)} \right\rangle, \tag{3}$$

which determine the character of these resonances. The general field operators $\hat{\psi}(\mathbf{x})$ and $\hat{\psi}^\dagger(\mathbf{x})$ can be expanded in terms of single-particle and single-hole creation operators

$$\hat{\psi}(\mathbf{x}) = \sum_{p,s} \phi_p(\mathbf{r}) \hat{a}_{p,s} \quad ; \quad \hat{\psi}^\dagger(\mathbf{x}) = \sum_{p,s} \phi^*_p(\mathbf{r}) \hat{a}^\dagger_{p,s}. \tag{4}$$

Substituting in Eq. (3) reveals the connection between the particle and hole functions

$$\chi^{(\lambda)}(\mathbf{r}_H, \mathbf{r}_P) = \sum_{pq,ss'} \phi^*_p(\mathbf{r}_H) \left\langle \Psi^{(0)} \left| \hat{a}^\dagger_{p,s} \hat{a}_{q,s'} \right| \Psi^{(\lambda)} \right\rangle \phi_q(\mathbf{r}_P) = \sum_{pq} \phi^*_p(\mathbf{r}_H) \mathbf{T}^{(\lambda)}_{pq} \phi_q(\mathbf{r}_P) \tag{5}$$

as well as with the transition density matrix $\mathbf{T}^{(\lambda)}_{pq}$.

The original formulation of NTOs uses the transition density matrix in order to determine unitary transformations linking the set of ground-state molecular orbitals (MOs) to the

NTOs. In the case of a single determinantal reference state, we can restrict the set of hole and particle creation operators to those defining the orbitals of the reference $|\Psi_0\rangle$. The many-body excited state wave function $\left|\Psi^{(\lambda)}\right\rangle$ is then expressed as a linear combination of single-particle/single-hole excitations as

$$\left|\Psi^{(\lambda)}\right\rangle = \sum_{pq} \mathbf{T}^{(\lambda)}_{pq} \hat{a}^{\dagger}_{q} \hat{a}_{p} \left|\Psi^{(0)}\right\rangle, \tag{6}$$

where p/q now runs only over occupied/unoccupied orbitals. To construct the NTOs, we first take the singular value decomposition of the transition density matrix

$$\mathbf{T}^{(\lambda)} = \mathbf{U}^{(\lambda)} \mathbf{\Sigma}^{(\lambda)} \left(\mathbf{V}^{(\lambda)}\right)^{*}, \tag{7}$$

where $\mathbf{\Sigma}^{(\lambda)} = \mathrm{diag}(\sigma^{(\lambda)}_{1}, \sigma^{(\lambda)}_{2}, \dots)$ is the diagonal matrix of the singular values of the transition density matrix. Substituting in Eq. (5) and simplifying yields

$$\chi^{(\lambda)}(\mathbf{r}_H, \mathbf{r}_P) = \sum_{a} \tilde{\phi}^{*}_{a}(\mathbf{r}_H) \sigma^{(\lambda)}_{a} \bar{\phi}_{a}(\mathbf{r}_P). \tag{8}$$

The transformation matrices in Eq. (7) are used to uniquely define the two sets of particle and hole orbitals as

$$\tilde{\phi}_{a}(\mathbf{r}_H) = \sum_{p} \mathbf{U}^{(\lambda)}_{pa} \phi_{p}(\mathbf{r}_H) \quad ; \quad \bar{\phi}_{a}(\mathbf{r}_P) = \sum_{q} \mathbf{V}^{(\lambda)}_{aq} \phi_{q}(\mathbf{r}_P). \tag{9}$$

The singular values $\sigma^{(\lambda)}_{a}$ serve as weights for the correlated particle-hole orbitals, which can be combined to yield an intuitive excitonic representation of the many-body excited state wave function.

Our method follows a similar rational but aims to circumvent the usage of a transition density matrix at the LR-TDDFT-RPA level of theory. To this end, we advocate using the transition dipole matrix to define transformation matrices from the basis of Kohn-Sham orbitals to the basis of correlated particle-hole orbitals. From the velocity gauge, the dipole matrix along a specific orientation α, $\mathbf{D}_{pq,\alpha}$, is given by

$$\mathbf{D}_{pq,\alpha} = \sum_{ss'} \frac{\hat{e}_{\alpha} \left\langle \psi_{p,s} \left| \nabla_{\alpha} \right| \psi_{q,s'} \right\rangle}{\epsilon_{p,s} - \epsilon_{q,s'}}, \tag{10}$$

where $\psi_{p,s}/\psi_{q,s'}$ are single-particle wave functions, and $\hat{e}_{\alpha}$ is the unit-vector along the three spatial direction, $\alpha \in \{x, y, z\}$. The reason for choosing the transition dipole moment matrices to construct the transition orbitals lies in its close connection to the imaginary part

of the frequency-dependent dielectric function in the LR-TDDFT-RPA ansatz, ($\mathcal{I}_\alpha\left[\varepsilon(\omega)\right]$). In the optical limit and neglecting local field effects, the imaginary part of the frequency-dependent dielectric function is given for a chosen direction (α) by

$$\mathcal{I}_\alpha\left[\varepsilon(\omega)\right] = \frac{4\pi\eta}{\Omega}\sum_{pq}\sum_{ss'}\frac{f_{q,s'}-f_{p,s}}{\left(\omega-\epsilon_{p,s}+\epsilon_{q,s'}\right)^2+\eta^2}\left|\frac{\hat{e}_\alpha\,\langle\psi_{p,s}\left|\nabla_\alpha\right|\psi_{q,s'}\rangle}{\epsilon_{p,s}-\epsilon_{q,s'}}\right|^2. \tag{11}$$

Here, η is a positive infinitesimal constant, and Ω is the volume of the unit cell. The transition dipole moment matrices contain the information about frequency-dependent intensity of the imaginary part of the LR-TDDFT-RPA, frequency-dependent dielectric function, which in turn is directly related to the optical absorption spectrum. The physics for the creation of a particle-hole pair via an external field is thus fully included in the $\mathbf{D}_\alpha$ matrices.

To analyze the character of the transitions using the new *dipole-induced transition orbitals* (DITOs), the various contributions to the LR-TDDFT-RPA spectrum in Eq. (11) must first be assigned to different bands. The subset of orbital transitions belonging to a specific band are subsequently used to define rectangular dipole matrices for each band. For a given band S in the spectrum with frequency $\omega^{(S)}$, the density matrix associated with the dipole-induced transition can then be approximated by first-order time-dependent perturbation theory as

$$\mathbf{T}^{(S)}_{pq,\alpha} = N_\alpha\left|\mathbf{D}_{pq,\alpha}\right|^2\delta\left(\epsilon_p-\epsilon_q-\hbar\omega^{(S)}\right) \tag{12}$$

with N_α as a normalization constant that ensures the particle/hole conservation. For practical applications, the delta distribution is replaced by a broadened Gaussian function obtained by fitting the spectrum for the subset of orbitals within a band. By computing the singular value decomposition of the resulting perturbative transition density matrix, we define two sets of transformation matrices

$$\mathbf{T}^{(S)}_\alpha = \mathbf{K}^{(S)}_\alpha\mathbf{\Sigma}^{(S)}_\alpha\left(\mathbf{L}^{(S)}_\alpha\right)^* \tag{13}$$

$$\tilde{\gamma}_{a,\alpha}(\mathbf{r}_H) = \sum_p \mathbf{K}^{(S)}_{pa,\alpha}\phi_p(\mathbf{r}_H) \tag{14}$$

$$\bar{\gamma}_{a,\alpha}(\mathbf{r}_P) = \sum_q\left(\mathbf{L}^{(S)}_{aq,\alpha}\right)^*\phi_q(\mathbf{r}_P), \tag{15}$$

where $\mathbf{\Sigma}^{(S)}_\alpha = \mathrm{diag}(\sigma^{(S)}_{1,\alpha},\sigma^{(S)}_{2,\alpha},\dots)$. The transformed sets of particle and hole orbitals can be used to approximate the transition density matrix as a weighed combination of DITOs, i.e.

$$\chi^{(S)}_\alpha(\mathbf{r}_H,\mathbf{r}_P) \simeq \sum_a \tilde{\gamma}^*_{a,\alpha}(\mathbf{r}_H)\sigma^{(S)}_{a,\alpha}\bar{\gamma}_{a,\alpha}(\mathbf{r}_P) \tag{16}$$

For extended systems, independent sets of DITOs along the three spatial directions $\alpha = x, y, z$ can be distinguished experimentally. For molecular spectra in the gas phase, where orientation plays no role, the density matrix elements in Eq. (12) are spherically averaged by summing over all three Cartesian contributions.

III. RESULTS AND DISCUSSION

In light of the previously discussed analogy between our definition of DITOs and the NTOs, we first compare the results obtained with both methods for a well-characterized benchmark system. For this purpose, we choose the $[\mathrm{Re(bpy)(CO)_3(4\text{-}Etpy)}]^+$ complex and analyze the particle and hole densities for the lowest-lying metal-to-ligand charge transfer (MLCT) absorption band as in Ref. 7. The electronic ground state structure for this metal complex is calculated at the density functional theory level (DFT) using a Def2-SVP basis set[12, 13] and the PBE0[14] functional. The corresponding orbitals serve as the computational basis for the DITOs and NTOs. In addition, the first low-lying excited eigenstates are required for the determination of the NTOs and specified by means of a time-dependent DFT (TDDFT) calculation in the linear response regime. As described above, the NTOs are calculated on the basis of the one-electron transition density matrices between the ground state and the excited states belonging to the MLCT absorption band. The DITOs are obtained from the molecular orbital transition dipole moments averaged over the given peak. All quantum chemistry calculations are performed using the TURBOMOLE program package[15], and both the NTOs and the DITOs are evaluated using the open source post-processing toolbox ORBKIT[16].

The comparison of the MLCT character obtained from the NTOs and the DITOs is shown in Fig. 1 for two orientations of the molecular complex. Despite marginal differences in the depth of the nodal structures, all qualitative features concur perfectly. The plots further demonstrate the power of both, the DITOs and the NTOs, to provide a quick and graphical tool for interpreting optical transitions and analyzing the spatial distribution of particles and holes. In sum, solely a small number of natural transition orbital pairs are usually required to determine the excitonic nature of a specific transition. This is in stark contrast to the respective characterization by means of many-body wave functions or fully-fledged TDDFT, which can quickly become a cumbersome task. In particular for complex extended

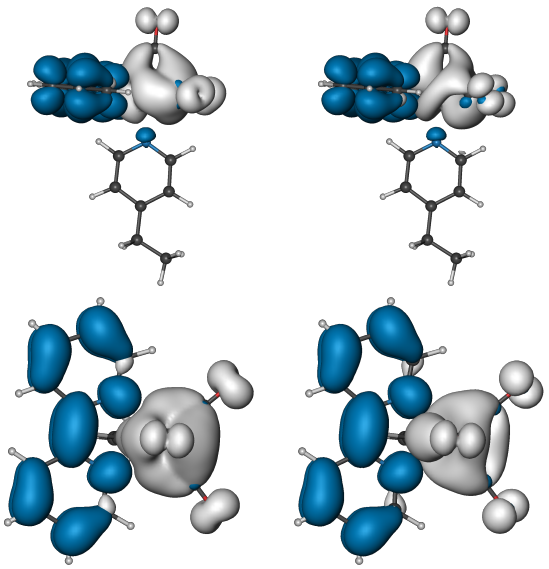

FIG. 1. Comparison of particle (blue) and hole (gray) densities between NTOs and (rotationally averaged) DITOs for the lowest-lying transition in $[Re(bpy)(CO)_3(4\text{-}Etpy)]^+$. The isosurface value of the densities is set to $0.001\,a_0^{-3}$

.

systems, a spectral feature often corresponds to a large number of individual (state-to-state) transitions. In order to further enhance the computational efficiency of the NTO formalism, the DITOs are obtained solely on the basis of orbital transitions, which renders the scheme numerically very advantageous. This comes at the expenses of accuracy losses in the optical spectrum at the LR-TDDFT-RPA level of theory, but qualifies them for high-throughput screening of optically active materials. In addition, its concept can be extended to semi-infinite systems.

As an example for such a semi-infinite system and to further demonstrate the capabilities of the DITOs, we investigate the excitonic properties of phenol-sensitized MoS_2 to elucidate the nature of specific electronic excitations in the optical spectrum. Over the past few years, MoS_2 has attracted much attention as an environmentally stable material possessing an attractive optical gap.[17–28] Its advantageous properties qualifies it for many applications including the construction of light-weight, ultra-thin solar-cells.

In light of the success of dye-sensitized solar cells (DSSC) employing TiO_2 substrates[29–35], it is reasonable to assume that the optical properties of MoS_2 might be further enhanced

by targeted functionalization.[36–40] In order to ascertain the performance of different potential functionalizing groups, a detailed mechanistic understanding of the optical excitations within such structures, i.e., the excitonic character and the degree of charge separation for certain features in the optical spectrum, is indispensable. To obtain these information, DITOs are ideally suited allowing a clear and physically meaningful visualization and evaluation of the optical excitations.

In the present study, the phenol molecules are chosen as sensitizers for the MoS_2 surface. These can be seen as analogues to the catechol dye, which is a typical chromophore used in dye-sensitized solar cells.[41–44] Different degrees of phenol coverage are modeled on a 6×6 MoS_2 supercell. The respective structure relaxations are performed using the GPAW program[45–50] and employing a LCAO representation for the pseudo wave functions. All calculations are carried out with a double-ζ polarized basis set and a Γ-centered 2×2 Monkhorst-Pack grid to sample the primitive Brillouin zone. The libvdwxc[51] implementation of the vdW-DF-CX functional[52–55] is employed throughout. The optimized structures of the prototypical dye-sensitized MoS_2 model systems are depicted in Fig. 2(a). The associated optical absorption spectra are determined at the LR-TDDFT-RPA level of theory, as implemented in ORBKIT[16]. The required orbitals are extracted from the results of periodic DFT calculations. These are performed with TURBOMOLE[15] using the LDA functional and a **k**-point sampling, which is limited to the Γ-point[56]. The results for the optical absorption spectra of the MoS_2 systems with a varying density of phenol-functionalization are shown in Fig 2(b). To verify the validity of our implementation of the LR-TDDFT-RPA formalism, we performed a comparative LR-TDDFT-RPA calculation using GPAW[57, 58] with a 9×9 Monkhorst-Pack grid and a numerical double-ζ polarized basis set. The resulting spectrum is illustrated in Fig. 2(b) (dashed lines). The energetic position of the bands satisfactorily coincides with the spectrum obtained on the basis of the TURBOMOLE calculation. The differences in the intensities of the optical features partially result from the incomplete **k**-point sampling in our implementation. Nonetheless, the spectrum is of sufficient quality for semi-quantitative analyses.

The examination of the excitonic nature of the phenol-sensitized MoS_2-surface, is solely focused on excitations caused by P-polarized light, since these proved to be most sensitive towards functionalizations. In contrast, excitations due to S-polarized light are largely dominated by MoS_2-localized transitions and are only weakly affected by the sensitization with

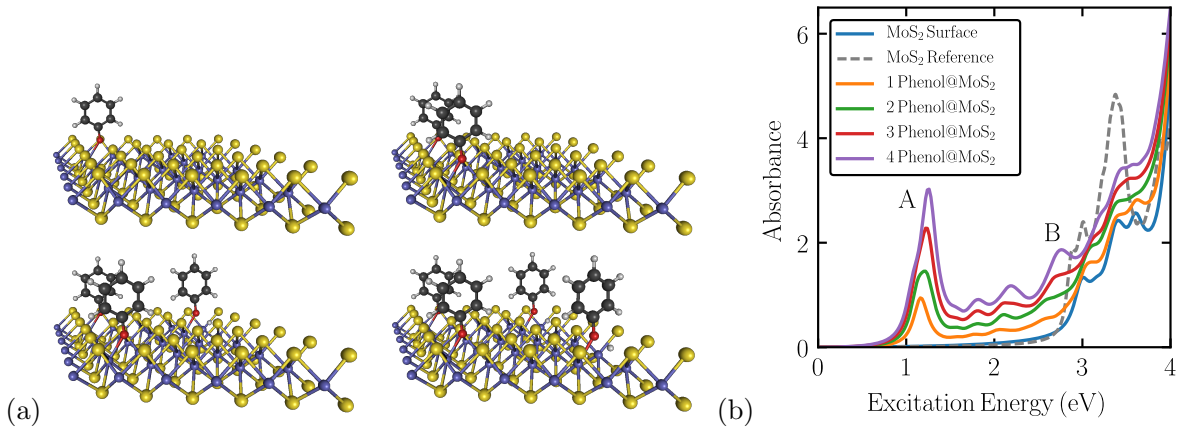

FIG. 2. (a) Structures of phenol-sensitized MoS_2-surface and (b) the associated optical RPA spectra in comparison to the clean MoS_2-surface.

the phenol molecules. From the optical spectra in Fig. 2(b), a very interesting trend can be immediately identified stemming from the functionalization of the MoS_2-surface. While pristine MoS_2 shows the onset of a large optical band at ≈ 2.5 eV with no discernible features below that threshold, a second peak appears in the low-energy part of the spectrum due to the sensitization with the phenol molecules. The peak becomes more prominent, as the density of phenol groups is increased. Furthermore, a shoulder below the high-intensity band and a few weaker peaks covering the $1.5 - 2.5$ eV energy region also exhibit an important coverage dependency. This in itself represents a highly desirable feature, if the aim is to increase the photovoltaic efficiency of a MoS_2-based solar cell by extending the photovoltaic response range. This information is also crucial for optimizing the performance of such a system by, e.g., chemically altering the phenol group. However, the spectrum itself provides no information about the spatial distribution of the electronic excitations in the low-energy/high-energy regions.

In order to gain more insights into the excitonic nature of the optical bands, we now take advantage of the capabilities of the DITOs for the analysis of the LR-TDDFT-RPA spectrum. As stated above, solely the molecular orbitals obtained at the DFT/LDA level of theory using atom-centered Gaussian basis functions are required for the computation of the DITOs. Their abilities to provide important visual and numerical data regarding optical excitations are demonstrated for the phenol-sensitized MoS_2 system at the highest coverage (cf. Fig. 2). The associated particle and hole densities are computed and depicted in Fig. 3

as blue and gray isosurfaces. Two bands are chosen to illustrate the marked change on the character in the spectrum from the infrared (band labeled "A" at circa 1.2 eV) to the visible regime (shoulder labeled "B" at circa 2.8 eV). By examining the particle (blue) and hole (gray) densities shown in Fig. 3, it can be observed that there is indeed a pronounced difference between low- and high-energy excitations. While the particle density lying within the MoS_2 surface is localized close to the phenol groups in the low-energy region A, it becomes almost evenly distributed over the MoS_2 layer in the high-energy region B. At the same time, the hole density remains highly localized on the phenol groups in both cases. From the visual inspection, the band A can be assigned to a charge transfer state, while the band B has a stronger charge separated character. The latter is thus expected to be more efficient for producing free charge carriers in the MoS_2 substrate and, therefore, be more useful for dye-sensitized solar cell applications.

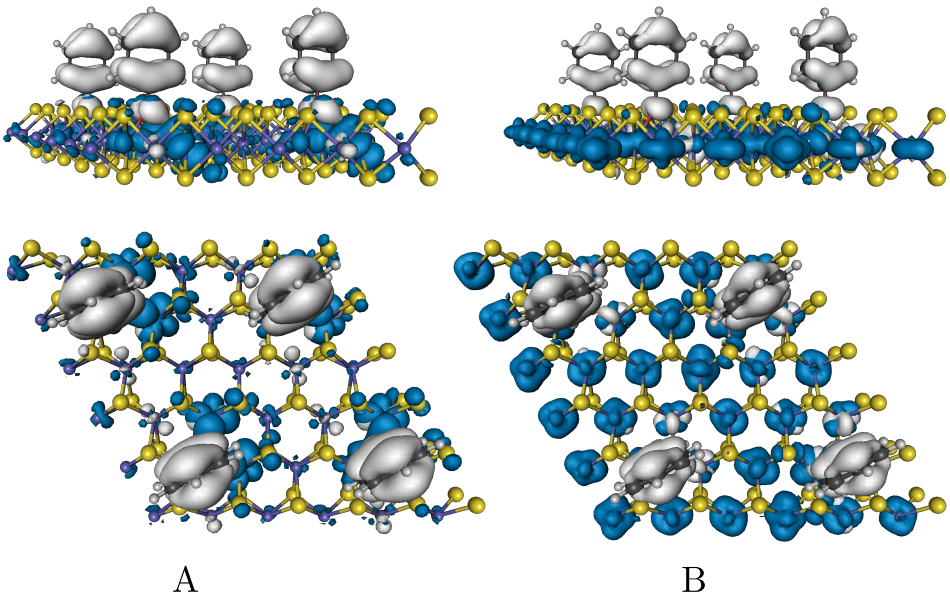

FIG. 3. Particle (blue) and hole (red) densities calculated from DITOs for sensitized MoS_2-surface with four phenol molecules.

IV. CONCLUSIONS

In this work, we extend the concept of natural transition orbitals to provide a novel, low-cost approach for analyzing spectra obtained from LR-TDDFT-RPA calculations. We

demonstrate how the resulting data can be used to complement the spectral data by providing a better *physical* and *visual* understanding of optical transitions. This should be particularly valuable as an analytical tool for complex, charge transfer transitions.

Our approach is in no way specific to LR-TDDFT-RPA and can easily be applied to every method, which allows the computation of transition dipole moments. In addition, these excitons could be used in subsequent BSE calculations to improve the quality of the optical spectrum in extended systems.

ACKNOWLEDGMENTS

L.E.M.S. acknowledges financial support from the Deutsche Forschungsgemeinschaft within the Priority Program (SPP) 1459 and the support form the Studienstiftung des deutschen Volkes e.V. and from the International Max Planck Research School "Functional Interfaces in Physics and Chemistry". J.C.T. and G.H. are grateful to the Deutsche Forschungsgemeinschaft for funding through projects TR1109/2-1 and Pe2297/1-1. The computer facilities of the Freie Universität Berlin (ZEDAT) are acknowledged for computer time. Further, we thank Hans-Christian Hege for providing the ZIBAmira visualization program [59].

---

[1] M. P. Balanay and D. H. Kim, Phys. Chem. Chem. Phys. **10**, 5121 (2008).

[2] F. D. Angelis, S. Fantacci, and A. Selloni, Nanotechnology **19**, 424002 (2008).

[3] A. K. Singh, K. Mathew, H. L. Zhuang, and R. G. Hennig, J. Phys. Chem. Lett. **6**, 1087 (2015).

[4] E. Runge and E. K. U. Gross, Phys. Rev. Lett. **52**, 997 (1984).

[5] F. Sottile, F. Bruneval, A. G. Marinopoulos, L. K. Dash, S. Botti, V. Olevano, N. Vast, A. Rubio, and L. Reining, Int. J. Quantum Chem. **102**, 684 (2005).

[6] M. S. Hybertsen and S. G. Louie, Phys. Rev. B **35**, 5585 (1987).

[7] R. L. Martin, J. Chem. Phys. **118**, 4775 (2003).

[8] G. Strinati, Phys. Rev. Lett. **49**, 1519 (1982).

[9] G. Strinati, Phys. Rev. B **29**, 5718 (1984).

[10] G. Strinati, Riv. Nuovo Cimento **11**, 1 (1988).

[11] M. Rohlfing and S. G. Louie, Phys. Rev. B **62**, 4927 (2000).

[12] A. Schäfer, H. Horn, and R. Ahlrichs, J. Chem. Phys. **97**, 2571 (1992).

[13] F. Weigend and R. Ahlrichs, Phys. Chem. Chem. Phys. **7**, 3297 (2005).

[14] C. Adamo and V. Barone, J. Chem. Phys. **110**, 6158 (1999).

[15] "TURBOMOLE V7.2 2017, a development of University of Karlsruhe and Forschungszentrum Karlsruhe GmbH, 1989-2007, TURBOMOLE GmbH, since 2007; available from `http://www.turbomole.com`.".

[16] G. Hermann, V. Pohl, J. C. Tremblay, B. Paulus, H.-C. Hege, and A. Schild, J. Comput. Chem. **37**, 1511 (2016).

[17] B. Radisavljevic, A. Radenovic, J. Brivio, V. Giacometti, and A. Kis, Nat. Nanotechnol. **6**, 147 (2011).

[18] O. Lopez-Sanchez, D. Lembke, M. Kayci, A. Radenovic, and A. Kis, Nat. Nanotechnol. **8**, 497 (2013).

[19] Z. Yin, H. Li, H. Li, L. Jiang, Y. Shi, Y. Sun, G. Lu, Q. Zhang, X. Chen, and H. Zhang, ACS Nano **6**, 74 (2011).

[20] H. Ramakrishna Matte, A. Gomathi, A. Manna, D. Late, R. Datta, S. Pati, and C. Rao, Angew. Chem. Int. Ed. **49**, 4059 (2010).

[21] G. Eda, H. Yamaguchi, D. Voiry, T. Fujita, M. Chen, and M. Chhowalla, Nano Lett. **11**, 5111 (2011).

[22] K. F. Mak, K. He, C. Lee, G. H. Lee, J. Hone, T. F. Heinz, and J. Shan, Nat. Mater. **12**, 207 (2012).

[23] A. K. Geim and K. S. Novoselov, Nat. Mater. **6**, 183 (2007).

[24] R. Mas-Ballesté, C. Gómez-Navarro, J. Gómez-Herrero, and F. Zamora, Nanoscale **3**, 20 (2011).

[25] K. S. Novoselov, D. Jiang, F. Schedin, T. J. Booth, V. V. Khotkevich, S. V. Morozov, and A. K. Geim, Proc. Natl. Acad. Sci. U.S.A. **102**, 10451 (2005).

[26] K. S. Novoselov, A. Mishchenko, A. Carvalho, and A. H. C. Neto, Science **353**, aac9439 (2016).

[27] A. Gupta, T. Sakthivel, and S. Seal, Prog. Mater. Sci. **73**, 44 (2015).

[28] F. A. Rasmussen and K. S. Thygesen, J. Phys. Chem. C **119**, 13169 (2015).

[29] B. O'Regan and M. Grätzel, Nature **353**, 737 (1991).

[30] A. Hagfeldt and M. Grätzel, Chem. Rev. **95**, 49 (1995).

[31] A. Hagfeldt and M. Grätzel, Acc. Chem. Res. **33**, 269 (2000).

[32] M. Grätzel, Nature **414**, 338 (2001).

[33] J. B. Asbury, E. Hao, Y. Wang, H. N. Ghosh, and T. Lian, J. Phys. Chem. B **105**, 4545 (2001).

[34] M. Grätzel, J. Photochem. Photobiol. C **4**, 145 (2003).

[35] A. Hagfeldt, G. Boschloo, L. Sun, L. Kloo, and H. Pettersson, Chem. Rev. **110**, 6595 (2010).

[36] S. H. Yu, Y. Lee, S. K. Jang, J. Kang, J. Jeon, C. Lee, J. Y. Lee, H. Kim, E. Hwang, S. Lee, and J. H. Cho, ACS Nano **8**, 8285 (2014).

[37] T. Jia, M. M. J. Li, L. Ye, S. Wiseman, G. Liu, J. Qu, K. Nakagawa, and S. C. E. Tsang, ChemComm **51**, 13496 (2015).

[38] Y. Huang, W. Zheng, Y. Qiu, and P. Hu, ACS Appl. Mater. Interfaces **8**, 23362 (2016).

[39] E. P. Nguyen, B. J. Carey, C. J. Harrison, P. Atkin, K. J. Berean, E. D. Gaspera, J. Z. Ou, R. B. Kaner, K. Kalantar-zadeh, and T. Daeneke, Nanoscale **8**, 16276 (2016).

[40] H. M. Le, V. Q. Bui, P. H. Tran, N.-N. Pham-Tran, Y. Kawazoe, and D. Nguyen-Manh, Chem. Phys. Lett. **667**, 290 (2017).

[41] W. R. Duncan and O. V. Prezhdo, Annu. Rev. Phys. Chem. **58**, 143 (2007).

[42] W. R. Duncan and O. V. Prezhdo, J. Phys. Chem. B **109**, 365 (2005).

[43] R. S. de Armas, M. San-Miguel, J. Oviedo, and J. F. Sanz, Comput. Theor. Chem. **975**, 99 (2011).

[44] Y. Ooyama, M. Kanda, K. Uenaka, and J. Ohshita, ChemPhysChem **16**, 3049 (2015).

[45] A. Larsen, J. Mortensen, J. Blomqvist, I. Castelli, R. Christensen, M. D. ak, J. Friis, M. Groves, B. Hammer, C. Hargus, E. Hermes, P. Jennings, P. Jensen, J. Kermode, J. Kitchin, E. Kolsbjerg, J. Kubal, K. Kaasbjerg, S. Lysgaard, J. Maronsson, T. Maxson, T. Olsen, L. Pastewka, A. Peterson, C. Rostgaard, J. Schiøtz, O. Schütt, M. Strange, K. Thygesen, T. Vegge, L. Vilhelmsen, M. Walter, Z. Zeng, and K. W. Jacobsen, J. Phys. Condens. Matter **29**, 273002 (2017).

[46] J. J. Mortensen, L. B. Hansen, and K. W. Jacobsen, Phys. Rev. B **71**, 035109 (2005).

[47] J. Enkovaara, C. Rostgaard, J. J. Mortensen, J. Chen, M. Dułak, L. Ferrighi, J. Gavnholt, C. Glinsvad, V. Haikola, H. A. Hansen, H. H. Kristoffersen, M. Kuisma, A. H. Larsen, L. Lehto-

vaara, M. Ljungberg, O. Lopez-Acevedo, P. G. Moses, J. Ojanen, T. Olsen, V. Petzold, N. A. Romero, J. Stausholm-Møller, M. Strange, G. A. Tritsaris, M. Vanin, M. Walter, B. Hammer, H. Häkkinen, G. K. H. Madsen, R. M. Nieminen, J. K. Nørskov, M. Puska, T. T. Rantala, J. Schiøtz, K. S. Thygesen, and K. W. Jacobsen, J. Phys. Condens. Matter **22**, 253202 (2010).

[48] A. H. Larsen, M. Vanin, J. J. Mortensen, K. S. Thygesen, and K. W. Jacobsen, Phys. Rev. B **80**, 195112 (2009).

[49] M. A. Marques, M. J. Oliveira, and T. Burnus, Comput. Phys. Commun. **183**, 2272 (2012).

[50] P. E. Blöchl, Phys. Rev. B **50**, 17953 (1994).

[51] A. H. Larsen, M. Kuisma, J. Löfgren, Y. Pouillon, P. Erhart, and P. Hyldgaard, Model. Simul. Mater. Sci. Eng. **25**, 065004 (2017).

[52] K. Berland, C. A. Arter, V. R. Cooper, K. Lee, B. I. Lundqvist, E. Schröder, T. Thonhauser, and P. Hyldgaard, J. Chem. Phys. **140**, 18A539 (2014).

[53] K. Berland and P. Hyldgaard, Phys. Rev. B **89**, 035412 (2014).

[54] G. Román-Pérez and J. M. Soler, Phys. Rev. Lett. **103**, 096102 (2009).

[55] L. Gharaee, P. Erhart, and P. Hyldgaard, Phys. Rev. B **95**, 085147 (2017).

[56] We used the molybdinum basis set proposed by Furio Corà [60] together with a Hay-Wadt type ECP [61], while a POB double-ζ polarized basis set [62] was used for all other elements.

[57] L. N. Glanzmann, D. J. Mowbray, D. G. F. del Valle, F. Scotognella, G. Lanzani, and A. Rubio, J. Phys. Chem. C **120**, 1926 (2016).

[58] L. N. Glanzmann and D. J. Mowbray, J. Phys. Chem. C **120**, 6336 (2016).

[59] D. Stalling, M. Westerhoff, and H.-C. Hege, in *The Visualization Handbook* (Elsevier, 2005) pp. 749–767.

[60] F. Corà, A. Patel, N. M. Harrison, C. Roetti, and C. R. A. Catlow, J. Mater. Chem. **7**, 959 (1997).

[61] P. J. Hay and W. R. Wadt, J. Chem. Phys. **82**, 270 (1985).

[62] M. F. Peintinger, D. V. Oliveira, and T. Bredow, J. Comput. Chem. **34**, 451 (2012).

Paper SM1

Charge Migration in Eyring, Walter and Kimball's 1944 Model of the Electronically Excited Hydrogen-Molecule Ion

D. J. Diestler, G. Hermann, and J. Manz

J. Phys. Chem. A **121**, 5332–5340 (2017)

DOI: 10.1021/acs.jpca.7b04714

URL: https://doi.org/10.1021/acs.jpca.7b04714

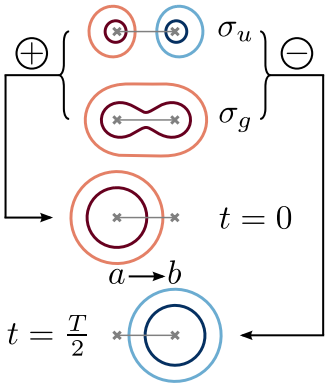

Figure 4.4: Graphical Abstract. Reprint with permission from Diestler et al.[SM1] (©2016 American Chemical Society)

Author contributions

Dennis J. Diestler first recognized that Eyring, Walter, and Kimball's model of the electronically excited hydrogen-molecule ion H_2^+ describes a charge migration process. He likewise derived analytical expressions for key dynamical quantities, i.e., the electronic probability density, the electronic flux density, the electronic flux, and the electronic yield, to characterize the charge migration in H_2^+. Jörn Manz discovered the related spatio-temporal symmetries. All static calculations, the dynamical simulation of the charge migration, and their visualization were carried out by myself. All authors contributed to the analysis of the charge migration process. The manuscript was prepared by Dennis J. Diestler with essential input from Jörn Manz and myself.

Paper SM2

Multidirectional Angular Electronic Flux during Adiabatic Attosecond Charge Migration in Excited Benzene

G. Hermann, C. Liu, J. Manz, B. Paulus, J. F. Pérez-Torres, V. Pohl, and J. C. Tremblay

J. Phys. Chem. A **120**, 5360–5369 (2016)

DOI: 10.1021/acs.jpca.6b01948

URL: https://doi.org/10.1021/acs.jpca.6b01948

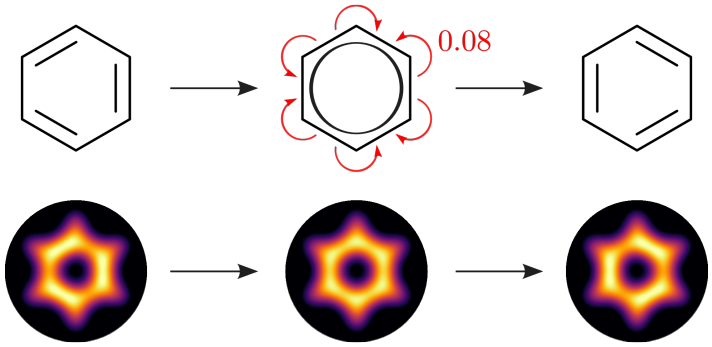

Figure 4.5: Graphical Abstract. Reprint with permission from Hermann et al.[SM2] (©2016 American Chemical Society)

Author contributions

The research question and the methodological framework of this work were outlined by Jörn Manz and Jhon Fredy Pérez-Torres. An initial characterization of the electronic structure of benzene and a preliminary simulation of the charge migration were carried out by Jhon Fredy Pérez-Torres with assistance of ChunMei Liu. For the final manuscript, Vincent Pohl determined the electronic structure of benzene with a CASSCF calculation after consultation with Beate Paulus and Jean Christophe Tremblay. The suggested methodology for the charge migration and its analysis tools were finally implemented by Vincent Pohl and myself in equal parts. In addition, Vincent Pohl and I prepared the figures for the publication with input from all other coauthors. All authors were involved in the concluding discussion of the results and contributed to the final version of the manuscript, which was mainly written by Jörn Manz.

Paper SM3

Attosecond Angular Flux of Partial Charges on the Carbon Atoms of Benzene in Non-Aromatic Excited State

G. Hermann, C. Liu, J. Manz, B. Paulus, V. Pohl, and J. C. Tremblay

Chem. Phys. Lett. **683**, 553–558 (2017)

DOI: 10.1016/j.cplett.2017.01.030

URL: https://doi.org/10.1016/j.cplett.2017.01.030

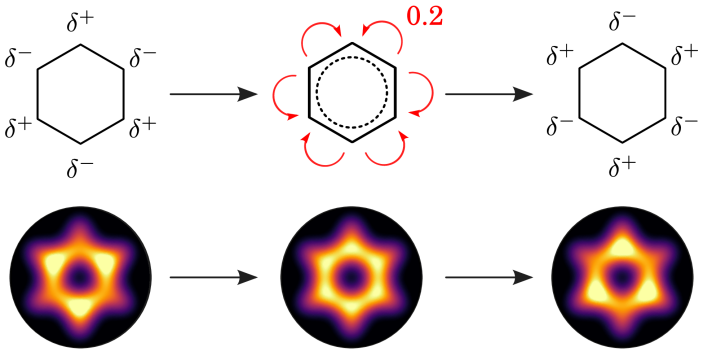

Figure 4.6: Graphical Abstract. Reprint with permission from Hermann et al.[SM3] (©2017 Elsevier B.V. All rights reserved.)

Author contributions

This work is a follow-up study of **Paper SM2** and was initially conceived by Jörn Manz. The CASSCF calculations for the electronic structure characterization were conducted by Vincent Pohl with advices from Beate Paulus and Jean Christophe Tremblay. The methodology of **Paper SM2** was further developed by Vincent Pohl and myself with considerable input from Jean Christophe Tremblay. This more sophisticated methodology was implemented by Vincent Pohl and myself, in equal parts, into the toolkit DETCI@ORBKIT.[TK1] Vincent Pohl and I applied the new methodology for the charge migration in a selected superposition state of benzene. The respective results based on the methodology from **Paper SM2** were generated by ChunMei Liu. The imaging of the collected data and the comparison between both methodologies were prepared by Vincent Pohl and myself. Jörn Manz predominantly wrote the first version of the manuscript and finalized it with contributions from all coauthors.

Paper SC1

Imaging the Ultrafast Photoelectron Transfer Process in Alizarin-TiO_2

T. Gomez, G. Hermann, X. Zarate, J. F. Pérez-Torres, and J. C. Tremblay

Molecules **20**, 13830–13853 (2015)

DOI: 10.3390/molecules200813830

URL: https://doi.org/10.3390/molecules200813830

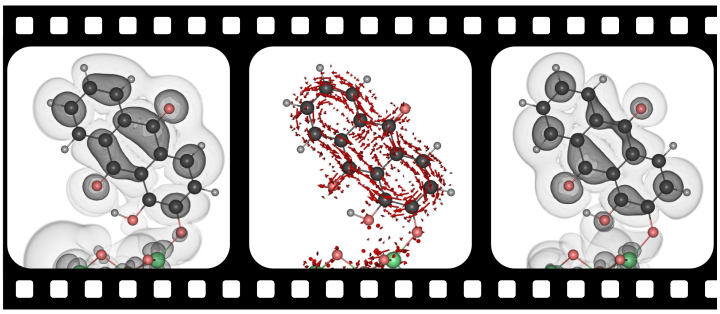

Figure 4.7: Graphical abstract, particularly created for this thesis on the basis of the figures from Paper SC1. ()

Author contributions

Tatiana Gomez and Ximena Zarate initialized the project and carried out the structure optimizations and the optical spectra calculations for the dye-sensitized solar cell model. The single active electron model for the electron dynamics and the electronic flux equations for its analysis and visualization were derived by Jean Christophe Tremblay and Jhon Fredy Pérez-Torres. I implemented the model, carried out the dynamical simulations, and created all figures. All authors contributed to the analysis of the time-independent and time-dependent data. The manuscript was written by Jean Christophe Tremblay with considerable input from all authors.

Paper SC2

Ultrafast Photoelectron Migration in Dye-Sensitized Solar Cells: Influence of the Binding Mode and Many-Body Interactions

G. Hermann, and J. C. Tremblay

J. Chem. Phys. **145**, 174704 (2016)

DOI: 10.1063/1.4966260

URL: https://doi.org/10.1063/1.4966260

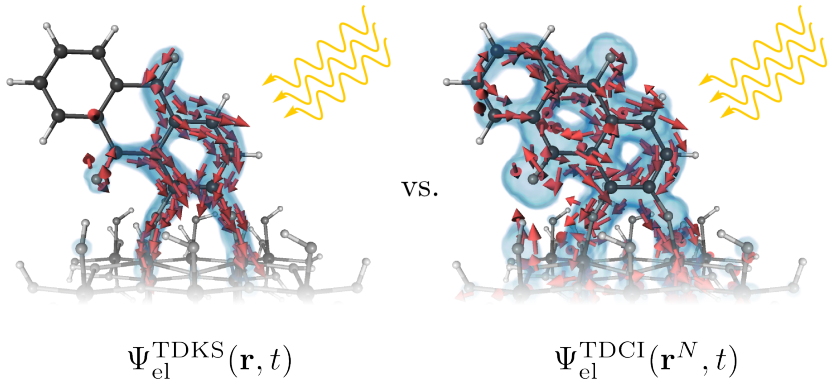

Figure 4.8: Graphical abstract, particularly created for this thesis on the basis of the figures from Paper SC2. ()

Author contributions

The initial idea of comparing the single active electron approach from **Paper SC1** with a time-dependent many-electron configuration interaction ansatz was proposed by Jean Christophe Tremblay and myself. For this purpose, Jean Christophe Tremblay developed a hybrid DFT/CI approach with assistance of myself. Johannes Dietschreit performed a preliminary characterization of the electronic structure of the dye-sensitized solar cells. I carried out all final quantum chemical calculations, the electron dynamics and prepared all figures to illustrate the data. The analysis of the findings and the writing of the manuscript were carried out by myself in collaboration with Jean Christophe Tremblay.

Paper SC3

Comparison of Donor-Acceptor π-Conjugated Dyes in Model Solar Cells: A Study of Interfacial Ultrafast Electron Migration

G. Hermann, F. Witte, and J. C. Tremblay

arXiv preprint arXiv:1707.01419 (2017)

URL: https://arxiv.org/abs/1707.01419 (2017)

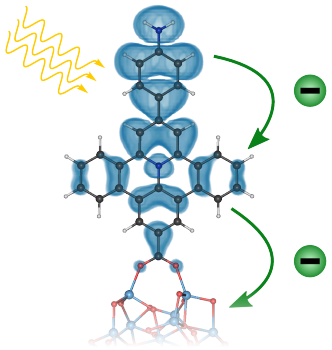

Figure 4.9: Graphical abstract, particularly created for this thesis on the basis of the figures from Paper SC3.

Author contributions

The conception for the project was formulated by myself. Felix Witte performed initial test calculations to characterize the electronic structure of the solar cell model systems. Jean Christophe Tremblay and myself extended the single active electron model from **Paper SC1** and **Paper SC2** for simulating the electron migration by parameter-free expressions for the injection time and current. In the final version of the paper, all electronic structure calculations, the dynamical simulations, and the visualization of the results were performed by myself. Jean Christophe and I summarized the final results. The manuscript was written by myself in collaboration with Jean Christophe Tremblay. Felix Witte helped in proofreading the paper.

Paper QD1

Laser-Driven Hole Trapping in a Ge/Si Core-Shell Nanocrystal: An Atomistic Configuration Interaction Perspective

G. Hermann and J. C. Tremblay

J. Phys. Chem. C **119**, 25606–25614 (2015)

DOI: 10.1021/acs.jpcc.5b08606

URL: https://doi.org/10.1021/acs.jpcc.5b08606

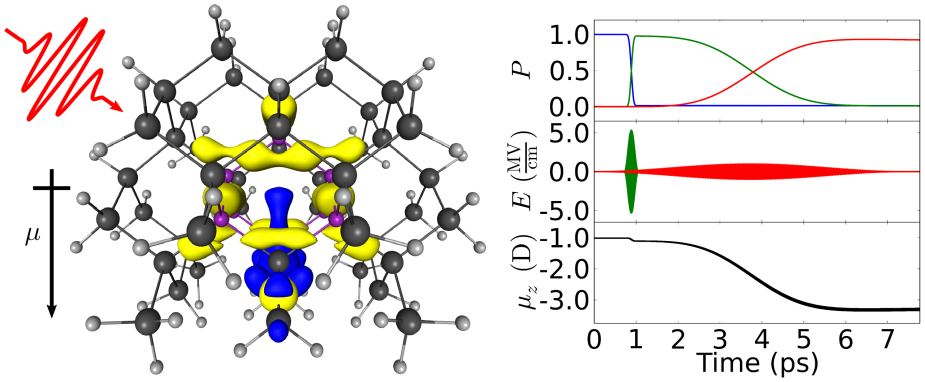

Figure 4.10: Graphical Abstract. Reprint with permission from Hermann et al.[QD1] (©2016 American Chemical Society)

Author contributions

The initial research question was proposed by Jean Christophe Tremblay, who also derived the expressions for the energy relaxation and dephasing rates with considerable input from myself. For the static analysis, I extended the program DETCI@ORBKIT by enabling the post-processing of CIS wave functions and the extraction of the necessary data from the respective quantum chemical program, GAMESS (US)[262]. The laser-driven many-electron dynamics as well as the visualization of the final results were performed by myself. In collaboration with Jean Christophe Tremblay, I prepared the manuscript.

Chapter 5

Conclusions

The main contributions of the present thesis are threefold: First, a computational framework for the post-processing of correlated many-electron wave functions was developed. Second, appropriate quantities and tools for the analysis and visualization of ultrafast electron dynamics were introduced and validated. Third, these analysis tools were applied to realistic charge migration processes in various molecular systems. Thus, the thesis provides both methodological and theoretical contributions to existing scholarly work on charge migration processes.

In modern quantum chemistry, several tools for post-processing many-electron wave function data are available. They range from stand-alone programs to add-on tools implemented in standard quantum chemistry software. As these tools often lack general applicability and ease of extensibility, the open-source framework DETCI@ORBKIT addresses these shortcomings and fulfills these requirements (cf. **Paper TK1** and **Paper TK2**). This toolbox is capable of reconstructing multi-determinantal Configuration Interaction (CI) wave functions obtained at various levels of theory. The required data are extracted from the output of various standard quantum chemical programs. Its extensibility is facilitated by its highly modular and easily comprehensible Python architecture (cf. **Paper AP2**).

By exploiting the functionalities of DETCI@ORBKIT, a set of quantum mechanical quantities is gathered allowing the time- and space-resolved analysis and visualization of many-electron dynamics. This set extends the standard investigation tools, i.e., the electron density, by the electronic flux and electronic flux density (cf. **Paper TK1** and **Paper TK2**). The validation of these tools by the example of various charge migration processes in small molecules disclose that a complete mechanistic enlightenment of the electron dynamics is only feasible by a combined examination of the electron density and electronic flux density. While the former reveals the probability distribution of the electrons, the latter unveils the spatially-resolved instantaneous flow of electrons.

In addition, the newly developed hybrid Time-Dependent Density Functional Theory (TDDFT)/CI singles (CIS) procedure enables the application of these analysis tools to more extended systems (cf. **Paper TK2** and **Paper SC2**). Within this scheme, the multi-determinantal wave functions are obtained from linear-response TDDFT calculations constructed as pseudo CI singles basis functions. This combination of electronic structure methods results in a favorable scaling with respect to the system size. In addition, this hybrid approach can be used for many-electron dynamics subject to strong laser fields and ensures the N_{el}-representability of the one-electron density and electronic flux density, contrary to real-time TDDFT and current DFT.

Furthermore, a universal and low-cost analysis strategy is devised to study the charge transfer character of a quantum system associated with a certain feature in its optical spectra. It approximates the concept of Natural Transition Orbitals (NTO)[69] by using the one-electron transition dipole matrix instead of the one-electron transition density matrix in the underlying unitary orbital transformation. By this means, pairs of particle and hole functions, i.e., the so-called Dipole-Induced Transition Orbitals (DITO), can be obtained for a particular optical transition (cf. **Paper TK3**). This allows to apply this novel approach also to 1D, 2D, and 3D periodic systems. While DITOs offer a straightforward, graphical way for interpreting electronic excitations, the underlying methodology can be applied to determine the expectation value of any one-electron operator.

The second part of this thesis focuses on the application of the introduced analysis tools to various charge migration processes and on their simulation. While the first system of interest, i.e., the hydrogen molecular ion (H_2^+), represents a well-studied system, the scientific originality behind its investigation (cf. **Paper SM1**) relies on the recognition that Eyring, Walter, and Kimball already predicted a possible charge migration process for H_2^+ in their theoretical textbook from 1944.[79] This was long before the experimental observation of charge migration phenomena.[26–28,263] Based on their model, analytical expressions and some fundamental symmetry relations are derived for the electron density, the axial electronic flux, and the electronic flux density. Both the axial electronic flux and the electronic flux density reveal an identical picture concerning the mechanistic details of the charge migration in H_2^+. A remarkable outcome of this examination is that electron migration can appear without the agency of electron coherences.

Moreover, the thesis' findings add knowledge to the mechanistic understanding of various charge migration processes in the benzene molecule. The related studies corroborate and extend the previous work of Ulusoy and Nest.[83] Specifically, their working hypothesis of a pincer-type electronic motion occurring for the two examined superposition states is confirmed (cf. **Paper SM2** and **Paper SM3**). In addition, the quantitative analysis of the angular electronic yields reveals the maximum number of

electrons flowing during the investigated charge migration processes for the first time. The findings are in stark contrast with the simple model, which describes the charge migration as the oscillation between two Lewis-type structures.[264] While this model suggests a number of six migrating electrons for the two monitored scenarios, the quantitative evaluation of the electronic yields give significantly smaller numbers. This discrepancy is assigned to the delocalization of the electrons, i.e., the transition between the two Lewis structures requires the reorganization of only a small fraction of the six electrons. In conclusion, the present methodology, i.e., the time- and space-resolved analysis of the electronic yields and electronic fluxes, facilitates the quantitative and qualitative description of charge migration processes and can be applied to refine the associated Lewis structure-based model. However, convenient boundary conditions have to be invoked for their determination.

Concerning the application of the introduced analysis tools to the charge migration in small molecules, its suitability for more extended systems is firstly verified for finite nanostructured models of Dye-Sensitized Solar Cells (DSSC). Generally, the findings add mechanistic insights to various charge migration scenarios in these systems (cf. **Papers SC1–SC3**). In addition to the analysis of the time-dependent electronic density and electronic flux density, a projector formalism using a Voronoi partitioning is introduced to study the electron dynamics. This scheme enables the time- and space-resolved evaluation of the electronic yield and electronic flux and thus the examination of the contribution of a certain molecular fragment during the charge migration. While the definition of the projectors is arbitrary to some extent, no boundary conditions for the electronic yields and fluxes are required. In addition to the mechanistic analysis, the thesis contributes to the modeling of different charge migration scenarios in various DSSC models. As these models are finite-sized, the electron dynamics is subject to a complex absorption potential to circumvent artificial reflection of the migrating electrons at the edges of the semiconductor substrate. For this reason, a parameter-free expression is derived yielding the same time scale as the experimental electron injection time (cf. **Paper SC3**). Furthermore, the thesis' findings contribute to the understanding of electron correlation effects during the charge migration in DSSCs. A comparison between a time-dependent many-electron configuration interaction ansatz and a single active electron approach reveals the suitability of both approaches for the description of electron migration processes in DSSCs (cf. **Paper SC2**). While the latter represents a low-cost approach allowing the investigation of more extended systems, the many-body approach sheds light on the electron-electron and hole-hole interactions during the charge migration. In sum, the studies on the DSSC models provide a computationally inexpensive one-electron approach for the real time simulation of charge migration processes and an appropriate set of tools for their analysis.

Finally, the investigation of the charge carrier confinement in a semiconductor quantum dot adds an

additional application for the density-based analysis tools (cf. **Paper QD1**). By their usage, a state-selective transition path for the laser-driven many-electron dynamics is defined for a Ge/Si core-shell model quantum dot. It enables a robust and effective hole confinement and the creation of a long-lived permanent dipole in the system. Furthermore, this work provides new microscopic perturbative expressions for energy relaxation and pure dephasing rates. This enables to simulate the dynamical coupling of the Ge/Si quantum dot with the vibrations of a surrounding Si environment. In sum, the study simultaneously introduces novel computational methodologies for dissipative electron dynamics and adds new insights to the nature of light-induced hole confinement in nanostructured solid state systems.

To conclude, this dissertation significantly contributes to the development of a robust and versatile set of tools to analyze and visualize many-electron dynamics, which are applied to a variety of charge migration processes. The corresponding findings do not only provide a deep mechanistic understanding of charge migration, but also highlight the relevance of ultrafast electron dynamics in molecular electronics.

Bibliography

[1] V. May and O. Kühn, *Charge and Energy Transfer Dynamics in Molecular Systems* (Wiley, 2011) (cit. on pp. 1, 29).

[2] R. A. Marcus, "On the Theory of Oxidation-Reduction Reactions Involving Electron Transfer. I", J. Chem. Phys. **24**, 966–978 (1956) (cit. on p. 1).

[3] R. A. Marcus, "Electrostatic Free Energy and Other Properties of States Having Nonequilibrium Polarization. I", J. Chem. Phys. **24**, 979–989 (1956) (cit. on p. 1).

[4] P. F. Barbara, T. J. Meyer, and M. A. Ratner, "Contemporary Issues in Electron Transfer Research", J. Phys. Chem. **100**, 13148–13168 (1996) (cit. on p. 1).

[5] T. Holstein, "Studies of Polaron Motion: Part I. The Molecular-Crystal Model", Ann. Phys. (N. Y.) **8**, 325–342 (1959) (cit. on p. 1).

[6] D. M. Adams, L. Brus, C. E. D. Chidsey, S. Creager, C. Creutz, C. R. Kagan, P. V. Kamat, M. Lieberman, S. Lindsay, R. A. Marcus, R. M. Metzger, M. E. Michel-Beyerle, J. R. Miller, M. D. Newton, D. R. Rolison, O. Sankey, K. S. Schanze, J. Yardley, and X. Zhu, "Charge Transfer on the Nanoscale: Current Status", J. Phys. Chem. B **107**, 6668–6697 (2003) (cit. on p. 1).

[7] M. Bixon and J. Jortner, "Electron Transfer-From Isolated Molecules to Biomolecules", in *Adv. Chem. Phys.* (John Wiley & Sons, Inc., 2007), pp. 35–202 (cit. on p. 1).

[8] L. S. Cederbaum and J. Zobeley, "Ultrafast Charge Migration by Electron Correlation", Chem. Phys. Lett. **307**, 205–210 (1999) (cit. on pp. 1, 2).

[9] A. I. Kuleff and L. S. Cederbaum, "Ultrafast Correlation-Driven Electron Dynamics", J. Phys. B: At., Mol. Opt. Phys. **47**, 124002 (2014) (cit. on pp. 1, 2).

[10] K. Ramasesha, S. R. Leone, and D. M. Neumark, "Real-Time Probing of Electron Dynamics Using Attosecond Time-Resolved Spectroscopy", Annu. Rev. Phys. Chem. **67**, 41–63 (2016) (cit. on p. 1).

[11] F. Calegari, A. Trabattoni, A. Palacios, D. Ayuso, M. C. Castrovilli, J. B. Greenwood, P. Decleva, F. Martín, and M. Nisoli, "Charge Migration Induced by Attosecond Pulses in Bio-Relevant Molecules", J. Phys. B: At. Mol. Opt. Phys. **49**, 142001 (2016) (cit. on p. 1).

[12] H. J. Wörner, C. A. Arrell, N. Banerji, A. Cannizzo, M. Chergui, A. K. Das, P. Hamm, U. Keller, P. M. Kraus, E. Liberatore, P. Lopez-Tarifa, M. Lucchini, M. Meuwly, C. Milne, J.-E. Moser, U. Rothlisberger, G. Smolentsev, J. Teuscher, J. A. van Bokhoven, and O. Wenger, "Charge Migration and Charge Transfer in Molecular Systems", Struct. Dyn. **4**, 061508 (2017) (cit. on p. 1).

[13] M. Nisoli, P. Decleva, F. Calegari, A. Palacios, and F. Martín, "Attosecond Electron Dynamics in Molecules", Chem. Rev. **117**, 10760–10825 (2017) (cit. on p. 1).

[14] P. M. Kraus and H. J. Wörner, "Perspectives of Attosecond Spectroscopy for the Understanding of Fundamental Electron Correlations", Angew. Chem. Int. Ed., 2–22 (2018) (cit. on p. 1).

[15] P. de Rege, S. Williams, and M. Therien, "Direct Evaluation of Electronic Coupling Mediated by Hydrogen Bonds: Implications for Biological Electron Transfer", Science **269**, 1409–1413 (1995) (cit. on p. 1).

[16] J. Lin, "The Nature of Aqueous Tunneling Pathways Between Electron-Transfer Proteins", Science **310**, 1311–1313 (2005) (cit. on p. 1).

[17] G. S. Engel, T. R. Calhoun, E. L. Read, T.-K. Ahn, T. Mančal, Y.-C. Cheng, R. E. Blankenship, and G. R. Fleming, "Evidence for Wavelike Energy Transfer through Quantum Coherence in Photosynthetic Systems", Nature **446**, 782–786 (2007) (cit. on p. 1).

[18] C. Consani, G. Aubock, F. van Mourik, and M. Chergui, "Ultrafast Tryptophan-To-Heme Electron Transfer in Myoglobins Revealed by UV 2D Spectroscopy", Science **339**, 1586–1589 (2013) (cit. on p. 1).

[19] R. Monni, A. A. Haddad, F. van Mourik, G. Auböck, and M. Chergui, "Tryptophan-To-Heme Electron Transfer in Ferrous Myoglobins", Proc. Natl. Acad. Sci. U.S.A. **112**, 5602–5606 (2015) (cit. on p. 1).

[20] G. Smolentsev, A. A. Guda, M. Janousch, C. Frieh, G. Jud, F. Zamponi, M. Chavarot-Kerlidou, V. Artero, J. A. van Bokhoven, and M. Nachtegaal, "X-Ray Absorption Spectroscopy with Time-Tagged Photon Counting: Application to Study the Structure of a Co(I) Intermediate of H_2 Evolving Photo-Catalyst", Faraday Discuss. **171**, 259–273 (2014) (cit. on p. 1).

[21] M. Wielopolski, M. Marszalek, F. G. Brunetti, D. Joly, J. Calbo, J. Aragó, J.-E. Moser, R. Humphry-Baker, S. M. Zakeeruddin, J. L. Delgado, M. Grätzel, E. Ortí, and N. Martín, "Synthesis and Optoelectronic Properties of Chemically Modified Bi-Fluorenylidenes", J. Mater. Chem. C **4**, 3798–3808 (2016) (cit. on p. 1).

[22] S. M. Falke, C. A. Rozzi, D. Brida, M. Maiuri, M. Amato, E. Sommer, A. D. Sio, A. Rubio, G. Cerullo, E. Molinari, and C. Lienau, "Coherent Ultrafast Charge Transfer in an Organic Photovoltaic Blend", Science **344**, 1001–1005 (2014) (cit. on p. 1).

[23] T. Plehn and V. May, "Charge and Energy Migration in Molecular Clusters: A Stochastic Schrödinger Equation Approach", J. Chem. Phys. **146**, 034107 (2017) (cit. on p. 1).

[24] M. Dantus, M. J. Rosker, and A. H. Zewail, "Real-Time Femtosecond Probing of ''Transition States" in Chemical Reactions", J. Chem. Phys. **87**, 2395–2397 (1987) (cit. on p. 1).

[25] T. S. Rose, M. J. Rosker, and A. H. Zewail, "Femtosecond Real-Time Observation of Wave Packet Oscillations (Resonance) in Dissociation Reactions", J. Chem. Phys. **88**, 6672–6673 (1988) (cit. on p. 1).

[26] R. Weinkauf, P. Schanen, D. Yang, S. Soukara, and E. W. Schlag, "Elementary Processes in Peptides: Electron Mobility and Dissociation in Peptide Cations in the Gas Phase", J. Phys. Chem. **99**, 11255–11265 (1995) (cit. on pp. 1, 214).

[27] R. Weinkauf, P. Schanen, A. Metsala, E. W. Schlag, M. Bürgle, and H. Kessler, "Highly Efficient Charge Transfer in Peptide Cations in the Gas Phase: Threshold Effects and Mechanism", J. Phys. Chem. **100**, 18567–18585 (1996) (cit. on pp. 1, 214).

[28] R. Weinkauf, E. W. Schlag, T. J. Martinez, and R. D. Levine, "Nonstationary Electronic States and Site-Selective Reactivity", J. Phys. Chem. A **101**, 7702–7710 (1997) (cit. on pp. 1, 214).

[29] M. Hentschel, R. Kienberger, C. Spielmann, G. A. Reider, N. Milosevic, T. Brabec, P. Corkum, U. Heinzmann, M. Drescher, and F. Krausz, "Attosecond Metrology", Nature **414**, 509–513 (2001) (cit. on p. 1).

[30] M. Drescher, M. Hentschel, R. Kienberger, M. Uiberacker, V. Yakovlev, A. Scrinzi, T. Westerwalbesloh, U. Kleineberg, U. Heinzmann, and F. Krausz, "Time-Resolved Atomic Inner-Shell Spectroscopy", Nature **419**, 803–807 (2002) (cit. on p. 1).

[31] R. Kienberger, "Steering Attosecond Electron Wave Packets with Light", Science **297**, 1144–1148 (2002) (cit. on p. 1).

[32] P. H. Bucksbaum, "Ultrafast Control", Nature **421**, 593–594 (2003) (cit. on p. 1).

[33] G. G. Paulus, F. Lindner, H. Walther, A. Baltuška, E. Goulielmakis, M. Lezius, and F. Krausz, "Measurement of the Phase of Few-Cycle Laser Pulses", Phys. Rev. Lett. **91**, 253004 (2003) (cit. on p. 1).

[34] J. Itatani, J. Levesque, D. Zeidler, H. Niikura, H. Pépin, J. C. Kieffer, P. B. Corkum, and D. M. Villeneuve, "Tomographic Imaging of Molecular Orbitals", Nature **432**, 867–871 (2004) (cit. on p. 1).

[35] A. Föhlisch, P. Feulner, F. Hennies, A. Fink, D. Menzel, D. Sanchez-Portal, P. M. Echenique, and W. Wurth, "Direct Observation of Electron Dynamics in the Attosecond Domain", Nature **436**, 373–376 (2005) (cit. on p. 1).

[36] M. F. Kling, "Control of Electron Localization in Molecular Dissociation", Science **312**, 246–248 (2006) (cit. on p. 1).

[37] P. B. Corkum and F. Krausz, "Attosecond Science", Nat. Phys. **3**, 381–387 (2007) (cit. on p. 1).

[38] F. Krausz and M. Ivanov, "Attosecond Physics", Rev. Mod. Phys. **81**, 163–234 (2009) (cit. on p. 1).

[39] H. J. Wörner, J. B. Bertrand, D. V. Kartashov, P. B. Corkum, and D. M. Villeneuve, "Following a Chemical Reaction Using High-Harmonic Interferometry", Nature **466**, 604–607 (2010) (cit. on p. 1).

[40] F. Calegari, D. Ayuso, A. Trabattoni, L. Belshaw, S. D. Camillis, S. Anumula, F. Frassetto, L. Poletto, A. Palacios, P. Decleva, J. B. Greenwood, F. Martin, and M. Nisoli, "Ultrafast Electron Dynamics in Phenylalanine Initiated by Attosecond Pulses", Science **346**, 336–339 (2014) (cit. on pp. 1, 2).

[41] P. M. Kraus, B. Mignolet, D. Baykusheva, A. Rupenyan, L. Horný, E. F. Penka, G. Grassi, O. I. Tolstikhin, J. Schneider, F. Jensen, L. B. Madsen, A. D. Bandrauk, F. Remacle, and H. J. Wörner, "Measurement and Laser Control of Attosecond Charge Migration in Ionized Iodoacetylene", Science **350**, 790–795 (2015) (cit. on p. 1).

[42] P. M. Kraus, S. B. Zhang, A. Gijsbertsen, R. R. Lucchese, N. Rohringer, and H. J. Wörner, "High-Harmonic Probing of Electronic Coherence in Dynamically Aligned Molecules", Phys. Rev. Lett. **111**, 243005 (2013) (cit. on p. 1).

[43] M. T. Hassan, T. T. Luu, A. Moulet, O. Raskazovskaya, P. Zhokhov, M. Garg, N. Karpowicz, A. M. Zheltikov, V. Pervak, F. Krausz, and E. Goulielmakis, "Optical Attosecond Pulses and Tracking the Nonlinear Response of Bound Electrons", Nature **530**, 66–70 (2016) (cit. on p. 1).

[44] F. Remacle, R. Levine, and M. Ratner, "Charge Directed Reactivity: A Simple Electronic Model, Exhibiting Site Selectivity, for the Dissociation of Ions", Chem. Phys. Lett. **285**, 25–33 (1998) (cit. on p. 2).

[45] F. Remacle and R. D. Levine, "An Electronic Time Scale in Chemistry", Proc. Natl. Acad. Sci. U.S.A. **103**, 6793–6798 (2006) (cit. on p. 2).

[46] B. Mignolet, R. D. Levine, and F. Remacle, "Charge Migration in the Bifunctional PENNA Cation Induced and Probed by Ultrafast Ionization: A Dynamical Study", J. Phys. B: At. Mol. Opt. Phys. **47**, 124011 (2014) (cit. on p. 2).

[47] J. Breidbach and L. S. Cederbaum, "Migration of Holes: Formalism, Mechanisms, and Illustrative Applications", J. Chem. Phys. **118**, 3983–3996 (2003) (cit. on p. 2).

[48] H. Hennig, J. Breidbach, and L. S. Cederbaum, "Electron Correlation as the Driving Force for Charge Transfer: Charge Migration Following Ionization in *N*-Methyl Acetamide", J. Phys. Chem. A **109**, 409–414 (2005) (cit. on p. 2).

[49] S. Lünnemann, A. I. Kuleff, and L. S. Cederbaum, "Ultrafast Charge Migration in 2-Phenylethyl-*N*,*N*-Dimethylamine", Chem. Phys. Lett. **450**, 232–235 (2008) (cit. on p. 2).

[50] A. I. Kuleff, S. Lünnemann, and L. S. Cederbaum, "Electron-Correlation-Driven Charge Migration in Oligopeptides", Chem. Phys. **414**, 100–105 (2013) (cit. on p. 2).

[51] A. I. Kuleff, N. V. Kryzhevoi, M. Pernpointner, and L. S. Cederbaum, "Core Ionization Initiates Subfemtosecond Charge Migration in the Valence Shell of Molecules", Phys. Rev. Lett. **117**, 093002 (2016) (cit. on p. 2).

[52] G. L. Yudin, S. Chelkowski, J. Itatani, A. D. Bandrauk, and P. B. Corkum, "Attosecond Photoionization of Coherently Coupled Electronic States", Phys. Rev. A **72**, 051401 (2005) (cit. on pp. 2, 3).

[53] A. D. Bandrauk, S. Chelkowski, P. B. Corkum, J. Manz, and G. L. Yudin, "Attosecond Photoionization of a Coherent Superposition of Bound and Dissociative Molecular States: Effect of Nuclear Motion", J. Phys. B: At. Mol. Opt. Phys. **42**, 134001 (2009) (cit. on pp. 2, 3).

[54] M. N. Daud, H. Lu, S. Chelkowski, and A. D. Bandrauk, "Quantum Control of Electron-Proton Symmetry Breaking in Dissociative Ionization of H_2 by Intense Laser Pulses", Int. J. Quantum Chem. **115**, 369–380 (2014) (cit. on p. 2).

[55] M. Kanno, H. Kono, and Y. Fujimura, "Control of π-Electron Rotation in Chiral Aromatic Molecules by Nonhelical Laser Pulses", Angew. Chem. Int. Ed. **45**, 7995–7998 (2006) (cit. on p. 2).

[56] H. Mineo, S. H. Lin, and Y. Fujimura, "Coherent π-Electron Dynamics of (P)-2,2′-Biphenol Induced by Ultrashort Linearly Polarized UV Pulses: Angular Momentum and Ring Current", J. Chem. Phys. **138**, 074304 (2013) (cit. on p. 2).

[57] H. Mineo, S. Lin, and Y. Fujimura, "Vibrational Effects on UV/Vis Laser-Driven π-Electron Ring Currents in Aromatic Ring Molecules", Chem. Phys. **442**, 103–110 (2014) (cit. on p. 2).

[58] M. F. Kling, P. von den Hoff, I. Znakovskaya, and R. de Vivie-Riedle, "(Sub-)femtosecond Control of Molecular Reactions via Tailoring the Electric Field of Light", Phys. Chem. Chem. Phys. **15**, 9448–9467 (2013) (cit. on p. 2).

[59] V. Despré, A. Marciniak, V. Loriot, M. C. E. Galbraith, A. Rouzée, M. J. J. Vrakking, F. Lépine, and A. I. Kuleff, "Attosecond Hole Migration in Benzene Molecules Surviving Nuclear Motion", J. Phys. Chem. Lett. **6**, 426–431 (2015) (cit. on p. 2).

[60] N. V. Golubev and A. I. Kuleff, "Control of Charge Migration in Molecules by Ultrashort Laser Pulses", Phys. Rev. A **91**, 051401 (2015) (cit. on p. 2).

[61] I. Barth and J. Manz, "Periodic Electron Circulation Induced by Circularly Polarized Laser Pulses: Quantum Model Simulations for Mg Porphyrin", Angew. Chem. Int. Ed. **45**, 2962–2965 (2006) (cit. on p. 2).

[62] L. A. Nafie, "Electron Transition Current Density in Molecules. 1. Non-Born-Oppenheimer Theory of Vibronic and Vibrational Transitions", J. Phys. Chem. A **101**, 7826–7833 (1997) (cit. on pp. 2, 38).

[63] T. B. Freedman, X. Gao, M.-L. Shih, and L. A. Nafie, "Electron Transition Current Density in Molecules. 2. Ab Initio Calculations for Electronic Transitions in Ethylene and Formaldehyde", J. Phys. Chem. A **102**, 3352–3357 (1998) (cit. on pp. 2, 38).

[64] L. F. Pacios, "CheckDen: A Computer Program to Generate 1D, 2D and 3D Grids of Functions Dependent on the Molecular Ab Initio Electron Density", Comput. Biol. Chem. **27**, 197–209 (2003) (cit. on p. 2).

[65] L. F. Pacios and A. Fernandez, "CheckDen, a Program to Compute Quantum Molecular Properties on Spatial Grids", J. Mol. Graph. Model. **28**, 102–112 (2009) (cit. on p. 2).

[66] T. Lu and F. Chen, "Multiwfn: A Multifunctional Wavefunction Analyzer", J. Comput. Chem. **33**, 580–592 (2011) (cit. on p. 2).

[67] J. Solano-Altamirano and J. M. Hernández-Pérez, "DensToolKit: A Comprehensive Open-Source Package for Analyzing the Electron Density and Its Derivative Scalar and Vector Fields", Comput. Phys. Commun. **196**, 362–371 (2015) (cit. on p. 2).

[68] M. Kohout, *DGrid, Version 5.0*, Dresden, 2017 (cit. on p. 2).

[69] R. L. Martin, "Natural Transition Orbitals", J. Chem. Phys. **118**, 4775–4777 (2003) (cit. on pp. 3, 27, 43, 214).

[70] A. Giusti-Suzor, F. H. Mies, L. F. DiMauro, E. Charron, and B. Yang, "Dynamics of H_2^+in Intense Laser Fields", J. Phys. B: At. Mol. Opt. Phys. **28**, 309–339 (1995) (cit. on p. 3).

[71] T. Zuo and A. D. Bandrauk, "Charge-Resonance-Enhanced Ionization of Diatomic Molecular Ions by Intense Lasers", Phys. Rev. A **52**, R2511–R2514 (1995) (cit. on p. 3).

[72] J. H. Posthumus, "The Dynamics of Small Molecules in Intense Laser Fields", Rep. Prog. Phys. **67**, 623–665 (2004) (cit. on p. 3).

[73] A. D. Bandrauk, S. Chelkowski, and H. S. Nguyen, "Attosecond Localization of Electrons in Molecules", Int. J. Quantum Chem. **100**, 834–844 (2004) (cit. on p. 3).

[74] M. Lein, "Molecular Imaging Using Recolliding Electrons", J. Phys. B: At. Mol. Opt. Phys. **40**, R135–R173 (2007) (cit. on p. 3).

[75] M. J. J. Vrakking, "Attosecond Imaging", Phys. Chem. Chem. Phys. **16**, 2775–2789 (2014) (cit. on p. 3).

[76] H. Xu, F. He, D. Kielpinski, R. Sang, and I. Litvinyuk, "Experimental Observation of the Elusive Double-Peak Structure in R-Dependent Strong-Field Ionization Rate of H_2^+", Sci. Rep. **5**, 13527 (2015) (cit. on p. 3).

[77] M. R. Miller, Y. Xia, A. Becker, and A. Jaroń-Becker, "Laser-Driven Nonadiabatic Electron Dynamics in Molecules", Optica **3**, 259–269 (2016) (cit. on p. 3).

[78] H. Ibrahim, C. Lefebvre, A. D. Bandrauk, A. Staudte, and F. Légaré, "H_2: the Benchmark Molecule for Ultrafast Science and Technologies", J. Phys. B: At. Mol. Opt. Phys. **51**, 042002 (2018) (cit. on p. 3).

[79] H. Eyring, J. Walter, and G. E. Kimball, in *Quantum Chemistry* (John Wiley & Sons, New York, 1944) Chap. 11 (cit. on pp. 3, 45, 214).

[80] A. T. Balaban, P. v. R. Schleyer, and H. S. Rzepa, "Crocker, Not Armit and Robinson, Begat the Six Aromatic Electrons", Chem. Rev. **105**, 3436–3447 (2005) (cit. on p. 3).

[81] D. E. Bean and P. W. Fowler, "Effect on Ring Current of the Kekulé Vibration in Aromatic and Antiaromatic Rings", J. Phys. Chem. A **115**, 13649–13656 (2011) (cit. on p. 3).

[82] A. Schild, D. Choudhary, V. D. Sambre, and B. Paulus, "Electron Density Dynamics in the Electronic Ground State: Motion Along the Kekulé Mode of Benzene", J. Phys. Chem. A **116**, 11355–11360 (2012) (cit. on pp. 3, 4).

[83] I. S. Ulusoy and M. Nest, "Correlated Electron Dynamics: How Aromaticity Can Be Controlled", J. Am. Chem. Soc. **133**, 20230–20236 (2011) (cit. on pp. 3, 4, 45, 214).

[84] B. Friedrich and D. Herschbach, "Alignment and Trapping of Molecules in Intense Laser Fields", Phys. Rev. Lett. **74**, 4623–4626 (1995) (cit. on p. 3).

[85] H. Stapelfeldt and T. Seideman, "Colloquium: Aligning Molecules with Strong Laser Pulses", Rev. Mod. Phys. **75**, 543–557 (2003) (cit. on p. 3).

[86] M. Leibscher, I. S. Averbukh, and H. Rabitz, "Molecular Alignment by Trains of Short Laser Pulses", Phys. Rev. Lett. **90**, 213001 (2003) (cit. on p. 3).

[87] R. d. Nalda, E. Heesel, M. Lein, N. Hay, R. Velotta, E. Springate, M. Castillejo, and J. P. Marangos, "Role of Orbital Symmetry in High-Order Harmonic Generation from Aligned Molecules", Phys. Rev. A **69**, 031804 (2004) (cit. on p. 3).

[88] S. Fleischer, I. S. Averbukh, and Y. Prior, "Selective Alignment of Molecular Spin Isomers", Phys. Rev. Lett. **99**, 093002 (2007) (cit. on p. 3).

[89] K. Oda, M. Hita, S. Minemoto, and H. Sakai, "All-Optical Molecular Orientation", Phys. Rev. Lett. **104**, 213901 (2010) (cit. on p. 3).

[90] T. Grohmann and M. Leibscher, "Nuclear Spin Selective Alignment of Ethylene and Analogues", J. Chem. Phys. **134**, 204316 (2011) (cit. on p. 3).

[91] G. Knizia and J. E. M. N. Klein, "Electron Flow in Reaction Mechanisms-Revealed from First Principles", Angew. Chem. Int. Ed. **54**, 5518–5522 (2015) (cit. on p. 3).

[92] H.-C. Hege, J. Manz, F. Marquardt, B. Paulus, and A. Schild, "Electron Flux during Pericyclic Reactions in the Tunneling Limit: Quantum Simulation for Cyclooctatetraene", Chem. Phys. **376**, 46–55 (2010) (cit. on p. 4).

[93] D. Andrae, I. Barth, T. Bredtmann, H.-C. Hege, J. Manz, F. Marquardt, and B. Paulus, "Electronic Quantum Fluxes during Pericyclic Reactions Exemplified for the Cope Rearrangement of Semibullvalene", J. Phys. Chem. B **115**, 5476–5483 (2011) (cit. on p. 4).

[94] T. Bredtmann and J. Manz, "Electronic Bond-To-Bond Fluxes in Pericyclic Reactions: Synchronous or Asynchronous?", Angew. Chem. Int. Ed. **50**, 12652–12654 (2011) (cit. on p. 4).

[95] T. Bredtmann, D. J. Diestler, S.-D. Li, J. Manz, J. F. Pérez-Torres, W.-J. Tian, Y.-B. Wu, Y. Yang, and H.-J. Zhai, "Quantum Theory of Concerted Electronic and Nuclear Fluxes Associated with Adiabatic Intramolecular Processes", Phys. Chem. Chem. Phys. **17**, 29421–29464 (2015) (cit. on p. 4).

[96] N. A. Anderson and T. Lian, "Ultrafast Electron Transfer at the Molecule-Semiconductor Nanoparticle Interface", Annu. Rev. Phys. Chem. **56**, 491–519 (2005) (cit. on p. 4).

[97] B. O'Regan and M. Grätzel, "A Low-Cost, High-Efficiency Solar Cell Based on Dye-Sensitized Colloidal TiO_2 Films", Nature **353**, 737–740 (1991) (cit. on p. 4).

[98] A. Hagfeldt and M. Grätzel, "Light-Induced Redox Reactions in Nanocrystalline Systems", Chem. Rev. **95**, 49–68 (1995) (cit. on p. 4).

[99] A. Hagfeldt and M. Grätzel, "Molecular Photovoltaics", Acc. Chem. Res. **33**, 269–277 (2000) (cit. on p. 4).

[100] M. Grätzel, "Photoelectrochemical Cells", Nature **414**, 338–344 (2001) (cit. on p. 4).

[101] J. B. Asbury, E. Hao, Y. Wang, H. N. Ghosh, and T. Lian, "Ultrafast Electron Transfer Dynamics from Molecular Adsorbates to Semiconductor Nanocrystalline Thin Films", J. Phys. Chem. B **105**, 4545–4557 (2001) (cit. on p. 4).

[102] M. Grätzel, "Dye-Sensitized Solar Cells", J. Photochem. Photobiol. C **4**, 145–153 (2003) (cit. on p. 4).

[103] A. Hagfeldt, G. Boschloo, L. Sun, L. Kloo, and H. Pettersson, "Dye-Sensitized Solar Cells", Chem. Rev. **110**, 6595–6663 (2010) (cit. on pp. 4, 5).

[104] R. Huber, J.-E. Moser, M. Grätzel, and J. Wachtveitl, "Real-Time Observation of Photoinduced Adiabatic Electron Transfer in Strongly Coupled Dye/Semiconductor Colloidal Systems with a 6 fs Time Constant", J. Phys. Chem. B **106**, 6494–6499 (2002) (cit. on pp. 5, 48).

[105] L. Dworak, V. V. Matylitsky, and J. Wachtveitl, "Ultrafast Photoinduced Processes in Alizarin-Sensitized Metal Oxide Mesoporous Films", ChemPhysChem **10**, 384–391 (2009) (cit. on pp. 5, 48).

[106] M. Thoss, I. Kondov, and H. Wang, "Theoretical Study of Ultrafast Heterogeneous Electron Transfer Reactions at Dye-Semiconductor Interfaces", Chem. Phys. **304**, 169–181 (2004) (cit. on p. 5).

[107] I. Kondov, M. Čížek, C. Benesch, H. Wang, and M. Thoss, "Quantum Dynamics of Photoinduced Electron-Transfer Reactions in Dye-Semiconductor Systems: First-Principles Description and Application to Coumarin 343-TiO_2", J. Phys. Chem. C **111**, 11970–11981 (2007) (cit. on p. 5).

[108] W. R. Duncan and O. V. Prezhdo, "Theoretical Studies of Photoinduced Electron Transfer in Dye-Sensitized TiO_2", Annu. Rev. Phys. Chem. **58**, 143–184 (2007) (cit. on p. 5).

[109] O. V. Prezhdo, W. R. Duncan, and V. V. Prezhdo, "Photoinduced Electron Dynamics at the Chromophore-Semiconductor Interface: A Time-Domain Ab Initio Perspective", Prog. Surf. Sci. **84**, 30–68 (2009) (cit. on p. 5).

[110] D. Rocca, R. Gebauer, F. D. Angelis, M. K. Nazeeruddin, and S. Baroni, "Time-Dependent Density Functional Theory Study of Squaraine Dye-Sensitized Solar Cells", Chem. Phys. Lett. **475**, 49–53 (2009) (cit. on p. 5).

[111] C. Anselmi, E. Mosconi, M. Pastore, E. Ronca, and F. D. Angelis, "Adsorption of Organic Dyes on TiO_2 Surfaces in Dye-Sensitized Solar Cells: Interplay of Theory and Experiment", Phys. Chem. Chem. Phys. **14**, 15963–15974 (2012) (cit. on p. 5).

[112] F. Ambrosio, N. Martsinovich, and A. Troisi, "Effect of the Anchoring Group on Electron Injection: Theoretical Study of Phosphonated Dyes for Dye-Sensitized Solar Cells", J. Phys. Chem. C **116**, 2622–2629 (2012) (cit. on p. 5).

[113] Y. Ooyama, M. Kanda, K. Uenaka, and J. Ohshita, "Effect of Substituents in Catechol Dye Sensitizers on Photovoltaic Performance of Type II Dye-Sensitized Solar Cells", ChemPhysChem **16**, 3049–3057 (2015) (cit. on p. 5).

[114] J. E. Moser and M. Grätzel, "Observation of Temperature Independent Heterogeneous Electron Transfer Reactions in the Inverted Marcus Region", Chem. Phys. **176**, 493–500 (1993) (cit. on p. 5).

[115] R. Huber, S. Spörlein, J. E. Moser, M. Grätzel, and J. Wachtveitl, "The Role of Surface States in the Ultrafast Photoinduced Electron Transfer from Sensitizing Dye Molecules to Semiconductor Colloids", J. Phys. Chem. B **104**, 8995–9003 (2000) (cit. on p. 5).

[116] R. Huber, J. E. Moser, M. Grätzel, and J. Wachtveitl, "Observation of Photoinduced Electron Transfer in Dye/Semiconductor Colloidal Systems with Different Coupling Strengths", Chem. Phys. **285**, 39–45 (2002) (cit. on p. 5).

[117] W. R. Duncan and O. V. Prezhdo, "Electronic Structure and Spectra of Catechol and Alizarin in the Gas Phase and Attached to Titanium", J. Phys. Chem. B **109**, 365–373 (2005) (cit. on p. 5).

[118] W. R. Duncan, W. M. Stier, and O. V. Prezhdo, "Ab Initio Nonadiabatic Molecular Dynamics of the Ultrafast Electron Injection across the Alizarin-TiO_2 Interface", J. Am. Chem. Soc. **127**, 7941–7951 (2005) (cit. on p. 5).

[119] V. V. Matylitsky, M. O. Lenz, and J. Wachtveitl, "Observation of pH-Dependent Back-Electron-Transfer Dynamics in Alizarin/TiO_2 Adsorbates: Importance of Trap States", J. Phys. Chem. B **110**, 8372–8379 (2006) (cit. on p. 5).

[120] Z. Guo, W. Liang, Y. Zhao, and G. Chen, "Real-Time Propagation of the Reduced One-Electron Density Matrix in Atom-Centered Orbitals: Application to Electron Injection Dynamics in Dye-Sensitized TiO_2 Clusters", J. Phys. Chem. C **112**, 16655–16662 (2008) (cit. on p. 5).

[121] A. Nawrocka and S. Krawczyk, "Electronic Excited State of Alizarin Dye Adsorbed on TiO_2 Nanoparticles: A Study by Electroabsorption (Stark Effect) Spectroscopy", J. Phys. Chem. C **112**, 10233–10241 (2008) (cit. on p. 5).

[122] S. Kaniyankandy, S. Verma, J. A. Mondal, D. K. Palit, and H. N. Ghosh, "Evidence of Multiple Electron Injection and Slow Back Electron Transfer in Alizarin-Sensitized Ultrasmall TiO_2 Particles", J. Phys. Chem. C **113**, 3593–3599 (2009) (cit. on p. 5).

[123] J. Li, I. Kondov, H. Wang, and M. Thoss, "Theoretical Study of Photoinduced Electron-Transfer Processes in the Dye-Semiconductor System Alizarin-TiO_2", J. Phys. Chem. C **114**, 18481–18493 (2010) (cit. on p. 5).

[124] R. Sánchez-de-Armas, J. O. López, M. A. San-Miguel, J. F. Sanz, P. Ordejón, and M. Pruneda, "Real-Time TD-DFT Simulations in Dye Sensitized Solar Cells: The Electronic Absorption Spectrum of Alizarin Supported on TiO_2 Nanoclusters", J. Chem. Theory Comput. **6**, 2856–2865 (2010) (cit. on p. 5).

[125] O. Lehtonen, D. Sundholm, and T. Vänskä, "Computational Studies of Semiconductor Quantum Dots", Phys. Chem. Chem. Phys. **10**, 4535–4550 (2008) (cit. on p. 5).

[126] A. J. Nozik, M. C. Beard, J. M. Luther, M. Law, R. J. Ellingson, and J. C. Johnson, "Semiconductor Quantum Dots and Quantum Dot Arrays and Applications of Multiple Exciton Generation to Third-Generation Photovoltaic Solar Cells", Chem. Rev. **110**, 6873–6890 (2010) (cit. on p. 5).

[127] A. P. Alivisatos, "Semiconductor Clusters, Nanocrystals, and Quantum Dots", Science **271**, 933–937 (1996) (cit. on p. 5).

[128] S. V. Kondratenko, O. V. Vakulenko, Y. N. Kozyrev, M. Y. Rubezhanska, A. G. Naumovets, A. S. Nikolenko, V. S. Lysenko, V. V. Strelchuk, and C. Teichert, "Photovoltaic Properties and Photoconductivity in Multilayer Ge/Si Heterostructures with Ge Nanoislands", J. Mater. Sci. **46**, 5737–5742 (2011) (cit. on p. 5).

[129] B. Bitnar, "Silicon, Germanium and Silicon/Germanium Photocells for Thermophotovoltaics Applications", Semicond. Sci. Technol. **18**, S221–S227 (2003) (cit. on p. 5).

[130] T. D. Ladd, F. Jelezko, R. Laflamme, Y. Nakamura, C. Monroe, and J. L. O'Brien, "Quantum Computers", Nature **464**, 45–53 (2010) (cit. on p. 5).

[131] R. Vrijen, E. Yablonovitch, K. Wang, H. W. Jiang, A. Balandin, V. Roychowdhury, T. Mor, and D. DiVincenzo, "Electron-Spin-Resonance Transistors for Quantum Computing in Silicon-Germanium Heterostructures", Phys. Rev. A **62**, 012306 (2000) (cit. on p. 5).

[132] S. Ciraci and I. P. Batra, "Strained Si/Ge Superlattices: Structural Stability, Growth, and Electronic Properties", Phys. Rev. B **38**, 1835–1848 (1988) (cit. on pp. 5, 6).

[133] J. E. Bernard and A. Zunger, "Strain Energy and Stability of Si-Ge Compounds, Alloys, and Superlattices", Phys. Rev. B **44**, 1663–1681 (1991) (cit. on p. 5).

[134] B. Voigtländer, "Fundamental Processes in Si/Si and Ge/Si Epitaxy Studied by Scanning Tunneling Microscopy during Growth", Surf. Sci. Rep. **43**, 127–254 (2001) (cit. on pp. 5, 6).

[135] C. Teichert, "Self-Organization of Nanostructures in Semiconductor Heteroepitaxy", Phys. Rep. **365**, 335–432 (2002) (cit. on p. 5).

[136] O. Kirfel, E. Müller, D. Grützmacher, K. Kern, A. Hesse, J. Stangl, V. Holý, and G. Bauer, "Shape and Composition Change of Ge Dots Due to Si Capping", Appl. Surf. Sci. **224**, 139–142 (2004) (cit. on pp. 5, 6).

[137] A. I. Yakimov, V. V. Kirienko, V. A. Armbrister, A. A. Bloshkin, and A. V. Dvurechenskii, "Electronic States in Vertically Ordered Ge/Si Quantum Dots Detected by Photocurrent Spectroscopy", Phys. Rev. B **90**, 035430 (2014) (cit. on pp. 5, 6).

[138] A. I. Yakimov, A. V. Dvurechenskii, A. I. Nikiforov, A. A. Bloshkin, A. V. Nenashev, and V. A. Volodin, "Electronic States in Ge/Si Quantum Dots with Type-II Band Alignment Initiated by Space-Charge Spectroscopy", Phys. Rev. B **73**, 115333 (2006) (cit. on p. 5).

[139] K. B. Wong, M. Jaros, I. Morrison, and J. P. Hagon, "Electronic Structure and Optical Properties of Si-Ge Superlattices", Phys. Rev. Lett. **60**, 2221–2224 (1988) (cit. on p. 6).

[140] V. L. Thanh, "Mechanisms of Self-Organization of Ge/Si(001) Quantum Dots", Phys. E **23**, 401–409 (2004) (cit. on p. 6).

[141] A. I. Yakimov, A. V. Dvurechenskii, V. A. Volodin, M. D. Efremov, A. I. Nikiforov, G. Y. Mikhalyov, E. I. Gatskevich, and G. D. Ivlev, "Effect of Pulsed Laser Action on Hole-Energy Spectrum of Ge/Si Self-Assembled Quantum Dots", Phys. Rev. B **72**, 115318 (2005) (cit. on p. 6).

[142] W.-Y. Chen, W.-H. Chang, A.-T. Chou, T.-M. Hsu, P.-S. Chen, Z. Pei, and L.-S. Lai, "Optical Properties of Stacked Ge/Si Quantum Dots with Different Spacer Thickness Grown by Chemical Vapor Deposition", Appl. Surf. Sci. **224**, 148–151 (2004) (cit. on p. 6).

[143] M. Larsson, A. Elfving, P. O. Holtz, G. V. Hansson, and W.-X. Ni, "Spatially Direct and Indirect Transitions Observed for Si/Ge Quantum Dots", Appl. Phys. Lett. **82**, 4785–4787 (2003) (cit. on p. 6).

[144] A. Franceschetti, H. Fu, L. W. Wang, and A. Zunger, "Many-Body Pseudopotential Theory of Excitons in InP and CdSe Quantum Dots", Phys. Rev. B **60**, 1819–1829 (1999) (cit. on p. 6).

[145] F. A. Reboredo, A. Franceschetti, and A. Zunger, "Dark Excitons Due to Direct Coulomb Interactions in Silicon Quantum Dots", Phys. Rev. B **61**, 13073–13087 (2000) (cit. on p. 6).

[146] E. L. de Oliveira, E. L. Albuquerque, J. S. de Sousa, G. A. Farias, and F. M. Peeters, "Configuration-Interaction Excitonic Absorption in Small Si/Ge and Ge/Si Core/Shell Nanocrystals", J. Phys. Chem. C **116**, 4399–4407 (2012) (cit. on p. 6).

[147] E. Schrödinger, "Quantisierung als Eigenwertproblem", Ann. Phys. (Leipzig) **81**, 109–139 (1926) (cit. on pp. 7, 38).

[148] C. Cohen-Tannoudji, B. Diu, and F. Laloë, *Quantenmechanik* (De Gruyter, 2007) (cit. on pp. 8, 37).

[149] A. Szabo and N. S. Ostlund, *Modern Quantum Chemistry* (Dover Publications, Mineola, 1996) (cit. on pp. 8–10, 12–15, 25, 26).

[150] F. Jensen, *Introduction to Computational Chemistry*, 3rd ed. (John Wiley & Sons, Chichester, Hoboken, 2017) (cit. on pp. 8–10, 13, 15, 18, 24, 26).

[151] M. Born and R. Oppenheimer, "Zur Quantentheorie Der Molekeln", Ann. Phys. (Berlin) **389**, 457–484 (1927) (cit. on pp. 9, 10).

[152] M. Born and K. Huang, *Dynamical Theory of Crystal Lattices*, International Series of Monographs on Physics (Clarendon Press, 1954) (cit. on p. 10).

[153] D. Tannor, *Introduction to Quantum Mechanics: A Time-Dependent Perspective* (University Science Books, Sausalito, Calif, 2007) (cit. on p. 10).

[154] W. Domcke, D. Yarkony, and H. Köppel, *Conical Intersections: Electronic Structure, Dynamics & Spectroscopy*, Advanced Series in Physical Chemistry (World Scientific, 2004) (cit. on p. 10).

[155] W. Koch and M. Holthausen, *A Chemist's Guide to Density Functional Theory* (Wiley, 2015) (cit. on pp. 10, 15, 18).

[156] T. Helgaker, P. Jørgensen, and J. Olsen, *Molecular Electronic-Structure Theory* (Wiley, Chichester, New York, 2000) (cit. on pp. 10, 13).

[157] D. R. Hartree, "The Wave Mechanics of an Atom with a Non-Coulomb Central Field. Part I. Theory and Methods", Math. Proc. Camb. Philos. Soc. **24**, 89–110 (1928) (cit. on p. 11).

[158] D. R. Hartree, "The Wave Mechanics of an Atom with a Non-Coulomb Central Field. Part II. Some Results and Discussion", Math. Proc. Camb. Philos. Soc. **24**, 111–132 (1928) (cit. on p. 11).

[159] V. Fock, "Näherungsmethode zur Lösung des Quantenmechanischen Mehrkörperproblems", Z. Phys. **61**, 126–148 (1930) (cit. on p. 11).

[160] W. Pauli, "Über den Zusammenhang des Abschlusses der Elektronengruppen im Atom mit der Komplexstruktur der Spektren", Z. Phys. **31**, 765–783 (1925) (cit. on p. 11).

[161] W. Pauli, "The Connection Between Spin and Statistics", Phys. Rev. **58**, 716–722 (1940) (cit. on p. 11).

[162] J. C. Slater, "A Simplification of the Hartree-Fock Method", Phys. Rev. **81**, 385–390 (1951) (cit. on p. 11).

[163] C. C. J. Roothaan, "New Developments in Molecular Orbital Theory", Rev. Mod. Phys. **23**, 69–89 (1951) (cit. on pp. 12, 13).

[164] G. G. Hall, "The Molecular Orbital Theory of Chemical Valency VIII. A Method of Calculating Ionization Potentials", Proc. R. Soc. Lond. A **205**, 541–552 (1951) (cit. on pp. 12, 13).

[165] J. C. Slater, "The Theory of Complex Spectra", Phys. Rev. **34**, 1293–1322 (1929) (cit. on p. 14).

[166] E. U. Condon, "The Theory of Complex Spectra", Phys. Rev. **36**, 1121–1133 (1930) (cit. on p. 14).

[167] J. C. Slater, "Molecular Energy Levels and Valence Bonds", Phys. Rev. **38**, 1109–1144 (1931) (cit. on p. 14).

[168] J. B. Foresman, M. Head-Gordon, J. A. Pople, and M. J. Frisch, "Toward a Systematic Molecular Orbital Theory for Excited States", J. Phys. Chem. **96**, 135–149 (1992) (cit. on p. 14).

[169] J. Olsen, B. O. Roos, P. Jørgensen, and H. J. A. Jensen, "Determinant Based Configuration Interaction Algorithms for Complete and Restricted Configuration Interaction Spaces", J. Chem. Phys. **89**, 2185–2192 (1988) (cit. on p. 15).

[170] P. G. Szalay, T. Müller, G. Gidofalvi, H. Lischka, and R. Shepard, "Multiconfiguration Self-Consistent Field and Multireference Configuration Interaction Methods and Applications", Chem. Rev. **112**, 108–181 (2012) (cit. on p. 15).

[171] B. O. Roos, P. R. Taylor, and P. E. Siegbahn, "A Complete Active Space SCF Method (CASSCF) Using a Density Matrix Formulated Super-CI Approach", Chem. Phys. **48**, 157–173 (1980) (cit. on p. 15).

[172] P. E. M. Siegbahn, J. Almlöf, A. Heiberg, and B. O. Roos, "The Complete Active Space SCF (CASSCF) Method in a Newton–Raphson Formulation with Application to the HNO Molecule", J. Chem. Phys. **74**, 2384–2396 (1981) (cit. on p. 15).

[173] B. O. Roos, "The Complete Active Space SCF Method in a Fock-Matrix-Based Super-CI Formulation", Int. J. Quantum Chem **18**, 175–189 (2009) (cit. on p. 15).

[174] R. J. Buenker and S. D. Peyerimhoff, "Individualized Configuration Selection in CI Calculations with Subsequent Energy Extrapolation", Theor. Chem. Acc. **35**, 33–58 (1974) (cit. on p. 15).

[175] H.-J. Werner and E.-A. Reinsch, "The Self-Consistent Electron Pairs Method for Multiconfiguration Reference State Functions", J. Chem. Phys. **76**, 3144–3156 (1982) (cit. on p. 15).

[176] R. Parr and Y. Weitao, *Density-Functional Theory of Atoms and Molecules*, International Series of Monographs on Chemistry (Oxford University Press, 1994) (cit. on pp. 15, 18).

[177] F. Neese, "Prediction of Molecular Properties and Molecular Spectroscopy with Density Functional Theory: From Fundamental Theory to Exchange-Coupling", Coord. Chem. Rev. **253**, 526–563 (2009) (cit. on pp. 15, 17–19).

[178] L. Piela, *Ideas of Quantum Chemistry* (Elsevier Science, 2013) (cit. on p. 15).

[179] N. Mardirossian and M. Head-Gordon, "Thirty Years of Density Functional Theory in Computational Chemistry: An Overview and Extensive Assessment of 200 Density Functionals", Mol. Phys. **115**, 2315–2372 (2017) (cit. on pp. 15, 17–19).

[180] P. Hohenberg and W. Kohn, "Inhomogeneous Electron Gas", Phys. Rev. **136**, B864–B871 (1964) (cit. on pp. 16, 20).

[181] W. Kohn and L. J. Sham, "Self-Consistent Equations Including Exchange and Correlation Effects", Phys. Rev. **140**, A1133–A1138 (1965) (cit. on p. 16).

[182] J. P. Perdew, A. Ruzsinszky, J. Tao, V. N. Staroverov, G. E. Scuseria, and G. I. Csonka, "Prescription for the Design and Selection of Density Functional Approximations: More Constraint Satisfaction with Fewer Fits", J. Chem. Phys. **123**, 062201 (2005) (cit. on p. 18).

[183] D. M. Ceperley and B. J. Alder, "Ground State of the Electron Gas by a Stochastic Method", Phys. Rev. Lett. **45**, 566–569 (1980) (cit. on p. 19).

[184] P. A. M. Dirac, "Note on Exchange Phenomena in the Thomas Atom", Math. Proc. Cambridge Philos. Soc. **26**, 376–385 (1930) (cit. on p. 19).

[185] J. C. Slater, "A Simplification of the Hartree-Fock Method", Phys. Rev. **81**, 385–390 (1951) (cit. on p. 19).

[186] S. H. Vosko, L. Wilk, and M. Nusair, "Accurate Spin-Dependent Electron Liquid Correlation Energies for Local Spin Density Calculations: A Critical Analysis", Can. J. Phys. **58**, 1200–1211 (1980) (cit. on p. 19).

[187] J. P. Perdew and Y. Wang, "Accurate and Simple Analytic Representation of the Electron-Gas Correlation Energy", Phys. Rev. B **45**, 13244–13249 (1992) (cit. on p. 19).

[188] T. Chachiyo, "Communication: Simple and Accurate Uniform Electron Gas Correlation Energy for the Full Range of Densities", J. Chem. Phys. **145**, 021101 (2016) (cit. on p. 19).

[189] D. M. Ceperley and B. J. Alder, "Ground State of the Electron Gas by a Stochastic Method", Phys. Rev. Lett. **45**, 566–569 (1980) (cit. on p. 19).

[190] J. P. Perdew, J. A. Chevary, S. H. Vosko, K. A. Jackson, M. R. Pederson, D. J. Singh, and C. Fiolhais, "Atoms, Molecules, Solids, and Surfaces: Applications of the Generalized Gradient Approximation for Exchange and Correlation", Phys. Rev. B **46**, 6671–6687 (1992) (cit. on p. 19).

[191] J. P. Perdew, K. Burke, and M. Ernzerhof, "Generalized Gradient Approximation Made Simple", Phys. Rev. Lett. **77**, 3865–3868 (1996) (cit. on p. 19).

[192] A. D. Becke, "A New Mixing of Hartree–Fock and Local Density-Functional Theories", J. Chem. Phys. **98**, 1372–1377 (1993) (cit. on p. 19).

[193] A. D. Becke, "Density-Functional Thermochemistry. III. The Role of Exact Exchange", J. Chem. Phys. **98**, 5648–5652 (1993) (cit. on p. 19).

[194] P. J. Stephens, F. J. Devlin, C. F. Chabalowski, and M. J. Frisch, "Ab Initio Calculation of Vibrational Absorption and Circular Dichroism Spectra Using Density Functional Force Fields", J. Phys. Chem. **98**, 11623–11627 (1994) (cit. on p. 19).

[195] C. Adamo and V. Barone, "Toward Reliable Density Functional Methods without Adjustable Parameters: The PBE0 Model", J. Chem. Phys. **110**, 6158–6170 (1999) (cit. on p. 19).

[196] S. Grimme, J. Antony, S. Ehrlich, and H. Krieg, "A Consistent and Accurate Ab Initio Parametrization of Density Functional Dispersion Correction (DFT-D) for the 94 Elements H-Pu", J. Chem. Phys. **132**, 154104 (2010) (cit. on p. 19).

[197] S. Grimme, "Accurate Description of Van der Waals Complexes by Density Functional Theory Including Empirical Corrections", J. Comput. Chem. **25**, 1463–1473 (2004) (cit. on p. 19).

[198] S. Grimme, "Semiempirical GGA-Type Density Functional Constructed with a Long-Range Dispersion Correction", J. Comput. Chem. **27**, 1787–1799 (2006) (cit. on p. 19).

[199] E. K. U. Gross, J. F. Dobson, and M. Petersilka, "Density Functional Theory of Time-Dependent Phenomena", in *Topics in Current Chemistry* (Springer-Verlag), pp. 81–172 (cit. on pp. 20, 21).

[200] M. Marques and E. Gross, "Time-Dependent Density Functional Theory", Annu. Rev. Phys. Chem. **55**, 427–455 (2004) (cit. on pp. 20, 21).

[201] M. Marques, *Time-Dependent Density Functional Theory*, Lecture Notes in Physics (Springer, 2006) (cit. on pp. 20, 21).

[202] M. E. Casida, "Time-Dependent Density-Functional Theory for Molecules and Molecular Solids", J. Mol. Struct. (Theochem.) **914**, 3–18 (2009) (cit. on pp. 20, 21).

[203] C. Ullrich, *Time-Dependent Density-Functional Theory: Concepts and Applications*, 1st ed. (Oxford University Press, Oxford, New YorK, 2012) (cit. on pp. 20, 21).

[204] M. Marques, N. Maitra, F. Nogueira, E. Gross, and A. Rubio, *Fundamentals of Time-Dependent Density Functional Theory*, Lecture Notes in Physics (Springer Berlin Heidelberg, 2012) (cit. on pp. 20, 21).

[205] E. Runge and E. Gross, "Density-Functional Theory for Time-Dependent Systems", Phys. Rev. Lett. **52**, 997–1000 (1984) (cit. on p. 20).

[206] R. van Leeuwen, "Mapping from Densities to Potentials in Time-Dependent Density-Functional Theory", Phys. Rev. Lett. **82**, 3863–3866 (1999) (cit. on p. 20).

[207] M. Ernzerhof, "Taylor-Series Expansion of Density Functionals", Phys. Rev. A **50**, 4593–4607 (1994) (cit. on p. 22).

[208] S. L. Adler, "Quantum Theory of the Dielectric Constant in Real Solids", Phys. Rev. **126**, 413–420 (1962) (cit. on p. 23).

[209] N. Wiser, "Dielectric Constant with Local Field Effects Included", Phys. Rev. **129**, 62–69 (1963) (cit. on p. 23).

[210] M. E. Casida, "Time-Dependent Density Functional Response Theory for Molecules", in *Recent Advances in Density Functional Methods* (WORLD SCIENTIFIC, 1995), pp. 155–192 (cit. on p. 24).

[211] S. Hirata and M. Head-Gordon, "Time-Dependent Density Functional Theory within the Tamm-Dancoff Approximation", Chem. Phys. Lett. **314**, 291–299 (1999) (cit. on p. 24).

[212] J. Leszczynski, *Handbook of Computational Chemistry* (Springer, 2012) (cit. on p. 24).

[213] E. Lewars, *Computational Chemistry: Introduction to the Theory and Applications of Molecular and Quantum Mechanics* (Springer Netherlands, 2010) (cit. on p. 24).

[214] M. Cossi, V. Barone, R. Cammi, and J. Tomasi, "Ab Initio Study of Solvated Molecules: A New Implementation of the Polarizable Continuum Model", Chem. Phys. Lett. **255**, 327–335 (1996) (cit. on p. 25).

[215] A. Klamt and G. Schüürmann, "COSMO: A New Approach to Dielectric Screening in Solvents with Explicit Expressions for the Screening Energy and Its Gradient", J. Chem. Soc., Perkin Trans. 2, 799–805 (1993) (cit. on p. 25).

[216] A. Klamt, "Conductor-Like Screening Model for Real Solvents: A New Approach to the Quantitative Calculation of Solvation Phenomena", J. Phys. Chem. **99**, 2224–2235 (1995) (cit. on p. 25).

[217] A. Klamt, V. Jonas, T. Bürger, and J. C. W. Lohrenz, "Refinement and Parametrization of COSMO-RS", J. Phys. Chem. A **102**, 5074–5085 (1998) (cit. on p. 25).

[218] A. Schäfer, A. Klamt, D. Sattel, J. C. W. Lohrenz, and F. Eckert, "COSMO Implementation in TURBOMOLE: Extension of an Efficient Quantum Chemical Code towards Liquid Systems", Phys. Chem. Chem. Phys. **2**, 2187–2193 (2000) (cit. on p. 25).

[219] F. Eckert and A. Klamt, "Fast Solvent Screening via Quantum Chemistry: COSMO-RS Approach", AIChE J. **48**, 369–385 (2002) (cit. on p. 25).

[220] S. F. Boys, "Electronic Wave Functions - I. A General Method of Calculation for the Stationary States of Any Molecular System", Proc. Royal Soc. Lond. **200**, 542–554 (1950) (cit. on p. 25).

[221] R. S. Mulliken, "Electronic Population Analysis on LCAO–MO Molecular Wave Functions. I", J. Chem. Phys. **23**, 1833–1840 (1955) (cit. on p. 26).

[222] R. S. Mulliken, "Electronic Population Analysis on LCAO–MO Molecular Wave Functions. II. Overlap Populations, Bond Orders, and Covalent Bond Energies", J. Chem. Phys. **23**, 1841–1846 (1955) (cit. on p. 26).

[223] R. S. Mulliken, "Electronic Population Analysis on LCAO-MO Molecular Wave Functions. III. Effects of Hybridization on Overlap and Gross AO Populations", J. Chem. Phys. **23**, 2338–2342 (1955) (cit. on p. 26).

[224] R. S. Mulliken, "Electronic Population Analysis on LCAO-MO Molecular Wave Functions. IV. Bonding and Antibonding in LCAO and Valence-Bond Theories", J. Chem. Phys. **23**, 2343–2346 (1955) (cit. on p. 26).

[225] F. L. Hirshfeld, "Bonded-Atom Fragments for Describing Molecular Charge Densities", Theor. Chim. Acta **44**, 129–138 (1977) (cit. on p. 26).

[226] C. F. Guerra, J.-W. Handgraaf, E. J. Baerends, and F. M. Bickelhaupt, "Voronoi Deformation Density (VDD) Charges: Assessment of the Mulliken, Bader, Hirshfeld, Weinhold, and VDD Methods for Charge Analysis", J. Comput. Chem. **25**, 189–210 (2003) (cit. on p. 27).

[227] F. Plasser, M. Wormit, and A. Dreuw, "New Tools for the Systematic Analysis and Visualization of Electronic Excitations. I. Formalism", J. Chem. Phys. **141**, 024106 (2014) (cit. on p. 28).

[228] H. Breuer and F. Petruccione, *The Theory of Open Quantum Systems* (Oxford University Press, 2002) (cit. on pp. 29, 31).

[229] K. Blum, *Density Matrix Theory and Applications*, Physics of Atoms and Molecules (Springer US, 2013) (cit. on pp. 29, 33).

[230] G. Schaller, *Open Quantum Systems Far from Equilibrium*, Lecture Notes in Physics (Springer International Publishing, Cham, 2014) (cit. on p. 29).

[231] A. G. Redfield, "On the Theory of Relaxation Processes", IBM J. Res. Dev. **1**, 19–31 (1957) (cit. on p. 33).

[232] E. B. Davies, "Markovian Master Equations", Commun. Math. Phys. **39**, 91–110 (1974) (cit. on p. 33).

[233] R. Dümcke and H. Spohn, "The Proper Form of the Generator in the Weak Coupling Limit", Z. Phys. B **34**, 419–422 (1979) (cit. on p. 33).

[234] G. Lindblad, "On the Generators of Quantum Dynamical Semigroups", Commun. Math. Phys. **48**, 119–130 (1976) (cit. on p. 36).

[235] E. Fermi, *Nuclear Physics: A Course Given by Enrico Fermi at the University of Chicago* (University of Chicago Press, 1950) (cit. on p. 36).

[236] B. Shore, *Manipulating Quantum Structures Using Laser Pulses* (Cambridge University Press, 2011) (cit. on pp. 36, 37).

[237] I. I. Rabi, "Space Quantization in a Gyrating Magnetic Field", Phys. Rev. **51**, 652–654 (1937) (cit. on p. 37).

[238] I. I. Rabi, N. F. Ramsey, and J. Schwinger, "Use of Rotating Coordinates in Magnetic Resonance Problems", Rev. Mod. Phys. **26**, 167–171 (1954) (cit. on p. 37).

[239] B. Shore, *The Theory of Coherent Atomic Excitation: Simple Atoms and Fields*, The Theory of Coherent Atomic Excitation (Wiley, 1990) (cit. on p. 37).

[240] G. Hermann, B. Paulus, J. F. Pérez-Torres, and V. Pohl, "Electronic and Nuclear Flux Densities in the H_2 Molecule", Phys. Rev. A **89**, 052504 (2014) (cit. on p. 38).

[241] M. Okuyama and K. Takatsuka, "Electron Flux in Molecules Induced by Nuclear Motion", Chem. Phys. Lett. **476**, 109–115 (2009) (cit. on p. 38).

[242] D. J. Diestler, "Coupled-Channels Quantum Theory of Electronic Flux Density in Electronically Adiabatic Processes: Fundamentals", J. Phys. Chem. A **116**, 2728–2735 (2011) (cit. on p. 38).

[243] D. J. Diestler, A. Kenfack, J. Manz, and B. Paulus, "Coupled-Channels Quantum Theory of Electronic Flux Density in Electronically Adiabatic Processes: Application to the Hydrogen Molecule Ion", J. Phys. Chem. A **116**, 2736–2742 (2011) (cit. on p. 38).

[244] S. Patchkovskii, "Electronic Currents and Born-Oppenheimer Molecular Dynamics", J. Chem. Phys. **137**, 084109 (2012) (cit. on p. 38).

[245] D. J. Diestler, "Beyond the Born–Oppenheimer Approximation: A Treatment of Electronic Flux Density in Electronically Adiabatic Molecular Processes", J. Phys. Chem. A **117**, 4698–4708 (2013) (cit. on p. 38).

[246] T. Bredtmann, D. J. Diestler, S.-D. Li, J. Manz, J. F. Pérez-Torres, W.-J. Tian, Y.-B. Wu, Y. Yang, and H.-J. Zhai, "Quantum Theory of Concerted Electronic and Nuclear Fluxes Associated with Adiabatic Intramolecular Processes", Phys. Chem. Chem. Phys. **17**, 29421–29464 (2015) (cit. on p. 38).

[247] V. Pohl and J. C. Tremblay, "Adiabatic Electronic Flux Density: A Born-Oppenheimer Broken-Symmetry Ansatz", Phys. Rev. A **93**, 012504 (2016) (cit. on p. 38).

[248] A. Schild, F. Agostini, and E. K. U. Gross, "Electronic Flux Density beyond the Born–Oppenheimer Approximation", J. Phys. Chem. A **120**, 3316–3325 (2016) (cit. on p. 38).

[249] I. Barth, H.-C. Hege, H. Ikeda, A. Kenfack, M. Koppitz, J. Manz, F. Marquardt, and G. K. Paramonov, "Concerted Quantum Effects of Electronic and Nuclear Fluxes in Molecules", Chem. Phys. Lett. **481**, 118–123 (2009) (cit. on pp. 38, 39).

[250] M. Berg, B. Paulus, and T. Bredtmann, "Electronic Quantum Fluxes in Vibrating Symmetric and Polar Single, Double and Triple Bonds", Mol. Phys. **114**, 1356–1364 (2015) (cit. on pp. 38, 39).

[251] B. H. Bransden and C. J. Joachain, *Physics of Atoms and Molecules*, Pearson Education (Longman, 1983) (cit. on p. 39).

[252] T. Bredtmann, J. Manz, and J.-M. Zhao, "Concerted Electronic and Nuclear Fluxes During Coherent Tunnelling in Asymmetric Double-Well Potentials", J. Phys. Chem. A **120**, 3142–3154 (2016) (cit. on p. 45).

[253] T. Klamroth, "Laser-Driven Electron Transfer through Metal-Insulator-Metal Contacts: Time-Dependent Configuration Interaction Singles Calculations for a Jellium Model", Phys. Rev. B **68**, 245421 (2003) (cit. on p. 52).

[254] N. Rohringer, A. Gordon, and R. Santra, "Configuration-Interaction-Based Time-Dependent Orbital Approach for Ab Initio Treatment of Electronic Dynamics in a Strong Optical Laser Field", Phys. Rev. A **74**, 043420 (2006) (cit. on p. 52).

[255] J. C. Tremblay, T. Klamroth, and P. Saalfrank, "Time-Dependent Configuration-Interaction Calculations of Laser-Driven Dynamics in Presence of Dissipation", J. Chem. Phys. **129**, 084302 (2008) (cit. on p. 52).

[256] J. C. Tremblay, P. Krause, T. Klamroth, and P. Saalfrank, "Time-Dependent Response of Dissipative Electron Systems", Phys. Rev. A **81**, 063420 (2010) (cit. on p. 52).

[257] J. C. Tremblay, S. Klinkusch, T. Klamroth, and P. Saalfrank, "Dissipative Many-Electron Dynamics of Ionizing Systems", J. Chem. Phys. **134**, 044311 (2011) (cit. on p. 52).

[258] M. Bauer and M. Aeschlimann, "Dynamics of Excited Electrons in Metals, Thin Films and Nanostructures", J. Electron. Spectrosc. Relat. Phenom. **124**, 225–243 (2002) (cit. on p. 52).

[259] J. M. Turney, A. C. Simmonett, R. M. Parrish, E. G. Hohenstein, F. A. Evangelista, J. T. Fermann, B. J. Mintz, L. A. Burns, J. J. Wilke, M. L. Abrams, N. J. Russ, M. L. Leininger, C. L. Janssen, E. T. Seidl, W. D. Allen, H. F. Schaefer, R. A. King, E. F. Valeev, C. D. Sherrill, and T. D. Crawford, "Psi4: An Open-Source Ab Initio Electronic Structure Program", WIREs Comput. Mol. Sci. **2**, 556–565 (2011) (cit. on p. 55).

[260] H.-J. Werner, P. J. Knowles, G. Knizia, F. R. Manby, M. Schütz, P. Celani, T. Korona, R. Lindh, A. Mitrushenkov, G. Rauhut, K. R. Shamasundar, T. B. Adler, R. D. Amos, A. Bernhardsson, A. Berning, D. L. Cooper, M. J. O. Deegan, A. J. Dobbyn, F. Eckert, E. Goll, C. Hampel, A. Hesselmann, G. Hetzer, T. Hrenar, G. Jansen, C. Köppl, Y. Liu, A. W. Lloyd, R. A. Mata,

A. J. May, S. J. McNicholas, W. Meyer, M. E. Mura, A. Nicklass, D. P. O'Neill, P. Palmieri, D. Peng, K. Pflüger, R. Pitzer, M. Reiher, T. Shiozaki, H. Stoll, A. J. Stone, R. Tarroni, T. Thorsteinsson, and M. Wang, *MOLPRO, Version 2012.1, A Package of Ab Initio Programs*, see http://www.molpro.net (accessed Nov 20, 2016), 2012 (cit. on p. 55).

[261] *TURBOMOLE V6.5 2013, a Development of University of Karlsruhe and Forschungszentrum Karlsruhe GmbH, 1989-2007, TURBOMOLE GmbH, since 2007*, see http://www.turbomole.com (accessed Nov 20, 2016). (cit. on p. 71).

[262] M. W. Schmidt, K. K. Baldridge, J. A. Boatz, S. T. Elbert, M. S. Gordon, J. H. Jensen, S. Koseki, N. Matsunaga, K. A. Nguyen, S. Su, T. L. Windus, M. Dupuis, and J. A. Montgomery, "General Atomic and Molecular Electronic Structure System", J. Comput. Chem. **14**, 1347–1363 (1993) (cit. on pp. 71, 201).

[263] E. W. Schlag, H. L. Selzle, P. Schanen, R. Weinkauf, and R. D. Levine, "Dissociation Kinetics of Peptide Ions†", J. Phys. Chem. A **110**, 8497–8500 (2006) (cit. on p. 214).

[264] G. N. Lewis, "THE ATOM AND THE MOLECULE.", J. Am. Chem. Soc. **38**, 762–785 (1916) (cit. on p. 215).

Danksagung

An dieser Stelle möchte ich all jenen von Herzen danken, die mir durch ihre fachliche und persönliche Unterstützung die Anfertigung dieser Dissertation ermöglicht haben. Mein erster Dank gilt meinem Betreuer Jean Christophe Tremblay für seine hervorragende und angenehme Betreuung meiner Doktor- und Masterarbeit. Sein großes Interesse und sein Enthusiasmus für meine Forschungsthemen sowie der Freiraum, den er mir gewährte, ermöglichten es mir meine Forschungsprojekte nach meinen Interessen zu entwickeln und viele verschiedene Aspekte zu untersuchen. Unsere unzähligen, angeregten und stimulierenden Diskussionen zu wissenschaftlichen Themen und Fragestellungen erweiterten mein naturwissenschaftliches Verständnis und gaben mir ständig neue Impulse für meine Forschungsprojekte. Neben seiner exzellenten wissenschaftlichen Unterstützung waren seine Freundlichkeit, seine Geduld, sein Humor und persönlicher Beistand während meiner Promotion und vor allem während einer sehr schweren Zeit in meinem Leben eine sehr große Stütze, die weit über die Arbeit hinausging. Das war und ist nicht selbstverständlich und dafür werde ich immer dankbar sein.

Weiterhin möchte ich Beate Paulus meinen Dank dafür aussprechen, dass sie mein Interesse an der Theoretischen Chemie durch ihre Vorlesungen geweckt und dadurch den Grundstein für diese Dissertation gelegt hat. Darüber hinaus hat sie mir die Möglichkeit gegeben Erfahrungen in der Lehre zu sammeln, was ich als eine sehr positive Erfahrung schätze.

Jörn Manz möchte ich dafür danken, dass er mir die Chance geboten hat an vielen interessanten wissenschaftlichen Themen mitzuarbeiten. Seine enorme Begeisterungsfähigkeit für die Ergebnisse zu unseren gemeinsamen Projekten motivierte mich stets in meinem wissenschaftlichen Arbeiten. Außerdem stellte er den Kontakt zu anderen Wissenschaftler/innen her, womit er den Weg für einige erfolgreiche Kooperationsprojekte ebnete.

I would like to express my sincere gratitude to Jhon Fredy Pérez Torres for arousing my interest in the calculation and visualization of the electronic flux density. The numerous constructive discussions during an internship under his supervision laid the foundation for this work, since the electronic flux density is an essential component in many of the studies of this dissertation. In addition, I acknowledge

him for the financial support through his project Pe2297/1-1 funded from the Deutsche Forschungsgemeinschaft. Furthermore, I would like to offer my special thanks to Dennis J. Diestler for the fruitful collaborations and fundamental discussions on the electron migration in small molecular systems.

Im Rahmen eines Kooperationsprojekt mit dem Konrad-Zuse-Zentrum für Informationstechnik Berlin durfte ich zusammen mit Axel Schild und Vincent Pohl das Programm ORBKIT entwickeln, welches ein fundamentales Werkzeug meiner Master- und Doktorarbeit ist. Ein großes Dankeschön geht an Hans-Christian Hege und Beate Paulus für die Finanzierung während der Initialisierung dieses Projektes. Des Weiteren möchte ich mich bei Axel Schild und Vincent Pohl für die harmonische Zusammenarbeit und die kritischen Diskussionen im Zusammenhang mit der Realisierung dieses Projektes bedanken. Danken möchte ich auch Jean Christophe Tremblay, dessen uneingeschränkte Unterstützung und sein wissenschaftlicher Beitrag eine erfolgreiche Weiterentwicklung des Programms erst ermöglicht haben, und Lukas Eugen Marsoner Steinkasserer für sein Mitwirken in späteren Entwicklungsphasen von ORBKIT.

Besonders möchte ich meinem Bruder, Erik Hermann, für seine unaufhörliche Unterstützung und ermutigenden Worte beim Verfassen dieser Doktorarbeit und meiner anderen Publikationen danken. Sein unermüdlicher Zuspruch während meiner gesamten akademischen Laufbahn spornten mich stets an, das Optimum erreichen zu wollen.

Danken möchte ich außerdem meinen Mitstreitern Vincent Pohl, Lukas Eugen Marsoner Steinkasserer, Johannes Horst Budau und Marcel Quennet. Unsere unzähligen Diskussionen zu meist nichtwissenschaftlichen Themen während unserer gemeinsamen Mittags- oder Kaffeepausen erheiterten stets meinen Alltag. Eine besondere Anerkennung gilt Vincent Pohl, der mich seit meiner Grundschulzeit begleitet und maßgeblich meinen wissenschaftlichen Werdegang mitgestaltet hat.

Im Übrigen danke ich den aktuellen und ehemaligen Mitgliedern der Arbeitsgruppen in der theoretischen Chemie (AG Tremblay, AG Paulus, AG Keller) für das entspannte und freundliche Arbeitsumfeld. Ein besonderer Dank gilt Julija Djordjevic für ihre stetige Hilfe in allen bürokratischen Angelegenheiten. Ich möchte mich auch bei allen Studenten bedanken, die ich während eines Forschungspraktikums betreuen durfte: Johannes Dietschreit, Felix Witte und Simon Petry. Danken möchte ich auch dem Hochschulrechenzentrum der Freien Universität Berlin (ZEDAT) für die Bereitstellung der Computereinrichtungen.

Der mit Abstand größte Dank gebührt meinen Eltern, die mich während meines ganzen bisherigen Lebens bedingungslos unterstützt haben und mir zur Seite standen. Insbesondere danke ich meinem Vater, der durch seine vielseitige Neugierde an politischen, geschichtlichen und naturwissenschaftlichen Themen immer ein Vorbild für mich war. Sein schwerwiegender Verlust wirft leider einen großen Schat-

ten auf das Ende meiner Promotionszeit. Ich wünschte er hätte diesen Abschluss, an dem er und meine Mutter sehr großen Anteil haben, noch erleben dürfen.

Danken möchte ich auch meinen Freunden, die für die nötige Ablenkung und Zerstreuung vom universitären Alltag gesorgt haben. Abschließend möchte ich mich bei meiner Freundin Stephanie Holz für ihre Geduld, die vielseitige Unterstützung und ihr Verständnis bedanken.

Vielen Dank!